

Universal Freezing Transitions of Dipole-Conserving Chains

J. Classen-Howes,^{1,*} R. Senese,^{1,*} and Abhishodh Prakash¹

¹*Rudolf Peierls Centre for Theoretical Physics, Parks Road, Oxford OX1 3PU, United Kingdom*

(Dated: August 21, 2024)

We argue for the existence of a universal phase diagram of k -local quantum chains subject to the conservation of a total charge and its dipole moment, which exhibits “freezing” transitions between strongly and weakly Hilbert space fragmented phases as charge filling ν is varied. We show that these continuous phase transitions occur at a critical charge filling of $\nu_c = (k-2)^{-1}$ *independently* of the on-site Hilbert space dimension d . To this end, we analytically prove that for any d , any state for $\nu < \nu_c$ hosts a finite density of sites belonging to “blockages”: local regions across which transport of charge and dipole moment cannot occur. We prove that this implies strong fragmentation of typical symmetry sectors into Krylov sectors that each form an exponentially-vanishing fraction of the total sector. By studying the distribution of blockages we analytically characterise how typical states are subdivided into dynamically-disconnected local “active bubbles”, and prove that typical states at these charge fillings exhibit area-law entanglement scaling, with rare “inverse quantum many-body scar” states featuring non-area-law scaling. We then numerically show that for $\nu > \nu_c$ and arbitrary d , typical symmetry sectors are weakly fragmented, with their dominant Krylov sectors constituted of states that are free of blockages. We also study the critical scaling of the dimensions of various Krylov sectors at $\nu = \nu_c$, as well as investigate the properties of certain special case models for which no phase transitions occur.

CONTENTS

I. Introduction and summary of main results	2	C. Distribution of blockages in typical states	14
II. Models and order parameters	3	D. Active bubble density function	15
A. Charge and dipole conserving local models	3	E. Numerical results	16
B. Order parameters for the degree of fragmentation	4	VII. Numerical results for the weakly fragmented phase	18
III. Blockages and fully extended states	5	A. Blockage-free extended states and contracted states	19
A. Blockages as local features of fully-extended states	5	B. Mapping a CS to a BES	19
B. The FES picture	7	C. Numerical evidence of weak fragmentation	20
C. Blockage-free FESs	7	VIII. Numerical results for the ratio of dimensions	21
IV. Size of symmetry sectors and typicality	8	IX. Models without a phase transition	22
A. Asymptotic formulas and typical symmetry sectors	8	A. Absolute blockages	23
B. Homogeneous filling and typicality	9	B. Exact active bubble density for $d = 2, k = 4$	23
V. Analytic characterisation of strong fragmentation	9	X. Entanglement entropy in the strongly fragmented phase	24
A. Strong fragmentation for $\nu < (k-1)^{-1}$	10	A. Type-1 blockages	24
B. Strong fragmentation for $(k-1)^{-1} \leq \nu < (k-2)^{-1}$	10	B. Type-2 blockages	25
VI. Distribution of blockages and active bubbles	12	XI. Conclusion and outlook	26
A. A sufficient condition for constrained particle mobility	12	Acknowledgments	26
B. Average density of type-1 blockages and type-2 edges	12	A. Uniqueness of fully extended states	27
		B. Proof of 2-colour connectivity	29
		C. Existence of blockage-free FESs and BESs for any N and X	30
		D. Scaling of the size of symmetry sectors	31
		E. Strong fragmentation in atypical (N, X) families	33

* These authors contributed equally to this work;

Contacts:

jonathan.classen-howes@physics.ox.ac.uk;

riccardo.senese@physics.ox.ac.uk

F. Calculation of densities of various particle configurations	34
1. Calculation of $b_1(k, n, \ell)$ and $b_1^\infty(k, n, \ell)$	34
2. Lower bound on the density of particular particle configurations	35
G. Lower bounds on $A_2(x, k, N, L)$ and $A_\infty(x, k, N, L)$	36
H. Algorithm for efficiently mapping to the FES	37
I. Proof of the CS-to-BES algorithm	38
J. Characterizing typical states for $d = 2$	39
K. Deriving $P_b(\nu)$ for $d = 2, k = 4$	41
References	42

I. INTRODUCTION AND SUMMARY OF MAIN RESULTS

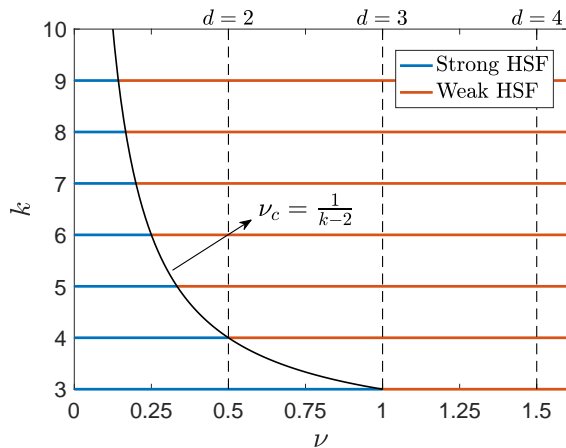


FIG. 1. Conjectured universal phase diagram in charge and dipole conserving k -local quantum chains featuring Hilbert space fragmentation (HSF). The relevant variables are the continuous particle filling $\nu \geq 0$ and the discrete locality of interactions $k \geq 3$. A first strong-to-weak fragmentation transition occurs at $\nu_c = 1/(k-2)$, a value independent of the on-site Hilbert space dimension d . Note that for each d value we report the corresponding phase diagram only below the half-filling $(d-1)/2$ (vertical dashed lines). Beyond half-filling the phase diagram is mirrored by particle-hole symmetry, leading to a second opposite transition (not depicted here) at $d-1-\nu_c$. Note that for $d = 2$ it is only meaningful to consider $k \geq 4$, as there can be no dynamical evolution at $k = 3$ which respects the global conservation laws.

When an interacting quantum many-body system undergoes dynamics it generically *thermalizes*, i.e. the long-time expectation value of local observables is found to coincide with the predictions of standard thermodynamic

ensembles. For quantum many-body systems, the condition for thermalisation is formalised by the so-called eigenstate thermalisation hypothesis (ETH) [1–3] which implies that the expectation value of local observables on eigenstates can be reproduced by appropriate thermal ensembles.

A long-standing quest in the study of quantum dynamics is to find generic settings robust to perturbations where ETH fails. One prominent example is many-body localization [3–6] which arises in systems with strong quenched disorder. An alternative, promising route following the recent discovery of fractons [7–12] are systems that exhibit Hilbert space fragmentation (HSF) [13–15] in the presence of multipole conservation. In fractonic models, kinetic constraints on the system’s dynamics inhibit thermalisation by preventing the model from exploring all of the states permitted by its local conservation laws. One widely studied class of fractonic models are 1D systems conserving a charge N and its dipole moment X , which can arise in the quantum Hall effect [16, 17] and in systems of charged particles exposed to a strong electric field [18, 19]. In these systems, the combined effect of the two conserved charges and the locality of interactions greatly inhibit mobility. In particular, isolated charges cannot propagate on their own, as they require other nearby charges to interact with. Hence, states in the same (N, X) quantum number sector can be dynamically disconnected.

Fractonic systems open up new possibilities for a rigorous characterization of ergodicity-breaking transitions in quantum many-body systems given that the underlying mechanisms rely only on symmetries and locality, which are easier to work with compared to, say, quenched disorder. In particular, there have been attempts to understand how fractonic systems undergo a continuous phase transition from “strong” to “weak” Hilbert space fragmentation [14] as the charge density ν is varied [20–22]. In the strongly fragmented phase, typical symmetry sectors can be subdivided into an exponentially-large (in system size) number of dynamically-disconnected “Krylov sectors”, all of which represent a vanishing fraction of the total sector. This results in a strong violation of ETH [14, 23]. In the weakly fragmented phase, although the number of Krylov sectors in a typical symmetry sector still grows exponentially with size, almost all states in a typical symmetry sector belong to a single dominant Krylov sector. Hence ETH is only weakly violated.

Quantum chains with any finite on-site dimension d , k -local interactions and charge-dipole symmetry can be analyzed by reformulating them as problems of hopping particles with maximal on-site occupation $d-1$ that conserve both total particle number N and center of mass X/N . Exploiting this, Ref. [21] analytically argued that for unbounded maximal on-site occupation ($d = \infty$), the critical density is located at $\nu_c = (k-2)^{-1}$, where k is the locality of interactions.

In this work, we show that the critical density $\nu_c =$

$(k-2)^{-1}$ of Ref. [21] is, in fact, “universal”: for any value of the on-site Hilbert space dimension d , there is a strong-to-weak transition at $\nu = \nu_c$, with a second weak-to-strong transition at $\nu = d - 1 - \nu_c$ by particle-hole symmetry. This leads to the universal d -independent phase diagram of Fig. 1. To achieve this we develop several new concepts and approaches for characterising strongly and weakly fragmented phases and the transition between them.

We introduce the concept of “blockages” to characterise the strongly fragmented phase, defining them as local regions of the system across which transport of particle number and dipole moment cannot occur. These constitute a generalisation of the “bottlenecks” introduced in Ref. [15]. The simplest example of a blockage is a contiguous sequence of $k-1$ or more “frozen” sites, i.e. sites with an unchanging particle occupation number under dynamics. Indeed, such a sequence necessarily disconnects the regions to its left and right from each other. We also demonstrate the existence of blockages that do not involve frozen sites at all.

Another crucial ingredient in our study of the strongly fragmented phase is that of a “fully extended state” (FES), introduced in Ref. [21] and whose scope we expand substantially. An FES is defined as a configuration of particles in a $d = \infty$ system to which no outward hops can be applied. We prove, for general locality k , that there exists a unique FES within each Krylov sector of a $d = \infty$ system, and furthermore that the structure of an FES can be used to determine the locations of certain types of blockages. Importantly, blockages can be located using FESs in finite- d systems as well: by embedding the latter into “auxiliary” $d = \infty$ chains, states in finite- d systems can be mapped to a corresponding FES, from which the location of some blockages can be readily inferred. We shall refer to this approach as “the FES picture”.

Using the FES picture we prove that for particle fillings $\nu < \nu_c$ and for any d , any configuration of particles features a finite density of sites belonging to blockages, and that this implies that typical symmetry sectors at these fillings are strongly fragmented. We also use the FES picture to analytically bound the density of blockages in typical states, as well as the density of “active bubbles”: local groups of interacting particles shielded from their surroundings by sequences of frozen sites. Additionally, we prove that due to the presence of blockages, typical eigenstates in the strongly fragmented phase feature area-law entanglement entropy scaling, although there exist rare exceptions which may constitute inverse quantum many body scars [24–27].

To characterise the weakly fragmented phase, we numerically show that for $\nu > \nu_c$ and arbitrary d , typical symmetry sectors feature a dominant Krylov sector in which all states are blockage-free and hence are weakly fragmented. We identify the dominant Krylov sector as the one containing a “blockage-free extended state” (BES), a particular state to which no outward hops can

be applied and which is unique to each symmetry sector. We develop an algorithm that maps arbitrary initial states to their corresponding BES with a high success rate for $\nu > \nu_c$, showing that typical states belong to the Krylov sector containing said BES.

Unlike previous analytical results on this phase transition [21], our FES picture can be used to analytically characterise not just individual symmetry sectors, but whole families of typical symmetry sectors at arbitrary on-site dimensions d , while also providing several analytical insights into the dynamical impacts of strong fragmentation. Furthermore, the numerical algorithms we develop are not only efficient at large system sizes but also exactly simulate the dynamics of the systems, unlike the approximate numerical methods developed in Ref. [20].

The remainder of the paper is organised as follows. In Section II, we begin by introducing our family of models and reviewing various probes that can be used to distinguish between the strongly and weakly fragmented phases. In Section III, we introduce two main types of blockages and the FES picture, and derive several key results regarding these. In Section IV, we define typical symmetry sectors and report some useful asymptotic formulas for their dimensions. We then make use of these formulas and the FES picture in Section V to demonstrate that for any on-site dimension d , typical symmetry sectors are strongly fragmented for $\nu < \nu_c$. We make further use of the FES picture in Section VI to analyse various properties of the strongly fragmented phase, such as the average density of frozen sites and different types of active bubbles. In Section VII, we present numerical evidence that typical symmetry sectors are weakly fragmented for $\nu > \nu_c$ and arbitrary d . We present further evidence that ν_c is the critical filling in Section VIII by numerically showing critical scaling in the dimension of the dominant Krylov sectors. In Section IX, we study special cases of the parameters d and k for which the model does not have phase transition. In Section X, we study the implications of the presence of blockages for the scaling of the entanglement entropy of eigenstates. We provide concluding remarks in Section XI.

II. MODELS AND ORDER PARAMETERS

A. Charge and dipole conserving local models

In this subsection we introduce the systems that are the focus of our study. It may be skipped by a reader familiar with previous works on HSF [14, 15].

Many of the fundamental features of the quantum models considered in this work are intrinsically classical, meaning that they can be studied by reasoning only in terms of quantum states that belong to a product-state basis [20–22]. For most purposes, it is hence sufficient to focus on classical 1D lattice models of hopping particles subject to finite-range interactions that conserve a charge

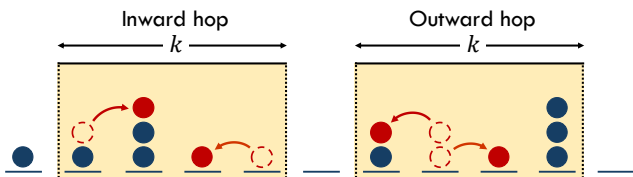


FIG. 2. Examples of inward hop and outward hop k -local gates ($k = 4$) that conserve N and X , acting on a local region of the chain with $d = 4$.

and its dipole moment. We consider a chain of L sites with open boundary conditions (OBC), where each site can host from 0 up to $d - 1$ particles, with $2 \leq d \leq \infty$, and the dynamics proceeds through sequences of hopping moves implemented via k -local gates, as depicted in Fig. 2. Calling n_i the number of particles on site i , every gate conserves the total number of particles N and the dipole moment X

$$N = \sum_{i=0}^{L-1} n_i \quad X = \sum_{i=0}^{L-1} i n_i. \quad (1)$$

We also define the filling ν and the intensive center of mass ν_x as

$$\nu = \frac{N}{L} \quad \nu_x = \frac{x}{L}, \quad (2)$$

where $x = X/N$ represents the center of mass. We require “gate-completeness”, i.e. that the set of chosen k -local gates and their combinations enable *all* possible rearrangements of particles compatible with k -locality, maximal occupancy of $d - 1$ and conservation of N and X . Violations of the previous condition, e.g. due to additional symmetries, further reduce mobility, and therefore do not alter most of the results derived in this work regarding the strongly fragmented phase. In the following, we will be mainly concerned with understanding which and how many configurations can be reached starting from a given initial configuration of particles and performing classical stochastic dynamics by randomly drawing sequences of k -local gates.

All the results derived in this work via classical reasoning have direct consequences on the physics of 1D lattice models with any on-site Hilbert space dimension d and k -local interactions that conserve a charge \hat{N} and its dipole moment \hat{X} , with $[\hat{N}, \hat{X}] = 0$. In the case of Hamiltonian dynamics, the Hamiltonian \hat{H} of these models is given by a sum of k -local terms $\hat{h}_j^{(k)}$ such that

$$\hat{H} = \sum_j \hat{h}_j^{(k)} + \text{H.c.}, \quad [\hat{h}_j^{(k)}, \hat{N}] = [\hat{h}_j^{(k)}, \hat{X}] = 0 \quad \forall j. \quad (3)$$

Here the possibly non-Hermitian $\hat{h}_j^{(k)}$'s can be chosen such that they map product states in a properly defined “particle basis” into other product states in the same

basis. Analogously to the classical case, we require gate-completeness of the set $\{\hat{h}_j^{(k)}\}$ and all their combinations. A standard example is a model of spin- s variables with $k = 4$ and Hamiltonian

$$\hat{H} = \sum_{i=0}^{L-4} J_i \hat{S}_i^+ \hat{S}_{i+1}^- \hat{S}_{i+2}^- \hat{S}_{i+3}^+ + \sum_{i=0}^{L-3} K_i \hat{S}_i^+ (\hat{S}_{i+1}^-)^2 \hat{S}_{i+2}^+ + \text{H.c.}, \quad (4)$$

where J_i, K_i are arbitrary non-zero complex scalars and \hat{S}_i^\pm represent on-site raising and lowering operators. Here, any product state in the \hat{S}^z basis can be mapped to a product state in a particle basis with $d = 2s + 1$, where the on-site particle occupation $\hat{n}_i = (\hat{S}_i^z + s)$ allows the defining of \hat{N}, \hat{X} analogous to Eq. (1). Identical considerations can be applied to fermionic ($d = 2$) and bosonic ($d = \infty$) models, and Hamiltonian dynamics can be easily replaced by stochastic quantum dynamics via quantum unitary circuits [13, 15].

In the following, we often refer to configurations of particles on the chain, or equivalently to product states in the particle basis, simply as “states”. In Section X, in which we study entanglement, we explicitly refer to vectors on Hilbert spaces as “quantum states”. From now on, we restrict our attention to fillings $0 \leq \nu \leq (d - 1)/2$. The regime $(d - 1)/2 \leq \nu \leq d - 1$ can be exactly mapped to the former by particle-hole symmetry; thus, identical results hold for both domains. Similarly, the domain $\nu_x \geq 1/2$ can be mapped to $\nu_x \leq 1/2$ by parity of the chain with respect to its center.

B. Order parameters for the degree of fragmentation

In the quantum setting, we refer to the dimension of a given (N, X) symmetry sector as $D_{N, X}^{(d)}$. Symmetry sectors can be decomposed into “Krylov sectors”, defined as the subspaces spanned by states connected by unitary evolution $\hat{U}(t)$ generated by \hat{H} from Eq. (3) (or its unitary circuit analogue). By the classical-quantum correspondence discussed in the previous section, Krylov sectors in the classical case are defined to be the set of product states in the particle basis that span its associated quantum Krylov sector. Hence, classical Krylov sectors coincide with the subsets of states within each classical symmetry sector that are connected by the classical stochastic dynamics, and they represent equivalence classes which partition the chosen (N, X) sector.

The interplay between k -locality and conservation of N and X necessarily fractures (N, X) sectors into exponentially many in system size Krylov sectors featuring a very wide range of dimensions [14, 15], in striking contrast with generic or integrable models. If we call $\mathcal{D}_i^{(d, k)} \geq 1$ the dimension of the i -th Krylov sector of a given (N, X)

sector, we have

$$D_{N,X}^{(d)} = \sum_{i=1}^{K_{d,k}(N,X)} \mathcal{D}_i^{(d,k)}, \quad (5)$$

where $K_{d,k}(N, X)$ is the total number of Krylov sectors in the (N, X) sector. In this work, we consider *families* of (N, X) sectors, where one family includes all the (N, X) sectors characterised by $N = \nu L$ and $X = \nu_x \nu L^2$ as we let L approach the thermodynamic limit, with ν and ν_x either fixed real numbers or fixed real functions of L . Then, following [14, 15], it is convenient to define the two phases of *strong* and *weak* fragmentation in terms of the ratio

$$r_{d,k}(N, X) = \frac{\mathcal{D}_{\max}^{(d,k)}}{D_{N,X}^{(d)}}, \quad (6)$$

$$\lim_{L \rightarrow \infty} r_{d,k}(N, X) = \begin{cases} 0 & \text{strong fragmentation} \\ 1 & \text{weak fragmentation} \end{cases}, \quad (7)$$

where $\mathcal{D}_{\max}^{(d,k)}$ represents the dimension of the largest Krylov sector in the given family of (N, X) sectors. In strongly fragmented families of symmetry sectors, each Krylov sector constitutes only a vanishingly small fraction of the corresponding symmetry sector, and numerical evidence has been given in Refs. [14, 15] that $r_{d,k}(N, X)$ decays to zero exponentially fast with system size. In contrast, in weakly fragmented families of symmetry sectors the largest Krylov sector includes in the thermodynamic limit a measure-1 fraction of all configurations present in the corresponding (N, X) sector.

In Section V we prove analytically that for any d , any $\nu < \nu_c$ and any typical family of (N, X) sectors, i.e. families characterized by $\nu_x = 1/2 + o(L^0)$ (cf. Section IV), $r_{d,k}(N, X)$ decays to zero exponentially with L . For these typical (N, X) families with $\nu < \nu_c$ we can therefore introduce the function $R_{d,k}(\nu)$ as

$$\lim_{L \rightarrow \infty} \frac{1}{L} \ln r_{d,k}(N, X) = R_{d,k}(\nu) < 0. \quad (8)$$

The importance of concentrating on $R_{d,k}$ compared to just considering the limit of Eq. (7) is that we conjecture the former to represent a *continuous* order parameter for the filling-induced phase transition. Indeed, in Section VIII we provide numerical evidence for $d = 2, 3$ and small L values that for $\nu \leq \nu_c$ the term $R_{d,k}(\nu)$ is an increasing function such that $R_{d,k}(\nu_c) = 0$. Note also that the main claim of Ref. [21] coincides with $R_{\infty,k}(\nu_c) = 0$. In Sections VII and VIII we provide strong numerical evidence for $d = 2, 3$ and ∞ that for $\nu > \nu_c$ the ratio $r_{d,k}(N, X)$ goes to 1 in the thermodynamic limit, i.e. $R_{d,k}(\nu) = 0 \forall \nu > \nu_c$. All this supports the fact that ν_c is the critical point for any d and that the continuous nature of the transition in typical symmetry sectors can be probed by looking at the scaling in Eq. (8) of $r_{d,k}(N, X)$ with L .

We note that a different probe for the nature of fragmentation has been introduced in Ref. [20]. Call $\rho_F(i)$ the density of frozen sites in the i -th Krylov sector of a given N sector, where a frozen site is a site whose occupation is the same throughout the Krylov sector. Then it was argued that in the thermodynamic limit the weighted average

$$\bar{\rho}_F^{(d)}(k, N, L) = \frac{\sum_{i=1}^{K_{d,k}(N)} \rho_F(i) \mathcal{D}_i^{(d,k)}}{\sum_{i=1}^{K_{d,k}(N)} \mathcal{D}_i^{(d,k)}} \quad (9)$$

is a non increasing function of ν which is exactly zero beyond a critical point. Here we have defined $K_{d,k}(N)$ to be the total number of Krylov sectors in fixed N sectors, i.e. we are not resolving over the different dipole moments compatible with N . The numerical results in Ref. [20] for $d = 3, k = 4$ suggest that the critical point coincides with ν_c . This supports the claim that $\lim_{L \rightarrow \infty} \bar{\rho}_F^{(d)}(k, N, L)$ is an alternative ordered parameter, different from $R_{d,k}(\nu)$ in Eq. (8), for the continuous filling-induced phase transition. In Section VI we analytically prove that $\lim_{L \rightarrow \infty} \bar{\rho}_F^{(d)}(k, N, L)$ is non-zero for $\nu < \nu_c$ in $d = 2$ and ∞ , and numerically show the same for other finite d values. We also provide in Section VII strong numerical evidence for $d = 2, 3$ and ∞ that the previous order parameter vanishes for $\nu > \nu_c$. However, note that, despite the powerful connection between the strongly fragmented phase and the presence of finite densities of frozen sites, as emphasised by these results, it is quite easy to verify that in the regime $(k-1)^{-1} \leq \nu < \nu_c$ Krylov sectors devoid of frozen sites exist for any d . Indeed, in Section V we prove that the presence of a finite density of frozen sites in the largest Krylov sector of a typical (N, X) family is a sufficient, but in principle not necessary condition for strong fragmentation according to the probe in Eq. (7).

III. BLOCKAGES AND FULLY EXTENDED STATES

A. Blockages as local features of fully-extended states

We present in this section a framework that will allow us to analytically characterise the strongly fragmented phase of models with any on-site dimension d . In the following, the concept of ‘‘fully extended state’’ (FES) originally introduced in Ref. [21] will play a crucial role. An FES is a configuration of particles of a $d = \infty$ system such that no pair of particles can perform an outward hop (cf. Fig. 2 for example of outward hop). FESs have a rather simple structure, which turns out to be particularly useful in identifying dynamical disconnections in systems of any on-site dimension d . Aside for the two boundary sites of the open chain, any site of an FES can host at most 1 particle, and different particles must be separated by sequences of at least $k - 3$ empty sites

(holes); otherwise it would still be possible to perform further outward hops. An indefinite number of particles can be stacked on the two boundary sites, and there is no lower bound on how many holes separate each of these stacks from the next closest particle. Importantly, in a $d = \infty$ system an FES can always be reached by starting from any initial configuration of particles and applying only outward hops [21]. In Appendix A we prove the “uniqueness” of FESs for general locality k :

In a $d = \infty$ system an FES cannot be dynamically connected to a different FES, i.e. each Krylov sector possesses a unique FES.

Blockages have been defined in Section I as local regions on the chain across which transport of particle number and dipole moment cannot occur. In other words, blockages prevent the regions to their left and right from exchanging particles and dipole moment quanta. We now show that in $d = \infty$ systems, thanks to the previous result on uniqueness, it is possible to easily identify blockages by analysing local features of FESs. This will later allow us to easily identify certain types of blockages in a system with finite d . An important property for the following derivation is that any subsystem (composed of adjacent sites) of an FES also represents an FES if considered in isolation. Indeed, if we consider any contiguous subregion of an FES and gates that act only within it, uniqueness applies to it too in that the subregion cannot be mapped by internal dynamics to a different FES. We call any contiguous subregion of an FES a “local FES”. We introduce the following two types of blockages that can be located by analysing the structure of FESs.

1. Consider a $d = \infty$ system and an FES that possesses a sequence of $k - 1$ or more consecutive holes somewhere along the chain.

$$\dots \frac{\bullet}{\geq k-1} \dots \frac{\bullet}{\geq k-1} \dots$$

Since it is not possible for 2 particles separated by $k - 1$ or more empty sites to interact, the subsystems on either side of these holes can only be dynamically connected if one of them expands further to bridge the divide. However, this would violate the uniqueness of FESs, given that both these subsystems are local FESs. This proves that the $k - 1$ empty sites are frozen, that is, they are empty in the entire Krylov sector, and hence the regions on their left and right are dynamically disconnected. A consequence of this is that any dynamics will conserve N and X separately on the left and right of the hole sequence. Thus, the hole sequence represents a blockage composed of empty frozen sites. We will refer to it as a type-1 blockage.

2. Consider a $d = \infty$ system in an FES and a subregion \mathcal{A} of the chain that is enclosed by two type-1 blockages, so that \mathcal{A} is dynamically disconnected from the rest of the chain. We also require that within \mathcal{A} there are no type-1 blockages. In cases where there are no type-1 blockages

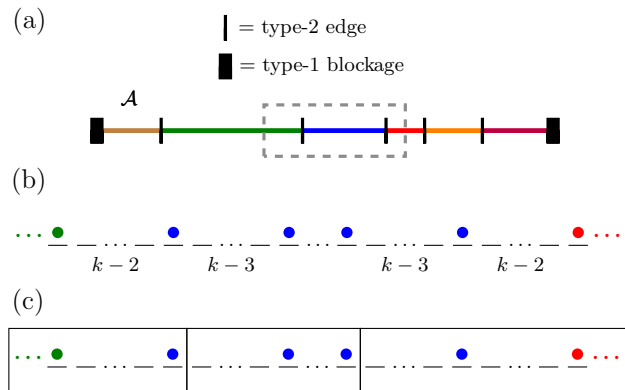


FIG. 3. Schematic representation of type-2 blockages, as identified from the local FES that occupies a region \mathcal{A} of the chain. (a) Example of region \mathcal{A} enclosed by two type-1 blockages. Subregions separated by a type-2 edge (i.e. a sequence of $k - 2$ holes in an FES) are associated with different colours. Any region consisting of two type-2 edges and the sites enclosed by them represents a type-2 blockage. (b) Zoom-in for the portion of region \mathcal{A} highlighted by the dashed gray rectangle in panel (a), where two sequences of $k - 2$ holes (type-2 edges) appear in the FES. In-between the two type-2 edges, particles are separated only by sequences of $k - 3$ holes. According to the colour scheme, regions separated by one type-2 edge have particles of different colour. (c) Example of a possible partition of the portion of \mathcal{A} from panel (b) into disjoint subregions that can at most host two different colours. Note that it is irrelevant where exactly in-between two chosen particles of the FES we place a given partition cut.

in the entire system, \mathcal{A} coincides with the whole chain. An example of region \mathcal{A} is presented in Fig. 3(a). Within \mathcal{A} we employ a useful colour scheme according to which regions separated by a sequence of $k - 2$ holes have particles of different colours, as represented in Fig. 3(b) where two sequences of $k - 2$ holes are separated by a non-zero number of sequences of $k - 3$ holes. Note that two sequences of $k - 2$ can also be next to each other, i.e. enclose just one particle and no sequence of $k - 3$ holes.

Consider the local Krylov sector composed of all the particle configurations in \mathcal{A} that can be reached starting from the local FES that originally occupies \mathcal{A} . In Appendix B we prove that:

Any configuration in this local Krylov sector can be dynamically reached by partitioning \mathcal{A} into disjoint subregions that contain at most two different colours each and, starting from the local FES, performing independent series of hops within each of these subregions.

An example of such a partition for the local subregion in Fig. 3(b) is represented in Fig. 3(c). Note that different particle configurations in the local Krylov sector might be associated with different partitions. In the following, we will refer to the statement above as “2-colour connectivity”.

With reference to the colours and particle configurations of Fig. 3(b)-(c), call “central” the region consisting of the two sequences of $k - 2$ holes and all the sites enclosed by them. An elementary consequence of the 2-colour connectivity is that the green and red regions cannot exchange particles or dipole moment quanta, and hence that the central region represents a blockage. Indeed, the 2-colour connectivity ensures that given any particle configuration in the local Krylov sector, we can find a cut somewhere along the central region such that the particle number and dipole moment to the left and right of the cut in the chosen configuration are the same as in the local FES. Contrary to type-1 blockages, here no frozen site is involved and the green and red regions can exchange particles and dipole moment with the blockage. Identical conclusions hold for all the other colours in \mathcal{A} , cf. Fig. 3(a).

In the following we will call any sequence of $k - 2$ holes enclosed between two particles in an FES a “type-2 edge”, and any region of an FES devoid of type-1 blockages and consisting of two type-2 edges and the sites enclosed by them a “type-2 blockage”.

B. The FES picture

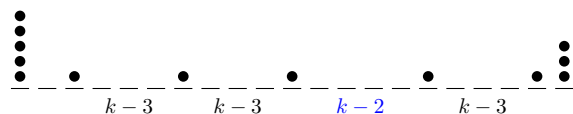
We have just seen how certain types of local configurations of particles and holes in the FES of a $d = \infty$ system allow us to identify blockages and frozen sites that characterise the entire Krylov sector. A key realisation is that this method based on FESs allows us to draw important conclusions about systems with any finite d . Consider a configuration of particles on the chain in a system S with d finite. Starting from this, we imagine performing dynamics in an auxiliary system \tilde{S} which is identical to S aside from having no upper bound on the maximal on-site occupancy, i.e. $\tilde{d} = \infty$. We then apply outward hops until we reach the corresponding unique FES. If in this FES some sequences of empty sites constitute type-1 blockages, the same sites will be empty and frozen also in the finite- d system S , thus representing there too type-1 blockages. This is because the Krylov sector associated with the chosen particle configuration in the finite- d system S is included in the Krylov sector associated with the $\tilde{d} = \infty$ system \tilde{S} . Similarly, type-2 blockages in \tilde{S} constitute type-2 blockages also in S , in that they prevent the propagation of particles and dipole moment between the regions on their left and right, while allowing interactions between the latter and the sites that form the blockage. In the following, we will refer to this approach that maps a configuration of the system S to its corresponding FES in the auxiliary system \tilde{S} as the “FES picture”.

Note that in general S might possess additional frozen sites and blockages in addition to those it has in common with \tilde{S} , due to the maximal occupation constraint of $d - 1$ particles per site. By particle-hole symmetry, some of these are trivial generalisations of those already derived and typically arise in N -sectors with filling ν be-

yond the half-filling $(d - 1)/2$. For example, a configuration of particles with some sites that form a type-1 block can be mapped to its particle-hole symmetric configuration, and in the latter the same sites will be frozen and have maximal occupation $d - 1$. Far more interesting are blockages in finite- d systems S that cannot be identified using the FES picture. The simplest example of these is a finite number of contiguous sites with maximal occupation $d - 1$ embedded in an otherwise empty chain. These sites are clearly frozen, but when applying the FES picture, there is no type-1 blockage signaling it, and thus this finite- d feature is invisible to the FES picture. We consider the effect of these types of finite- d blockages in Section VII.

C. Blockage-free FESs

A particularly interesting class of FESs is those devoid of any type-1 and type-2 blockages. Calling n_1 and n_2 respectively the number of type-1 blockages and of type-2 edges in an FES, we call a “blockage-free FES” a fully-extended state characterized by $n_1 = 0$ and $n_2 \leq 1$. Thus, if one considers all the separations between neighbouring particles in a blockage-free FES, there can be at most one separation of $k - 2$ holes while all the other separations must be of $k - 3$ holes, with the only exception being the separations next to the two boundary sites which can be composed of fewer than $k - 3$ holes. Note that stacking remains allowed at the two boundary sites and that the single sequence of $k - 2$ holes, if present, can also be in-between one of the boundary sites and the next closest particle. An example of a blockage-free FES for $k = 6$, $L = 21$, $N = 13$, $X = 112$ is given by



Importantly, blockage-free FESs can only exist for states with filling $\nu \geq \nu_c$, cf. Section V. The appendices A and C prove that:

For any pair of (N, X) values compatible with a given L and with $\nu \geq \nu_c$ there exists one and only one blockage-free FES for each value of k .

Later in Section VII we will argue on the basis of numerical evidence that in the weakly fragmented phase of a system S with any on-site dimension d , a necessary condition for a Krylov sector to be the dominant one which appears in the limit in Eq. (7) of $r_{d,k}(N, X)$ going to 1, is for it to be mapped by the FES picture to the unique blockage-free FES associated with the chosen (N, X) sector. The intuition behind this is that a dominant Krylov sector cannot possess the strong dynamical disconnections induced by the presence of type-1 and type-2 blockages.

In Section VII we will define “blockage-free extended states” (BES) as generalisations of blockage-free FESs that take into account the maximal on-site occupation of $d - 1$ for finite- d systems. These will have the same blockage-free FES structure in the bulk of the chain but will differ in proximity of the boundaries, given that the maximal on-site occupation prevents stacking of an indefinite number of particles on the boundary sites. BESs, for which an existence and uniqueness property analogous to the one for blockage-free FESs holds, will allow us to numerically argue that a *necessary and sufficient* condition for a Krylov sector of a finite- d system S in the weakly fragmented phase to be the dominant one in a given (N, X) sector is for it to contain the unique BES associated with the chosen (N, X) sector. This perspective offers an interesting interpretation of the uniqueness of dominant Krylov sectors in the weakly fragmented phase, attributing it to the uniqueness of BESs.

Given the identical structure of blockage-free FESs and BESs in the bulk of the chain, for the following it will be useful to define a “local BES” to be any subregion of the chain that has

1. At most one particle on each site.
2. Separations between neighbouring particles of exactly $k - 3$ holes, with the exception of at most one separation of $k - 2$ holes.

Note that making use of the definition of local BESs the previous existence and uniqueness properties can be extended to states with $\nu < \nu_c$: in this case the uniqueness refers to a state composed of a local BES surrounded by only empty sites (up to the boundaries). Finally, it is important to note that, in connection with the 2-colour connectivity, each contiguous subregion in an FESs hosting at most 2-colours coincides with a local BES.

IV. SIZE OF SYMMETRY SECTORS AND TYPICALITY

In this section, we present a few technical results that are needed in the analytic proofs discussed in the following sections. The reader not interested in technical details can skip it. In Section IV A we introduce asymptotic formulas for the dimension of symmetry sectors and define what we mean by a “typical symmetry sector”. In Section IV B we show that typical states for any d are spatially homogeneous over extensive length scales.

A. Asymptotic formulas and typical symmetry sectors

The total number of configurations on a chain of L sites with on-site dimension d , i.e. on-site occupation ranging from 0 to $d - 1$, is d^L . We start by restricting the number of particles to a fixed value N and refer to the total

number of configurations in this symmetry sector as $D_N^{(d)}$. There are $L(d - 1) + 1$ distinct N -sectors, corresponding in the thermodynamic limit to the real values in the interval $0 \leq \nu \leq d - 1$. The fact that these are only polynomially many in L , while the total number of configurations scales exponentially with L , shows that there must be large N -sectors with dimension $D_N^{(d)}$ whose exponential scaling coincides with d^L . For $d = 2$ and $d = \infty$ the expression for $D_N^{(d)}$ can be easily derived using Stirling’s asymptotic formula, in the limit of large L , on the two exact expressions

$$D_N^{(2)}(L) = \binom{L}{N} \quad D_N^{(\infty)}(L) = \binom{N + L - 1}{L - 1}. \quad (10)$$

We obtain for $0 < \nu < d - 1$

$$\ln D_N^{(d)}(L) = L\eta_d(\nu) - \frac{1}{2} \ln L + \mathcal{O}(L^0), \quad (11)$$

where

$$\begin{aligned} \eta_2(\nu) &= -\nu \ln \nu - (1 - \nu) \ln(1 - \nu) \\ \eta_\infty(\nu) &= -\nu \ln \nu + (1 + \nu) \ln(1 + \nu). \end{aligned} \quad (12)$$

In Appendix D we prove that the functional form of the leading term in Eq. (11) applies to all $2 \leq d \leq \infty$. There we also provide numerical evidence that the first subleading term $-\ln L/2$ in Eq. (11) is d -independent. For $d = 2$ and ∞ it is straightforward to check analytically that $\eta_d(\nu)$ is a strictly concave function, given that $\eta_d''(\nu) < 0$ for any ν in the allowed domain. In Appendix D we analytically derive, for any d , an exact implicit expression for $\eta_d(\nu)$. This allows us to show that $\eta_d(\nu)$ is strictly concave for any d , by (numerically) solving a single equation of $(d + 1)$ order. By particle-hole symmetry and strict concavity it follows that $\eta_d(\nu)$ has a unique global maximum at the half-filling $\nu^* = (d - 1)/2$, where it takes the value $\eta_d(\nu^*) = \ln d$.

Furthermore, we consider the size $D_{N,X}^{(d)}$ of (N, X) sectors. For a given N -family such that $0 < \nu < d - 1$, the number of distinct X -sectors scales asymptotically as $N(L - N/(d - 1)) = \mathcal{O}(L^2)$. In the thermodynamic limit, these correspond to the interval $\nu/(2d - 2) \leq \nu_x \leq 1 - \nu/(2d - 2)$. Given that the exponential scaling of the size of an $N = \nu L$ sector is governed by $\eta_d(\nu)$ and that there are only polynomially many X -sectors for each N , the largest X -sectors must have an exponential scaling of their size equal to $\exp(L\eta_d(\nu))$. Recently, Ref. [28] derived a sharp asymptotic formula for $D_{N,X}^{(d)}$ in the case of $d = \infty$. In Appendix D we show how from this we can also derive an exact asymptotic formula for $d = 2$. For these two values of d the asymptotic scaling of $D_{N,X}^{(d)}$ is given by

$$\begin{aligned} \ln D_{N,X}^{(d)}(L) &= L \left(\eta_d(\nu) - \Lambda_d(\nu, \nu_x) \right) \\ &\quad - 2 \ln L + \mathcal{O}(L^0), \end{aligned} \quad (13)$$

with $\Lambda(\nu, \nu_x) \geq 0$. As we show in Appendix D, for ν_x sufficiently close to $1/2$ the function $\Lambda_d(\nu, \nu_x)$ can be expanded as

$$\Lambda_d(\nu, \nu_x) = \lambda_d(\nu) \nu_{x_0}^2 + o(\nu_{x_0}^2), \quad (14)$$

where $\lambda_d(\nu)$ is a positive function of ν and $\nu_{x_0} = \nu_x - 1/2$ is the intensive center of mass when the origin is in the middle of the chain. In Appendix D we provide numerical evidence that the functional forms in Eq. (13) and Eq. (14) apply to any finite value of d . If we fix ν , then for any family of (N, X) sectors characterized by a $\nu_{x_0} = o(L^0)$ one gets

$$\frac{1}{L} \ln D_{N,X}^{(d)} = \eta_d(\nu) + o(L^0). \quad (15)$$

These families are thus *typical*, i.e. together they contain a fraction that tends to 1 exponentially with L of all the configurations in the chosen $N = \nu L$ sector.

B. Homogeneous filling and typicality

In the upcoming sections, the following property derived from the strict concavity of $\eta_d(\nu)$ will be especially important. Consider a chain of length L with $N = \nu L$ particles, characterised by Eq. (11). Create a bipartition of this system in such a way that one of the two subregions contains wL (possibly non-contiguous) sites and σL particles, with $0 < w < 1$, and assume that the two subregions cannot exchange particles. As a function of σ , the scaling of the total number W_d of configurations compatible with the bipartition is

$$\begin{aligned} g_d(\sigma | \nu, w) &= \lim_{L \rightarrow \infty} \frac{1}{L} \ln W_d \\ &= w \eta_d\left(\frac{\sigma}{w}\right) + (1-w) \eta_d\left(\frac{\nu - \sigma}{1-w}\right). \end{aligned} \quad (16)$$

Given that the global chain contains all the configurations of the bipartite one, by comparing Eq. (11) and Eq. (16) in the thermodynamic limit we have $\eta_d(\nu) \geq g_d(\sigma | \nu, w)$ for every σ in the domain determined by w and the maximal occupancy of $d-1$. We also notice that trivially $g_d(\sigma^* | \nu, w) = \eta_d(\nu)$, where $\sigma^* = \nu w$. Given that $\eta_d(\nu)$ is strictly concave, it follows that $\eta_d(\nu) > g_d(\sigma | \nu, w)$ for any $\sigma \neq \sigma^*$, that is, σ^* is the unique global maximum of $g_d(\sigma | \nu, w)$. Given that there are only $\mathcal{O}(L)$ ways to distribute the total number of particles over the two subregions, we see that configurations in which both subregions have local filling equal to the global ν (in the thermodynamic limit) are typical, i.e. their number exponentially dominates in system size over all other configurations. It is trivial to generalise the previous argument to the case in which we partition the system into any $G = \mathcal{O}(L^0)$ number of extensively large subregions of size $w_i L$, with $w_1 + \dots + w_G = 1$. Here we find again that if one or more of these subregions has local filling

different from ν (in the thermodynamic limit), the number of configurations compatible with this distribution of the N particles over the G subregions represents an exponentially vanishing with L fraction of the entire $N = \nu L$ symmetry sector. Given that there are only polynomially many ways of distributing the total number of particles over these G extensive subregions, we deduce that typical states in a given family of $N = \nu L$ sectors for any d have, in any extensive contiguous subregion, local filling equal to the global filling ν (in the thermodynamic limit), i.e. they are maximally homogeneous over extensive length scales [29]. Note that the previous typicality condition is consistent with the typicality of (N, X) sectors with vanishingly small ν_{x_0} . Thanks to the typicality of homogeneous configurations we will be able to show in the next sections that many classes of Krylov sectors, for global fillings $\nu < \nu_c$, occupy an exponentially vanishing fraction of their symmetry sector.

We can also generalise the inequality between η_d and g_d to the case in which we take into account the dipole moment conservation. Consider a chain characterised by $N = \nu L$ and $X = \nu_x \nu L^2$ and create a bipartition into two subregions of size wL and $(1-w)L$ that cannot exchange particles and dipole moment. Say that one of the two subregions has $N_1 = \sigma L$ particles and dipole moment $X_1 = \sigma_x \sigma w L^2$. The second subregion has N_2, X_2 such that $N_1 + N_2 = N$ and $X_1 + X_2 = X$. Define $\tilde{g}_d(\sigma, \sigma_x | \nu, \nu_x, w)$ as

$$\begin{aligned} \tilde{g}_d(\sigma, \sigma_x | \nu, \nu_x, w) &= \lim_{L \rightarrow \infty} \frac{1}{L} \ln \widetilde{W}_d, \\ \widetilde{W}_d &= D_{N_1, X_1}^{(d)}(wL) D_{N_2, X_2}^{(d)}(L-wL), \end{aligned} \quad (17)$$

where \widetilde{W}_d is the total number of particle configurations compatible with the bipartition. Then, since every configuration in the bipartite case is also a configuration of the global (N, X) sector chosen, using Eq. (13) and taking the thermodynamic limit we get

$$\eta_d(\nu) - \Lambda_d(\nu, \nu_x) \geq \tilde{g}_d(\sigma, \sigma_x | \nu, \nu_x, w) \quad (18)$$

for any σ and σ_x in their respective domains. The inequality Eq. (18) trivially generalises to the case in which we partition the system into more than 2 subregions. Note that identifying the global maxima of \tilde{g}_d requires a more precise determination of the function $\Lambda_d(\nu, \nu_x)$ compared to the numerical one performed in Appendix D.

V. ANALYTIC CHARACTERISATION OF STRONG FRAGMENTATION

In this section, we prove that, given any on-site dimension d , any typical symmetry sector with $\nu < \nu_c = (k-2)^{-1}$ is strongly fragmented. It is instructive to first focus on the region $\nu < (k-1)^{-1}$, where there are necessarily an extensive number of frozen sites. We then consider the more interesting region $(k-1)^{-1} \leq \nu < (k-2)^{-1} = \nu_c$, where there are Krylov sectors with no frozen sites.

A. Strong fragmentation for $\nu < (k-1)^{-1}$

We consider here a system S with $2 \leq d \leq \infty$ that is characterized by $\nu < (k-1)^{-1}$. Starting from any configuration of particles on the chain, we employ the FES picture in Section III and reach an FES in the auxiliary system \tilde{S} . We call f the fraction of sites in the chosen Krylov of S that are part of a type-1 blockage. Given the upper bound on ν , we automatically know from the FES picture that

$$f \geq 1 - \nu(k-1) > 0. \quad (19)$$

The lower bound is obtained by noticing that in the FES of \tilde{S} the lowest number of sites involved in a type-1 blockage is obtained when each one of the N particles is separated from its neighbours by exactly $k-2$ holes. We now prove that as a consequence of Eq. (19), any typical (N, X) family (*cf.* Section IV) in S is strongly fragmented according to the ratio test in Eq. (7). For any typical (N, X) family, the exponential scaling of $D_{N,X}^{(d)}$ is given by Eq. (15). On the other hand, the fL empty frozen sites induce a natural bipartition of the chain in which they represent one of the two (possibly non-contiguous) independent subregions that cannot exchange particles or dipole moment. The total number W_d of particle configurations, of any dipole moment, compatible with this bipartition is clearly larger than the dimension of any Krylov sector in the chosen (N, X) sector, i.e.

$$\mathcal{D}_{\max}^{(d)} < W_d. \quad (20)$$

From the uniqueness of the maximum of $g_d(\sigma|\nu, f)$ discussed in Section IV and the fact that here $\sigma = 0 \neq \nu f = \sigma^*$, we automatically see that

$$\lim_{L \rightarrow \infty} \frac{1}{L} \ln r_{d,k}(N, X) \leq g_d(0|\nu, f) - \eta_d(\nu) < 0. \quad (21)$$

This proves for any d that all the typical (N, X) families characterized by $\nu < (k-1)^{-1}$ and $\nu_{x_0} = o(L^0)$ are strongly fragmented according to the ratio test, given that the ratio in Eq. (6) decays to zero exponentially with L .

B. Strong fragmentation for $(k-1)^{-1} \leq \nu < (k-2)^{-1}$

In the region $(k-1)^{-1} \leq \nu < (k-2)^{-1}$ there still exist exponentially many FESs of \tilde{S} that possess a non-vanishing fraction $f > 0$ of frozen sites that are part of a type-1 blockage. Thus, by reasoning identical to the one of the previous section, any Krylov in S that is part of a typical (N, X) family and that can be connected within \tilde{S} to an FES of this type includes only an exponentially vanishing fraction of the configurations present in the corresponding (N, X) sector. Thus, if the largest Krylov

of a typical (N, X) family happens to have $f > 0$, the (N, X) family is strongly fragmented.

The important difference with respect to before is that in the region of ν values considered here it is possible to have Krylov sectors with $f = 0$, because the inequality in Eq. (19) doesn't hold anymore. Assume then $f = 0$ and that there are no particles stacked on the two boundary sites of the FES of \tilde{S} . If we call ρ_2 and ρ_3 the density of particles that are separated from the closest particle to their right by respectively $k-2$ and $k-3$ holes, in the thermodynamic limit we must have

$$\rho_2 + \rho_3 = \nu \quad \rho_2(k-1) + \rho_3(k-2) = 1. \quad (22)$$

The solution of the previous system is

$$\rho_2 = 1 - \nu(k-2) \quad \rho_3 = \nu(k-1) - 1. \quad (23)$$

Given that here $(k-1)^{-1} \leq \nu < (k-2)^{-1}$, we obtain $\rho_2 > 0$ and $\rho_3 \geq 0$. If we keep $f = 0$ but allow stacking of particles at the two boundary sites, then ρ_2 necessarily increases with respect to the case with no stacking. Thus every Krylov sector with $f = 0$ must possess an extensive number of type-2 edges, and thus, of type-2 blockages. We now prove that, in the region of ν values considered, every typical (N, X) family that has largest Krylov sector characterized by $f = 0$, must also be strongly fragmented. Say we select one among the $\mathcal{O}(L)$ many type-2 blockages. Given the extensive number of possible choices, we can always select a type-2 blockage (\mathcal{B}) of L -independent size such that the regions to its left (\mathcal{A}_1) and right (\mathcal{A}_2), up to the boundaries, are both extensively large. Given that \mathcal{A}_1 and \mathcal{A}_2 are prevented from exchanging particles and dipole moment, we can upper bound the dimension of the largest Krylov sector as

$$\mathcal{D}_{\max}^{(d)} < D_{N_{\mathcal{A}_1+\mathcal{B}}, X_{\mathcal{A}_1+\mathcal{B}}}^{(d)} D_{N_{\mathcal{A}_2+\mathcal{B}}, X_{\mathcal{A}_2+\mathcal{B}}}^{(d)}. \quad (24)$$

We notice that starting from a chain with L sites and N particles that possesses $D_N^{(d)}$ configurations, if we add to it $\ell = \mathcal{O}(L^0)$ sites which contain $n = \mathcal{O}(L^0)$ particles, then

$$1 < \lim_{L \rightarrow \infty} \frac{D_{N+n}^{(d)}(L+\ell)}{D_N^{(d)}(L)} < \infty, \quad (25)$$

as seen by applying Eq. (11). The same is true when we consider the sizes of (N, X) sectors $D_{N,X}^{(d)}(L)$. This implies that there always exists an L -independent constant Q such that from Eq. (24) we can arrive to

$$\mathcal{D}_{\max}^{(d)} < Q D_{N_{\mathcal{A}_1+\mathcal{B}}, X_{\mathcal{A}_1+\mathcal{B}}}^{(d)} D_{N_{\mathcal{A}_2}, X_{\mathcal{A}_2}}^{(d)}. \quad (26)$$

Consider the case in which in the largest Krylov sector the bipartition into $\mathcal{A}_1 + \mathcal{B}$ and \mathcal{A}_2 appearing in the previous inequality can be chosen in such a way that \mathcal{A}_2 has local filling different from ν (even in the thermodynamic limit), and hence hosts only atypical configurations. Then, similarly to Eq. (21), we obtain from the

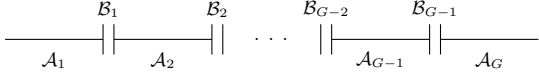


FIG. 4. Partition of the chain into contiguous subregions (\mathcal{A}_i) separated by type-2 blockages of L -independent size (\mathcal{B}_i). Each vertical line represents a type-2 edge.

typicality of homogeneous configuration proved in Section IV that

$$\lim_{L \rightarrow \infty} \frac{1}{L} \ln r_{d,k}(N, X) < 0. \quad (27)$$

This shows that $r_{d,k}$ decays to zero exponentially with L and thus implies strong fragmentation whenever the largest Krylov sector of a typical symmetry sector happens to be of the form just discussed.

Consider on the other the possibility of having a largest Krylov sector with $f = 0$ and for which we cannot find a bipartition of the system via a type-2 blockage such that the two subregions have local filling different from ν in the thermodynamic limit. This implies that any extensive subregion of the chain has local filling approaching the global ν for large L values. We now exploit a trivial property of the FES picture starting from any state of the system S with on-site dimension d : if an extensive subregion of the chain is enclosed by two blockages of either type-1 or type-2 with $o(L)$ size, then for asymptotically large L values this region has identical local filling in the FES of the auxiliary system \tilde{S} and in the chosen state of the system S . This provides us with an algorithm to partition the system into G subregions (\mathcal{A}_i) that are separated by type-2 blockages (\mathcal{B}_i) of L -independent size, as pictured in Fig. 4. The first subregion \mathcal{A}_1 must necessarily have size ℓ_1 scaling as $\mathcal{O}(L^{\gamma_1})$, with $0 \leq \gamma_1 < 1$. Indeed, assume for the sake of contradiction that the first L -independent in size type-2 blockage is encountered only extensively far away from from the left boundary, and so $\ell_1 = \mathcal{O}(L)$. This means that either \mathcal{A}_1 doesn't possess type-2 edges at all or that the ones present are at least an $\mathcal{O}(h(L))$ apart from each other, with $h(L)$ a function that diverges for $L \rightarrow \infty$. This would however imply that for large L the local filling in \mathcal{A}_1 is greater (in presence of stacking on the left boundary) or equal to ν_c , which is not possible given the condition of having local filling equal to $\nu < \nu_c$ in any extensive subregion of the chain. Exactly the same reasoning can be applied to all the remaining \mathcal{A}_i regions. In particular, after each blockage \mathcal{B}_{i-1} we try to look for the next type-2 blockage of L -independent size at a fixed distance $\ell = \mathcal{O}(L^0)$ to the right of \mathcal{B}_i , with $\ell \gg 1$. If no such blockage is found at this distance, we keep scanning to the right, until we find \mathcal{B}_i at a distance ℓ_i from \mathcal{B}_{i-1} . From the argument above we are guaranteed that for any subregion \mathcal{A}_i the size $\ell_i \geq \ell$ is subextensive, i.e. it scales as $\ell_i = \mathcal{O}(L^{\gamma_i})$ for some $0 \leq \gamma_i < 1$. We can now generalize Eq. (24) to

the multipartite case as (to simplify the notation we now indicate $D_{N_{\mathcal{A}}, X_{\mathcal{A}}}^{(d)}$ simply as $D_{\mathcal{A}}^{(d)}$)

$$\mathcal{D}_{\max}^{(d)} < D_{\mathcal{A}_1 + \mathcal{B}_1}^{(d)} \left[\prod_{i=2}^{G-1} D_{\mathcal{B}_{i-1} + \mathcal{A}_i + \mathcal{B}_i}^{(d)} \right] D_{\mathcal{B}_{G-1} + \mathcal{A}_G}^{(d)}. \quad (28)$$

Using the analogue of Eq. (25) for the dimension $D_{N, X}^{(d)}$ of (N, X) sectors, we obtain similarly to Eq. (26)

$$\mathcal{D}_{\max}^{(d)} < Q^{G-1} \left[\prod_{i=1}^{G-1} D_{\mathcal{A}_i + \mathcal{B}_i}^{(d)} \right] D_{\mathcal{A}_G}^{(d)}, \quad (29)$$

where Q is again an L -independent positive constant. The right-hand side of the previous inequality involves the total number of configurations in a partition of the chain into G regions that cannot exchange particles and dipole moment with each other. Using Eq. (13) together with the generalization of Eq. (18) to the multipartite case, we obtain

$$r_{d,k}(N, X) < L^2 \prod_{i=1}^G \frac{\tilde{Q}}{\ell_i^2}. \quad (30)$$

Here \tilde{Q} is an L -independent positive constant that has absorbed the Q factors from Eq. (29) and the $\mathcal{O}(L^0)$ constants arising from the use of Eq. (13) on every $D_{\mathcal{A}_i + \mathcal{B}_i}^{(d)}$ from Eq. (29) and on $D_{N, X}^{(d)}$ from Eq. (6). Importantly, we choose the L -independent distance ℓ to be much larger than the size of any \mathcal{B}_i . In this way we can always guarantee that $\ell_i^2 \geq \ell^2 > \tilde{Q}$. We see that if G is extensively large, i.e. if after applying the subdivision algorithm we find among the set of all \mathcal{A}_i regions a subset of extensively many sizes $\ell_i = \mathcal{O}(L^0)$, then $r_{d,k}$ in Eq. (30) decays to zero exponentially with L . The fact that $G = \mathcal{O}(L)$ is guaranteed by our requirement of having an extensive number of type-2 edges in the system. Indeed, assume by contradiction that $G = \mathcal{O}(L^{\gamma_g})$, with $\gamma_g < 1$. The total number of type-2 edges in the system are obtained by summing the following contributions:

1. Two type-2 edges per \mathcal{B}_i blockage and at most $\mathcal{O}(L^0)$ type-2 edges per each \mathcal{A}_i region with size $\ell_i = \mathcal{O}(L^0)$.
2. At most $\ell_i/h(L)$ type-2 edges in each \mathcal{A}_i region of size $\ell_i = \mathcal{O}(L^{\gamma_i})$ with $0 < \gamma_i < 1$. Here $h(L)$ is again a function that diverges for $L \rightarrow \infty$.

Summing these contributions under the assumption of a subextensive G yields a subextensive number of type-2 edges in the chain, which contradicts our requirements of having an extensive number of them.

To summarise, equations Eq. (21), Eq. (27) and Eq. (30) prove that:

For any d and in any typical family of (N, X) sectors characterized by $\nu < \nu_c$, the ratio $r_{d,k}(N, X)$ decays to

zero exponentially with L .

Therefore, these typical (N, X) families are strongly fragmented. Note that we have not determined the form of the largest Krylov sector in a given (N, X) sector. What we have achieved is showing that regardless of the characteristics of the Krylov sector, its dimension must represent an exponentially small fraction in L of the corresponding dimension of the (N, X) sector.

In the following section, we shall prove that the typical states for $d = 2$ and $d = \infty$ host an extensive number of type-1 blockages for $\nu < \nu_c$. We note that if one could easily prove the same for any d , then the previous proof could be limited to the case of $f > 0$.

In Appendix E we briefly discuss the fate of strong fragmentation in atypical families of (N, X) sectors.

VI. DISTRIBUTION OF BLOCKAGES AND ACTIVE BUBBLES

In the previous section, the FES picture allowed us to demonstrate for general d that typical symmetry sectors are strongly fragmented for fillings $\nu < \nu_c$. We will now use the FES picture and the 2-colour connectivity to develop an analytic framework for studying key dynamical characteristics of the strongly fragmented phase.

A. A sufficient condition for constrained particle mobility

We introduce here a sufficient condition which, when satisfied by a group of particles, places strong bounds on how far they can propagate from their point of origin. This condition can only generally be satisfied in the strongly fragmented phase, where fractonic restrictions on particle mobility give rise to the presence of blockages and local active bubbles. As such, the condition can be used to efficiently identify many (though not all) of the type-1 blockages in a system, and it is in some respects more analytically tractable than the FES picture (which on the other hand identifies all type-1 blockages). We will use it in the following subsections to analytically lower bound the average density of type-1 blockages and type-2 edges, as well as the average density of active bubbles.

We consider a system S with on-site dimension d . Pick a site of the chain as the origin, that is, call it site 0. Assume that there are N_R particles in the region \mathcal{A}_R of the chain that goes from site 0 to the right boundary of the chain, and let L_R denote the total number of sites in \mathcal{A}_R . Assume furthermore that either the rest of the system is empty or that the particles to the left of site 0 are sufficiently far away that they never interact with the particles in \mathcal{A}_R . Label the initial positions of the particles in \mathcal{A}_R , from leftmost to rightmost, as $\{i_n^0\}_{n=1}^{N_R}$, and say those positions satisfy

$$i_n^0 \geq (n-1)(k-2). \quad (31)$$

We note that this constraint requires $L_R \geq (N_R - 1)(k - 2) + 1$, which implies that in the thermodynamic limit $\lim_{L \rightarrow \infty} N_R/L_R \leq \nu_c$. We will show that condition Eq. (31) ensures that, under dynamical evolution of the system S , none of those N_R particles ever leaves the region \mathcal{A}_R .

Assume, for the sake of contradiction, that it is possible to start from an initial state satisfying Eq. (31) and to propagate particles originally in \mathcal{A}_R to the left of site 0. From the point of view of the FES picture, this implies that in the auxiliary system \tilde{S} , the leftmost of the particles initially in \mathcal{A}_R is mapped to a position i_1 in the FES that satisfies $i_1 < 0$. Due to the 2-colour connectivity of Section III, we know that the FES picture expansion from the initial state in \mathcal{A}_R to the final auxiliary FES will occur independently within different subregions of the system. As stressed before, the particles in each of these subregions form a local BES in the final FES, with at most one pair of particles in each local BES separated by a sequence of $k-2$ holes and with no pairs separated by sequences of $k-1$ or more holes.

Consider the leftmost of these local BESs, and say that it is constituted of m particles in total. Since these particles only interacted amongst themselves during the expansion in \tilde{S} , they must have conserved their initial dipole moment, and by Eq. (31) they must satisfy

$$\sum_{j=1}^m i_j \geq \sum_{j=1}^m (j-1)(k-2) = \frac{m(m-1)}{2}(k-2). \quad (32)$$

We next consider what local BES made of m particles would have the highest possible dipole moment while satisfying $i_1 < 0$. Clearly, this is given by $i_1 = -1$ and $i_j = (j-1)(k-2)$ for $j = 2, \dots, m$. Hence, the leftmost local BES must have a dipole moment of at most

$$-1 + \sum_{j=2}^m (j-1)(k-2) = -1 + \frac{m(m-1)}{2}(k-2). \quad (33)$$

This is less than the lower bound in Eq. (32), and so this propagation cannot happen. Hence, regardless of the value of d , particles that have initial positions satisfying Eq. (31) cannot propagate left of site 0 by interacting solely among themselves.

B. Average density of type-1 blockages and type-2 edges

Using the sufficient condition in Eq. (31) we now rigorously derive a lower bound on the average density of type-1 blockages and type-2 edges in a typical state for $d = 2$ and $d = \infty$, where the average is taken over all particle configurations in a specified N sector. We define the average densities of type-1 blockages and type-2 edges $\bar{\rho}_t^{(d)}$ (with $t = 1, 2$ respectively) in a system with

on-site dimension d to be given by

$$\bar{\rho}_t^{(d)}(k, N, L) = \frac{1}{L} \frac{\beta_t^{(d)}(k, N, L)}{D_N^{(d)}(L)}, \quad (34)$$

where $\beta_t^{(d)}$ is the total number of type-1 blockages and type-2 edges with locality k across all states in the N sector for $t = 1, 2$ respectively. Since the holes within a type-1 blockage are frozen, a finite density of type-1 blockages, in turn, implies a lower bound on the average density of frozen sites $\bar{\rho}_F^{(d)}(k, N, L)$, defined in Eq. (9) from Section II B. We expect by self-averaging that these lower bounds also apply to individual states in the thermodynamic limit, an argument we elaborate further on in Section VI C and demonstrate numerically in Section VI E. The lower bound on the density of frozen sites is particularly noteworthy for the regime $(k-1)^{-1} < \nu < (k-2)^{-1}$ as it indicates that, despite the existence of Krylov sectors without any frozen sites, states from those sectors are extremely rare.

We first consider the case of type-1 blockages. For simplicity, we will only compute a lower bound on the density of type-1 blockages of a particular format. In particular, we consider the configuration of holes and particles be-

tween the dashed vertical lines in the following figure:

$$\cdots \left| \begin{array}{c} \vdots \\ \vdots \\ \vdots \end{array} \right| \cdots \text{---} \text{---} \text{---} \bullet \text{---} \text{---} \text{---} \left| \begin{array}{c} \vdots \\ \vdots \\ \vdots \end{array} \right| \cdots \quad (35)$$

It is clear that, if the above configuration is embedded in a system such that the particles to the right of the right vertical dashed line satisfy the no-propagation constraints in Eq. (31) (with site 0 corresponding to the first site after the vertical line), and the particles to the left of the left line satisfy a mirrored version of the constraints (with site 0 being the first site to the left of the left line), then the $k-1$ holes in the configuration will be frozen and constitute a type-1 blockage. Hence, by counting the number of times the configuration in Eq. (35) occurs in a given state with the particles to its left and right satisfying the no-propagation constraints, we can lower bound the total number of type-1 blockages. The reason we include a particle in the configuration in Eq. (35), and don't just count occurrences of sequences of $k-1$ holes with Eq. (31) satisfied on either side, is to avoid double-counting issues later on. The density of other possible constructions of type-1 blockages can be calculated using an identical method.

We begin with the case of $d = 2$, and study the average density of type-1 blockages $\bar{\rho}_1^{(2)}(k, N, L)$ (recalling that $D_N^{(2)}(L) = \binom{L}{N}$). We can lower bound $\beta_1^{(2)}(k, N, L)$ by solely counting the total number of blockages of the type presented in Eq. (35). This sum is computed by summing first over all $\mathcal{O}(L)$ possible positions in the chain for at which the configuration in Eq. (35) can be situated, and then for each such position summing over all possible positions compatible with Eq. (31) for the remaining particles in the system. This yields

$$\beta_1^{(2)}(k, N, L) \geq \sum_{L_R=0}^{L-2k+3} \sum_{N_R=N_{\min}}^{N_{\max}} b_1(k, N_R, L_R) b_1(k, N - N_R - 1, L - L_R - 2k + 3) \equiv \tilde{\beta}_1^{(2)}(k, N, L). \quad (36)$$

In the expression above, $b_1(k, N_R, L_R)$ denotes the total number of ways to arrange N_R particles over L_R sites such that the particles obey the constraint in Eq. (31). The second appearance of the b_1 function hence gives the analogous quantity for the region to the left of the configuration.

We compute this function explicitly in Appendix F, and find it to be

$$b_1(k, N_R, L_R) = \binom{L_R + (k-2)}{N_R} \frac{L_R - (N_R - 1)(k-2)}{L_R + (k-2)}. \quad (37)$$

The upper and lower bounds on the summation over N_R

in Eq. (36) are

$$N_{\max} = \max(0, N - \lfloor (L - L_R - k)/(k-2) \rfloor) \quad (38)$$

$$N_{\min} = \min(N, \lfloor (L_R + k - 3)/(k-2) \rfloor), \quad (39)$$

where the brackets $\lfloor \dots \rfloor$ denote the floor function. These bounds ensure that the number of particles to the right and left of the blockage configuration is small enough that the conditions of Eq. (31) are satisfied; if N_R was greater than N_{\max} , it would be impossible to arrange the particles on the right of the blockage in a way that satisfied Eq. (31), as well as for N_{\min} and the particles on the left.

With this result in hand, we may bound the mean den-

sity of type-1 blockages as

$$\bar{\rho}_1^{(2)}(k, N, L) \geq \frac{\tilde{\beta}_1^{(2)}(k, N, L)}{L \binom{L}{N}}. \quad (40)$$

In the thermodynamic limit, the sums in Eq. (36) become integrals, and the sum over N_R can be approximated using Laplace's method. We perform this calculation in Appendix F, yielding the final result

$$\lim_{L \rightarrow \infty} \bar{\rho}_1^{(2)}(k, \nu L, L) \geq \nu(1 - \nu/\nu_c)^2, \quad (41)$$

where $\nu = \nu_c$ as before. This proves that the average density of type-1 blockages in a given N -sector with $\nu < \nu_c$ is non-zero in the thermodynamic limit.

This result also allows us to put a lower bound on the average density $\bar{\rho}_F^{(2)}(k, N, L)$ of frozen sites in a fixed N family. Since there are at least $k - 1$ frozen sites per blockage configuration of the type in Eq. (35), we immediately have that $\bar{\rho}_F^{(2)}(k, N, L) \geq (k - 1)\bar{\rho}_1^{(2)}(k, N, L)$, from which it follows that in the thermodynamic limit

$$\lim_{L \rightarrow \infty} \bar{\rho}_F^{(2)}(k, \nu L, L) \geq (k - 1)\nu(1 - \nu/\nu_c)^2. \quad (42)$$

This is non-vanishing for $\nu < \nu_c$, proving that $\bar{\rho}_F^{(2)}(k, N, L)$ is a valid order parameter for the strongly fragmented phase for $d = 2$. Moving on to the case of type-2 edges, we compute a lower bound on their average density by considering edges of the format:

$$\begin{array}{ccccccc} \vdots & & & & & & \vdots \\ \cdots & \cdots & \cdots & \cdots & \cdots & \cdots & \cdots \\ \vdots & & \bullet & & \bullet & & \vdots \\ \cdots & \cdots & \cdots & \cdots & \cdots & \cdots & \cdots \\ \vdots & & & & & & \vdots \\ & k-3 & & k-2 & & k-3 & \end{array}, \quad (43)$$

where again the particles to the right and left of the dashed vertical lines follow the no-propagation constraints of Eq. 31. Making use of identical logic as for the type-1 blockage case and again using the thermodynamic-limit results of Appendix F, we get that the average density $\bar{\rho}_2^{(2)}(k, N, L)$ of type-2 edges is lower bounded in the thermodynamic limit by

$$\lim_{L \rightarrow \infty} \bar{\rho}_2^{(2)}(k, \nu L, L) \geq \nu^2(1 - \nu)^{k-3}(1 - \nu/\nu_c)^2. \quad (44)$$

The bounds derived above in the $d = 2$ case can also be derived in the $d = \infty$ case using an almost identical approach. We carry out the calculation explicitly in Appendix F, and find the average density of type-1 blockages in the thermodynamic limit to be bounded by

$$\lim_{L \rightarrow \infty} \bar{\rho}_1^{(\infty)}(k, \nu L, L) \geq \nu(1 + \nu)^{-3}(1 - \nu/\nu_c)^2, \quad (45)$$

leading to a corresponding bound on the average density of frozen sites

$$\lim_{L \rightarrow \infty} \bar{\rho}_F^{(\infty)}(k, \nu L, L) \geq (k - 1)\nu(1 + \nu)^{-3}(1 - \nu/\nu_c)^2. \quad (46)$$

Likewise the average density of type-2 edges can also be lower-bounded, yielding the result

$$\lim_{L \rightarrow \infty} \bar{\rho}_2^{(\infty)}(k, \nu L, L) \geq \nu^2(1 + \nu)^{-(k+5)}(1 - \nu/\nu_c)^2. \quad (47)$$

C. Distribution of blockages in typical states

It is ubiquitous in statistical mechanics to find that properties averaged over an ensemble of states match the properties of individual states in the typicality class that dominates the average, *cf.* Appendix J. Also in the present case we expect the density of type-1 or type-2 blockages in an individual typical state of any d system to approach the average density of blockages in the chosen $N = \nu L$ sector in the thermodynamic limit. We show this explicitly by making use of self-averaging [30] arguments.

Given the regime $\nu < \nu_c$, we know from Section V any state must host an extensive number of sites that are part of either type-1 blockages or type-2 edges. We restrict our attention to typical states, which as proved in Section IV have, in any extensive subregion, local filling approaching the global ν for $L \rightarrow \infty$. Given these premises, we can imagine to apply the FES picture to any given typical state and in the FES obtained apply the same subdivision algorithm used in Section VB and depicted in Fig. 4. In this way, we partition the chain into G dynamically disconnected subregions \mathcal{A}_i , with sizes $\ell_i \geq \ell \gg 1$ such that $\ell_i = \mathcal{O}(L^{\gamma_i})$ for some $0 \leq \gamma_i < 1$, and that are separated by blockages \mathcal{B}_i of L -independent size. The only two differences with respect to the algorithm applied in Section VB are

1. Now the \mathcal{B}_i 's can be either type-1 or type-2 blockages. In this regard notice that a type-1 blockage of any size can be counted as a blockage of L -independent size, by considering as a blockage only a subpart of it, if necessary.
2. Starting from blockage \mathcal{B}_{i-1} , the search for the next blockage is only stopped when we find an L -independent blockage \mathcal{B}_i such that the region \mathcal{A}_i has local filling sufficiently close to the global one ν . This is always possible to achieve while retaining $\gamma_i < 1$, given that from typicality any extensively large region enclosed by two blockages of L -independent size must have filling approaching ν in the thermodynamic limit.

Also, here we are choosing ℓ much larger than the size of any \mathcal{B}_i blockage, so that the dynamical overlap associated with the presence of type-2 blockages among the \mathcal{B}_i 's is negligible. Furthermore, we notice that by construction G diverges for $L \rightarrow \infty$. Having obtained G dynamically disconnected subregions all with local filling close to the global ν , we can compute the density of both type-1 blockages and type-2 edges in each of the G many \mathcal{A}_i subregions. Over asymptotically large chains, these can be regarded as many independent realisations of a random variable whose expected value coincides with the average density of type-1 blockages or type-2 edges calculated over the entire $N = \nu L$ sector. By the central limit theorem we thus expect the global density of type-1 blockages and type-2 edges, in any asymptotically large

typical state for $\nu < \nu_c$ and any d , to match the ones obtained by computing the average densities over the entire N sector. The previous argument based on the subdivision algorithm and self-average also proves that type-1 blockages and type-2 edges must be quite uniform along the chain in any typical state.

Note that combining the present results with the lower bounds on the average density of type-1 blockages and type-2 edges from the previous section, we prove for $d = 2$ and $d = \infty$ that individual typical states possess a non-vanishing density of type-1 blockages and type-2 edges for $\nu < \nu_c$. We expect the same to be true for any other value of d and numerically show it in the next Section [VIE](#).

D. Active bubble density function

Since typical states in the strongly fragmented phase contain a finite density of uniformly distributed type-1 blockages, dynamical evolution in these states must be confined to dynamically-disconnected local regions that are L -independent in size. Following the terminology of Ref. [\[20\]](#), we refer to these regions as “active bubbles”. More specifically, we define an active bubble to be a set of neighbouring sites containing at least 2 particles and such that:

- Nowhere in the active bubble is there a sequence of $k - 1$ or more frozen sites.
- The leftmost and rightmost sites of the active bubble are not frozen sites.
- The first $k - 1$ sites to the left and right of the active bubble are frozen sites and therefore constitute a blockage.

Since the active bubbles are dynamically disconnected from each other, we may independently map out the local Krylov sectors associated with each active bubble, where a local Krylov sector consists of all particle configurations available to an active bubble under dynamical evolution. A simple example in a $d = 2$, $k = 5$ system is an active bubble consisting of $x = 2$ particles spread out over $\ell = 4$ sites, which would have two states in its local Krylov sector:

$$\{ \text{---} \bullet \bullet \text{---} , \text{---} \bullet \text{---} \bullet \text{---} \}, \quad (48)$$

and an active bubble with $x = 2$, $\ell = 5$ would have

$$\{ \text{---} \bullet \bullet \text{---} , \text{---} \bullet \text{---} \text{---} \bullet \text{---} \}. \quad (49)$$

We shall refer to the different particle configurations within local Krylov sectors as “active bubble configurations”.

We shall now make use of the results of the previous sections to analytically study the average densities of different types of active bubbles. Similarly to the mean

density of type-1 blockages, we take the average over an entire N sector, and we expect thermodynamically-large states to reflect the average densities of various active bubbles by self-averaging as well. We begin by considering the case of $d = 2$. We define the active bubble density function, $A_2(x, k, N, L)$, to give the average density of occurrences of active bubbles that contain x particles. We may expand $A_2(x, k, N, L)$ as a sum over ℓ , where ℓ is the total number of sites a given active bubble occupies:

$$A_2(x, k, N, L) = \sum_{\ell=\ell_{2,\min}(x,k)}^{\ell_{2,\max}(x,k)} m_2(x, \ell, k) a_2(x, \ell, k, N, L). \quad (50)$$

In the above expression, the multiplicity function $m_2(x, \ell, k)$ gives the total number of active bubble configurations compatible with a particular x , ℓ , and k ; the function $a_2(x, \ell, k, N, L)$ gives the average density of occurrences of any particular active bubble configuration compatible with x , ℓ , and k (we note that this density is independent of how the particles are actually arranged); and $\ell_{2,\min}(x, k)$ and $\ell_{2,\max}(x, k)$ are respectively the smallest and largest number of sites compatible with an active bubble with x particles at locality k . The value of the function $\ell_{2,\min}(x, k)$ has to be determined on a case by case basis; $\ell_{2,\max}(x, k)$, on the other hand, has an exact expression. Since an active bubble cannot have any sequences of $k - 1$ frozen sites, its corresponding local FES in the FES picture will have particles that are all at most separated by $k - 2$ holes. Hence, we have that

$$\ell_{2,\max}(x, k) = 1 + (k - 1)(x - 1). \quad (51)$$

As a simple example, returning to the case of $k = 5$ and $x = 2$ mentioned above, we see that

$$\begin{aligned} \ell_{2,\min}(2, 5) &= 4, \\ \ell_{2,\max}(2, 5) &= 5, \\ m_2(2, 4, 5) &= m_2(2, 5, 5) = 2. \end{aligned} \quad (52)$$

To lower bound the function $a_2(x, \ell, k, N, L)$, we restrict our attention to active bubbles for which the $k - 1$ frozen sites to the right and left of the active bubble are holes, and for which the remaining particles in the system obey the no-propagation condition in Eq. [\(31\)](#) (we note that although the $k - 1$ frozen holes will constitute a blockage, they will not necessarily constitute a type-1 blockage, as it may be than in the FES picture, the active bubble in question would expand further than in the finite d case). This allows us to lower-bound $a_2(x, \ell, k, N, L)$ using an identical approach to the one used for the average density of type-1 blockages. We perform the calculation explicitly in Appendix [F](#), and find that in the thermodynamic limit

$$\lim_{L \rightarrow \infty} a_2(x, \ell, k, \nu L, L) \geq \nu^x (1 - \nu)^{\ell - x + 2} (1 - \nu / \nu_c)^2. \quad (53)$$

Applying this to the $x = 2$, $k = 5$ example, we find that

in the thermodynamic limit

$$\begin{aligned} \lim_{L \rightarrow \infty} A_2(x=2, k=5, \nu L, L) \\ \geq 2\nu((1-\nu)^4 + (1-\nu)^5)(1-3\nu)^2. \end{aligned} \quad (54)$$

In Appendix G, we also work out $\lim_{L \rightarrow \infty} A_2(x, k=5, \nu L, L)$ for $x=3$ to $x=5$. We plot the derived lower bounds explicitly in Fig. 6, where we compare them to the results of numerical simulations.

The active bubble density function $A_\infty(x, k, N, L)$ for $d = \infty$ can be lower-bounded following almost identical steps. We again decompose in terms of the different active bubble configuration densities:

$$A_\infty(x, k, N, L) = \sum_{\ell=\ell_{\infty, \min}(x, k)}^{\ell_{\infty, \max}(x, k)} m_\infty(x, \ell, k) a_\infty(x, \ell, k, N, L). \quad (55)$$

The above functions have the same definitions as their $d=2$ counterparts, with the only difference being they take into account $d = \infty$ dynamics. It's apparent that $\ell_{\infty, \max}(x, k) = 1 + (x-1)(k-1)$; furthermore, since an active bubble in a $d = \infty$ system can always be expanded out to its local FES, we also have that

$$\ell_{\infty, \min}(x, k) = 1 + (x-1)(k-2), \quad (56)$$

corresponding to an FES where all pairs of particles are separated by $k-3$ holes.

In the thermodynamic limit, we have from the general expression in Appendix F that

$$\begin{aligned} \lim_{L \rightarrow \infty} a_\infty(x, \ell, k, \nu L, L) \\ \geq \nu^x (1+\nu)^{-(x+\ell+2)} (1-\nu/\nu_c)^2 \end{aligned} \quad (57)$$

Returning to our $x=2, k=5$ example, we note that

$$\begin{aligned} \ell_{\infty, \min}(2, 5) &= 4, \\ \ell_{\infty, \max}(2, 5) &= 5, \\ m_\infty(2, 4, 5) &= 2, \\ m_\infty(2, 5, 5) &= 3. \end{aligned} \quad (58)$$

The difference in value between $m_\infty(2, 5, 5)$ and $m_2(2, 5, 5)$ arises due to the possibility for particles to be stacked for $d = \infty$. Hence we find that

$$\begin{aligned} \lim_{L \rightarrow \infty} \mathcal{A}^\infty(x=2, k=5, \nu L, L) \\ \geq \nu^2(2(1+\nu)^{-8} + 3(1+\nu)^{-9})(1-3\nu)^2. \end{aligned} \quad (59)$$

We compute lower bounds for $x=3$ to $x=6$ for this function in Appendix G. We shall make use of these results in the following subsection, where we shall numerically demonstrate that the derived lower bounds are valid at all ν and tight for $\nu \ll \nu_c$. Hence, the constraints in Eq. (31) lead to an accurate analytic understanding of how typical states in the $\nu \ll \nu_c$ regime subdivide into active bubbles of different sizes.

E. Numerical results

We now proceed to numerically confirm the results of the previous subsections, as well as to provide evidence that several of the main conclusions drawn for $d=2$ and ∞ hold for any finite d . These results support the claim that typical states in the strongly fragmented phase feature an extensive number of evenly-distributed type-1 blockages and type-2 edges, confining dynamical evolution to finite-sized active bubbles. We also show that, for any d , type-1 blockages and type-2 edges become vanishingly rare for $\nu > \nu_c$. For $d = \infty$, where no blockages exist other than type-1 and type-2, we show how this represents direct numerical evidence of the strong-to-weak fragmentation transition happening at ν_c . For finite d , blockages beyond type-1 and type-2 can exist, and so the results from this section, despite being consistent with the existence of a universal d independent phase transition at $\nu = \nu_c$, are not sufficient to prove the latter. Numerical evidence for the universal phase transition will be discussed in Section VII, by numerically probing the presence or absence of blockages of any kind.

1. Type-1 blockages and type-2 edges distributions

We can numerically determine the location of type-1 and type-2 blockages associated with a generic state using the FES picture, i.e. mapping the state of the S system with local space dimension d to its associated FES in the auxiliary system \tilde{S} . An efficient algorithm for performing this task, which makes use of the structure of local BESs, is presented in Appendix H. We then count the total number n_1 of type-1 blockages, i.e. sequences of $k-1$ or more holes, and the total number n_2 of type-2 edges, i.e. sequences of exactly $k-2$ holes. We also record the positions of these sequences of holes along the chain.

In Fig. 5(a)-(c), we plot the numerical estimates from random sampling for $\bar{\rho}_t^{(d)}$ introduced in Section VI B, obtained by computing average densities $\langle n_t \rangle / L$, with $t \in \{1, 2\}$, for several different values of k, d , and ν . The averages are taken over several randomly-drawn states, all of which were found to have vanishingly-small intensive centers of mass ν_{x_0} , as expected for typical states. In Fig. 5(a), where the system is in its strongly fragmented phase given that $\nu < \nu_c$, we see that the mean densities tend to a constant with increasing L . The corresponding standard deviations also appear to decrease with L , indicating the onset of self-averaging. In Fig. 5(b) blockages of type-1 and type-2 are, on the other hand, seen to become vanishingly rare with increasing L for $\nu > \nu_c$, which is consistent with the onset of the weakly fragmented phase. More evidence for a transition at ν_c is reported in Fig. 5(c). Here we fix L and study $\bar{\rho}_t^{(d)}$ as a function of ν . Below ν_c we find $\bar{\rho}_t^{(d)}$ to be a smooth positive function that tends to zero linearly as $\nu \rightarrow \nu_c$. Given that above the critical filling the average density $\bar{\rho}_t^{(d)}$ is

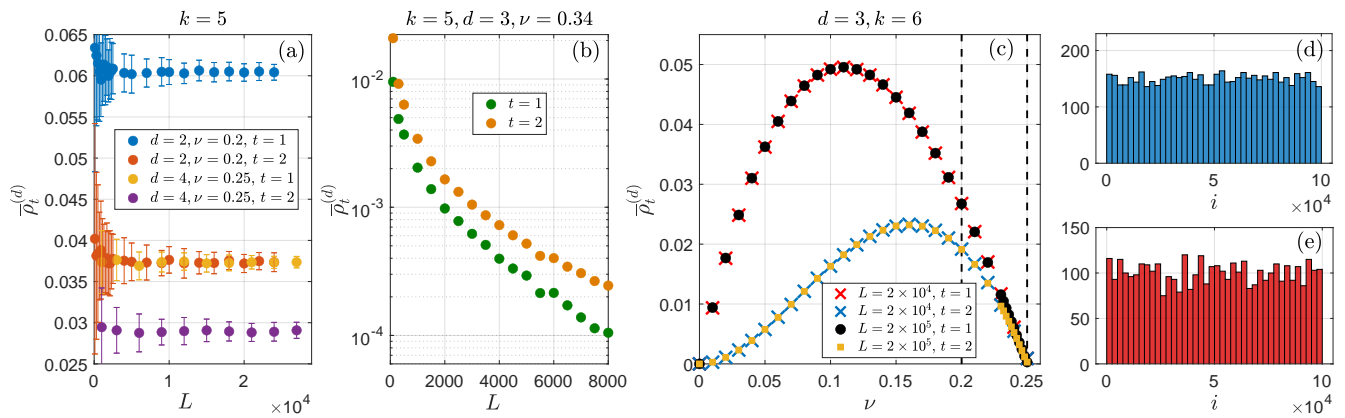


FIG. 5. (a) Numerical estimates for $\bar{\rho}_t^{(d)}$ (from random sampling) as a function of L for 100 randomly generated states at local dimensions $d = 2, 4$, for $k = 5$ and fillings $\nu < \nu_c = 1/3$. The error bars show the standard deviation associated with the set of 100 random states at each L value. (b) $\bar{\rho}_t^{(d)}$ as a function of L for 1000 randomly generated states at $\nu = 0.34 > 1/3 = \nu_c$, $k = 5$ and $d = 3$. (c) $\bar{\rho}_t^{(d)}$ for $d = 3, k = 6$ as a function of $\nu < \nu_c = 0.25$ for $L = 2 \times 10^4$ (1000 randomly generated states) and $L = 2 \times 10^5$ (100 randomly generated states). The leftmost vertical line coincides with $(k - 1)^{-1}$ and the rightmost with $\nu_c = (k - 2)^{-1}$. (d) Spatial distribution for $k = 5$ of type-1 blockages in a single randomly drawn state with $L = 10^5$, $d = 2$, $\nu = 0.2 < \nu_c$. Here, $i = 1, \dots, L$ labels the sites of the chain. The histogram shows the number of type-1 blockages that occurred in each bin. (e) Analogous histogram for $k = 5$, $L = 10^5$, $d = 4$, $\nu = 0.25 < \nu_c$.

zero in the thermodynamic limit, the latter is seen to have a discontinuous first derivative with respect to ν at ν_c , signalling a phase transition. We also note that there is no evidence of a phase transition at $\nu = (k - 1)^{-1}$. Thus, even if the latter value marks the filling after which it becomes possible to generate states that have no type-1 blockages, *cf.* Section VB, our numerical analysis suggests that these type of configurations are extremely rare and do not lead to additional transitions as long as typical states at a given ν are considered. Note also that $\bar{\rho}_t^{(d)}$ has a peak at some finite value of ν , and decreases both for fillings above and below it, as expected. Indeed, even if more sites are involved in type-1 blockages at a given filling ν_1 compared to any other filling $\nu_2 > \nu_1$, the number of distinct type-1 blockages n_1 is strongly suppressed at small ν values given that many different type-1 blockages merge, thus forming longer and longer type-1 blockages. On the other hand, type-2 edges have a fixed length, and it is clear that at very low fillings $\nu \rightarrow 0$ their number must tend to zero, given that sequences of holes involving many more than $k - 2$ sites become more likely than type-2 edges.

In Figs. 5(d)-(e) we report the spatial distribution of type-1 blockages along the chain for two randomly generated states at large L , for the values of $\nu < \nu_c$ and d from Fig. 5(a). The distribution of positions is seen to be quite homogeneous along the entire chain. This was also found to be the case for all other randomly generated states tested, for which the spatial distribution of type-2 edges was also found to be generally uniform. Finally, from the numerical results described in Fig. 5(b) and other tests for $d = \infty$ that we report in Fig. 7(d) of Section VIIC, we notice that for $\nu > \nu_c$ typical ran-

domly drawn states for any d are mapped by the FES picture to an FES with $n_1 = 0$ and $n_2 \leq 1$, i.e to the unique blockage-free FES compatible with the given values of L, N and X . Exceptions to this become rarer and rarer as we increase L at fixed $\nu > \nu_c$, or if at fixed L we increase ν . For example, in the case of $d = 3, k = 5$ from Fig. 5(b), if we set the value of ν slightly higher, say $\nu = 0.38$, already for $L = 500$ all the 100 randomly generated states have $n_1 = 0$ and $n_2 \leq 1$.

Note that we *cannot* directly infer the presence of a weak-to-strong fragmentation transition at ν_c for finite d values just from the numerical evidence of a phase transition for $\bar{\rho}_t^{(d)}$ at the critical filling. Indeed, in finite- d systems blockages and frozen sites invisible to the FES picture might exist, and states that end up in the same FES of the auxiliary system \tilde{S} via the FES picture are not guaranteed to be in the same Krylov in the finite- d system S . These issues are addressed in Section VII, where we characterise the weakly fragmented phase of finite- d systems by showing that blockages of any kind disappear for $\nu > \nu_c$ and that typical states belong to the same Krylov sector, confirming the universality in d of the strong-to-weak transition at $\nu = \nu_c$. However, it is worth noticing that the equivalence of the critical filling for the weak-to-strong transition and the $\bar{\rho}_t^{(d)}$ transition leaves space for conjecturing that type-1 and type-2 blockages might represent the main cause of dynamical disconnections also in finite d systems for $\nu < \nu_c$, with other types of blockages playing a less central role.

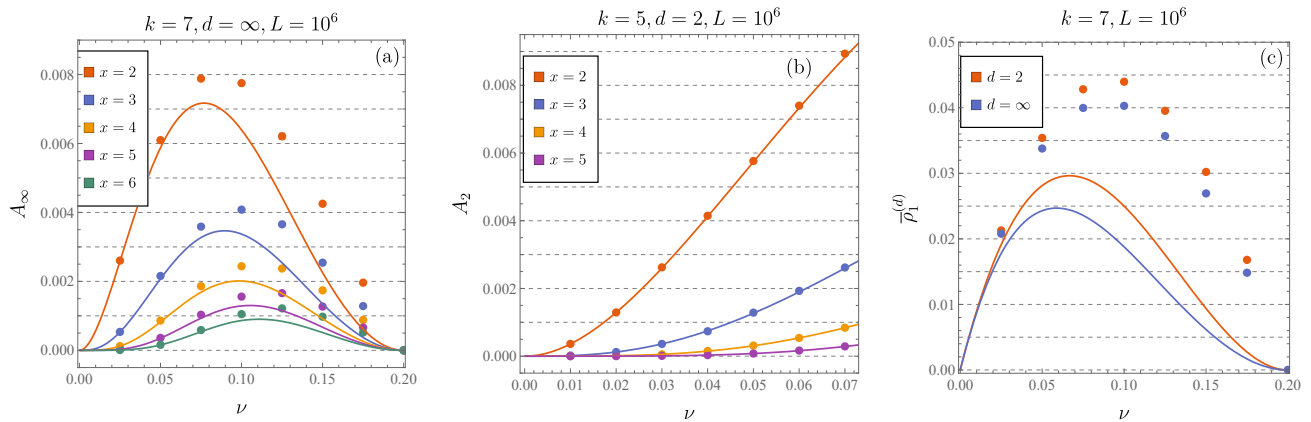


FIG. 6. Comparisons between numerical densities and analytic lower bounds for systems of size $L = 10^6$. The functions used for the lower bounds are derived in Sections VI B, VI D, and Appendix G. In (a), the active bubble densities of 100 random states were averaged over per value of ν at $k = 7$ and $d = \infty$. In (b) 10 random states were sampled per value of ν at $k = 5$. We note the tightness of the bound for $\nu \ll \nu_c$ in both cases. In (c), the type-1 blockage densities of 100 random initial states were averaged over per data point for $d = 2$ and $d = \infty$. Error bars in all plots are given by the standard deviation divided by square root of sample size, and are generally too small to see.

2. Comparison with analytic bounds

We may also use our numerical results to assess how tight the analytic lower bounds computed in the previous subsections are. This allows us to determine to what extent the simplifying assumptions used to compute those bounds are representative of the structure of a typical state. We present three comparative graphs in Fig. 6. The analytic lower bounds for the average density of active bubbles are computed in Appendix G. In Fig. 6(a), we compare analytic and numerical results for the mean active bubble densities of a $d = \infty$ system. For $d = \infty$, the active bubble densities of a given state can be exactly obtained by mapping the state to its FES and then subdividing the FES into active bubbles separated by type-1 blockages. For the numerical results, the active bubble densities of 100 randomly drawn states were averaged over for each value of ν , with $L = 10^6$. We note that for small fillings ν , the analytic lower bounds are very close to the numerical densities, whereas the two start to diverge for intermediate values of ν . The close match for small ν indicates that for most active bubbles in the system at these densities, the no-propagation conditions in Eq. (31) are satisfied by the particles outside the active bubble. This is to be expected: for the condition to be violated, there would have to be a group of particles close to the active bubble with a local density greater than ν_c , which is highly unlikely for $\nu \ll \nu_c$ even for small groups of particles.

We further confirm the tightness of the lower bounds on the active bubble densities for small ν in $d = 2$ systems in Fig. 6(b). In this case, the FES picture cannot be used as it can overlook the contributions of finite- d blockages. Instead, the numerical active bubble densities were determined by dividing randomly drawn states with

filling ν into “initial” active bubbles, mapping out the local Krylov sectors of these active bubbles, merging active bubbles, which then overlapped, and then continuing to map out local Krylov sectors of the new merged active bubbles and merging the results until no further merging occurred. As this was a numerically intensive procedure, only small values of ν could be studied, with 10 samples per data point. The small standard deviation in the resulting data, however, indicates that self-averaging was ensuring the accuracy of the data collected.

The analytic lower-bound for the density of type-1 blockages is compared to its numerical counterpart in Fig. 6(c). The numerical values were determined via the FES picture in the same fashion as those of Fig. 5(c). We remark that here, the analytic lower bound is less tight than in the case of the active bubble densities. This is to be expected, since only the type-1 blockages of the form presented in Eq. (35) were considered for the analytic bound. Also of note is the lower density of type-1 blockages for $d = \infty$ compared to $d = 2$. We intuit this to be related to the particle stacking that becomes possible for $d = \infty$, as this stacking means that on average there will be fewer sites occupied by particles in a $d = \infty$ state than in a $d = 2$ state at the same filling. Since type-1 blockages are distinguished from each other by sites containing particles, this implies a smaller number of distinct type-1 blockages for $d = \infty$, though the number of sites in each type-1 blockage may also consequently increase.

VII. NUMERICAL RESULTS FOR THE WEAKLY FRAGMENTED PHASE

Next, we provide numerical evidence that, for $\nu > \nu_c$ and generic d , the model is in its weakly fragmented

phase. This implies that typical symmetry sectors at these fillings will have a dominant Krylov sector, to which almost all states belong in the thermodynamic limit. Indeed, we will show numerically that states with $\nu > \nu_c$ are almost always in the same Krylov sector as the “blockage-free extended state” (BES) associated with their (N, X) sector. These BESs, which we will define shortly, constitute a generalisation to finite d of the structure of blockage-free FESs defined in Section III C. Our numerical results indicate that the Krylov sectors which contain BESs are dominant within their quantum number sectors and hence that typical symmetry sectors are weakly fragmented.

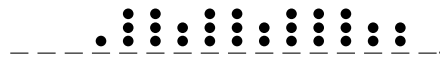
A. Blockage-free extended states and contracted states

Blockage-free extended states (BES) are a finite- d generalisation of the blockage-free FESs defined in Section III C. For the case of BESs with no particles on the leftmost and rightmost boundary sites, we define them to be identical in structure to blockage-free FESs: they consist of a series of particles separated by holes, with at most one pair of particles being separated by $k-2$ holes and all other pairs being separated by $k-3$ holes. The particular value of d comes into play when the particles in the BES overlap with the boundaries, leading to a “pile-up”. In a $d = \infty$ blockage-free FES, this pile-up is entirely confined to the boundary sites; the maximal on-site occupancy of finite- d systems, however, implies that the pile-up must be spread out over several sites. The general form of this pile-up is as follows. Say there is a pile-up of m particles on the left boundary of the system: we then have that in a BES, the particles in the pile-up will occupy the $\lceil m/(d-1) \rceil$ leftmost sites of the system, with the first $\lfloor m/(d-1) \rfloor$ of these sites having the maximal number $d-1$ of particles, and the last site of the pileup containing the remaining particles (if there is a remainder). The next occupied site to the right of the pile-up can be separated by $k-2$ holes or fewer from the rightmost occupied site in the pile-up; though we note that if the separation is of $k-2$ holes, then no other separations of $k-2$ holes can be present in the BES. An identical structure characterizes the right-boundary pile-up, if there is one. We note that setting $d = \infty$ in the above description, we recover the structure of a blockage-free FES from Section III C. An example of a BES with $d = 3$, $k = 5$, $L = 16$, $N = 15$, $X = 67$ would be:



The proof that there is a unique BES corresponding to each (N, X) sector for finite d follows identical logic to the proof for $d = \infty$ presented in Appendix C, in which it is shown that a unique blockage-free FES corresponds to each (N, X) sector in a $d = \infty$ system.

We define a contracted state (CS), on the other hand, to be the particle-hole conjugate of a BES. It consists of sites with $d-2$ particles separated from each other by sequences of $k-3$ sites with $d-1$ particles, up to one possible pair of sites with $d-2$ particles separated by $k-2$ sites with $d-1$ particles, as well as the possibility of “tails” on either side. A tail will first consist of a sequence of sites with occupancy $d-1$, possibly followed by a site with occupancy $d-2$ and a further site with occupancy less than or equal to $d-2$, or otherwise just followed by a single site with occupancy lesser or equal to $d-2$. The sequence in the tail of sites with occupancy $d-1$ will consist of at most $k-2$ sites with $d-1$ particles if no other sequence of $k-2$ maximally occupied sites is present in the CS; otherwise, it will consist of at most $k-3$ sites. An example of a CS with $d = 3$, $k = 5$, $L = 16$, $N = 29$, $X = 258$ is given by



We note the tails on either side.

B. Mapping a CS to a BES

Next, we present an algorithm for mapping from a CS to a BES for general finite d . The corresponding derivation is presented in Appendix I. This algorithm will be central to our main algorithm for demonstrating weak fragmentation.

In what follows, we denote an outward hop gate, sending a single particle on site $i+1$ and a particle on site $j-1$ to sites i and j respectively, by $U_{i,j}^+$, and an inward hop gate sending them from sites i and j to sites $i+1$ and $j-1$ by $U_{i,j}^-$. A gate is only applied in the following algorithm if it is compatible with the constraints of on-site dimension d and system length L . The algorithm is given by:

- For site $i \in \{0, \dots, L-1\}$ in increasing order, if the sites i and $i+k-1$ are within the system (i.e. are within $\{0, \dots, L-1\}$) and have occupancy at most $d-2$, and all sites in-between them have occupancy $d-1$, then apply the gate $U_{i,i+k-1}^+$. Repeat the loop over sites until it is no longer possible to apply this gate.
- For $\ell = k-4$ to $\ell = 0$ in decreasing order, for site $i \in \{0, \dots, L-1\}$ in increasing order, if the sites i and $i+\ell+2$ are within the system and have occupancy at most $d-2$, and all sites in-between have occupancy $d-1$, apply the gate $U_{i,i+\ell+2}^+$ (where $U_{i,i+2}^+$ for $\ell = 0$ is an outward hop of two particles on a same site); if the gate cannot be applied, then if the sites i and $i+\ell+3$ are within the system and have occupancy at most $d-2$, and all sites in-between have occupancy $d-1$, apply $U_{i,i+\ell+3}^+$ instead.

- For $\ell = 0$ to $\ell = k - 4$ in increasing order, for site $i \in \{0, \dots, L - 1\}$ in increasing order, apply the gate $U_{i, i+\ell+2}^+$ if possible, and if not, apply the gate $U_{i, i+\ell+3}^+$ if possible.

For the case of $d = 2$, since no stacking can occur, ℓ ranges from $k - 4$ to 1 in the second step and from 1 to $k - 4$ in the third.

Starting from a CS, the algorithm operates as follows. If the CS contains a sequence of $k - 2$ sites with occupancy $d - 1$, the first step of the algorithm shifts the position of that sequence toward the boundaries until either the sequence is no longer present, or otherwise a boundary pile-up is obtained. Likewise, the second step of the algorithm also “unstacks” particles by shifting them toward the boundaries, until no sites apart from the boundary pile-ups have occupancy greater than 1. The third step then expands the spacings between particles until a BES is obtained.

An algorithm for mapping from the BES to the CS is obtained by replacing outward hops $U_{i,j}^+$ in the above algorithm with inward hops $U_{i,j}^-$.

The existence of the CS-to-BES and BES-to-CS algorithms is proof that if the BES corresponding to a particular Krylov sector extends to the boundaries of the system and the corresponding CS does not, then there are no blockages in that Krylov sector. Indeed, it is immediately apparent that there are no frozen sites and that there can be no type-2 blockages, since if type-2 blockages were present, then it would be impossible to map from the BES to the CS using the two-colour property of Section III A. It is furthermore apparent that, since exchange of particle number and dipole moment between subregions can occur throughout a system in a BES, there must be no finite- d blockages as well. This strongly suggests that, for typical (N, X) sectors with $\nu > \nu_c$, the Krylov sector containing the BES will be ergodic, and hence the system will be in its weakly fragmented phase.

We note that the BES-to-CS algorithm also works when acting on a local BES, i.e. a group of particles that has the same structure as a BES but which does not span the entirety of the system. The resulting configuration after the application of the algorithm will then also follow the same general structure as a CS; and likewise, if the CS-to-BES algorithm is subsequently applied, the original local BES is obtained again.

C. Numerical evidence of weak fragmentation

In searching to numerically demonstrate weak fragmentation, we cannot make use of the FES picture to establish the absence of blockages, as blockages that prevent ergodicity could exist at finite d and yet not be captured by the FES picture. For example, dense groups of particles, such as a sequence of $k - 1$ or more sites all containing $d - 1$ particles, can potentially constitute a blockage for finite- d systems, but not for a $d = \infty$ system.

To overcome these limitations, we develop an algorithm that, using only hopping moves compatible with finite values of d , tests for the presence of weak Hilbert space fragmentation in typical symmetry sectors for $\nu > \nu_c$.

In particular, the algorithm attempts to map from a random initial state at a given ν and L to either the corresponding BES or CS (both of which share a same Krylov sector by the algorithms of the previous subsection). The success rate of the algorithm hence lower bounds the probability that a typical initial state will be in the same Krylov sectors as the BES and CS. Since there is a unique BES for each (N, X) sector for $\nu > \nu_c$, if this success rate goes to 1 for $\nu > \nu_c$, that indicates that typical symmetry sectors are dominated by the Krylov sectors containing the BES, and therefore the model is in its weakly fragmented phase. For $\nu < \nu_c$ where the BES is not defined (as there will necessarily be a blockage somewhere), the algorithm instead attempts to map all particles in the state into a single local BES (or the corresponding CS), with all sites outside the local BES being empty. This remains well defined, as there is a single local BES for each (N, X) sector at $\nu < \nu_c$ as well. Here, however, we expect the success rate of the algorithm to drop to 0 due to strong fragmentation.

We apply the following algorithm to an arbitrary state at a particular value of ν and L :

- Apply the CS-to-BES expansion algorithm to the state. If a BES is obtained (or all particles are in a same local BES), terminate the algorithm and register a success; if not, proceed to the next step.
- Apply the BES-to-CS contraction algorithm. Again, register a success if a CS (or single local CS) is obtained, and proceed to the next step if not.
- Apply the previous two steps in sequence in total for an arbitrary number Q of times. If the algorithm still hasn't terminated, then register an ambiguous result.

In what follows, we will set $Q = 3$. The rationale behind the above algorithm is as follows. After the first application of the CS-to-BES algorithm, if the state does not reach a BES (or a single local BES), often the resulting state is found to be composed of individual local BESs. These will often be separated from each other by sequences of $k - 1$ or more sites containing $d - 1$ particles or sequences of $k - 1$ or more holes. During the subsequent BES-to-CS contraction, the sequences of $k - 1$ or more sites with $d - 1$ particles are “melted” by the contraction process as their edges are peeled off, but the sequences of $k - 1$ or more holes remain. These hole sequences are then potentially bridged during the following CS-to-BES expansion step, though this may introduce the presence of new dense regions of $k - 1$ or more maximally occupied sites. In this alternating fashion, the aim of the algorithm is to “melt” the dense regions and

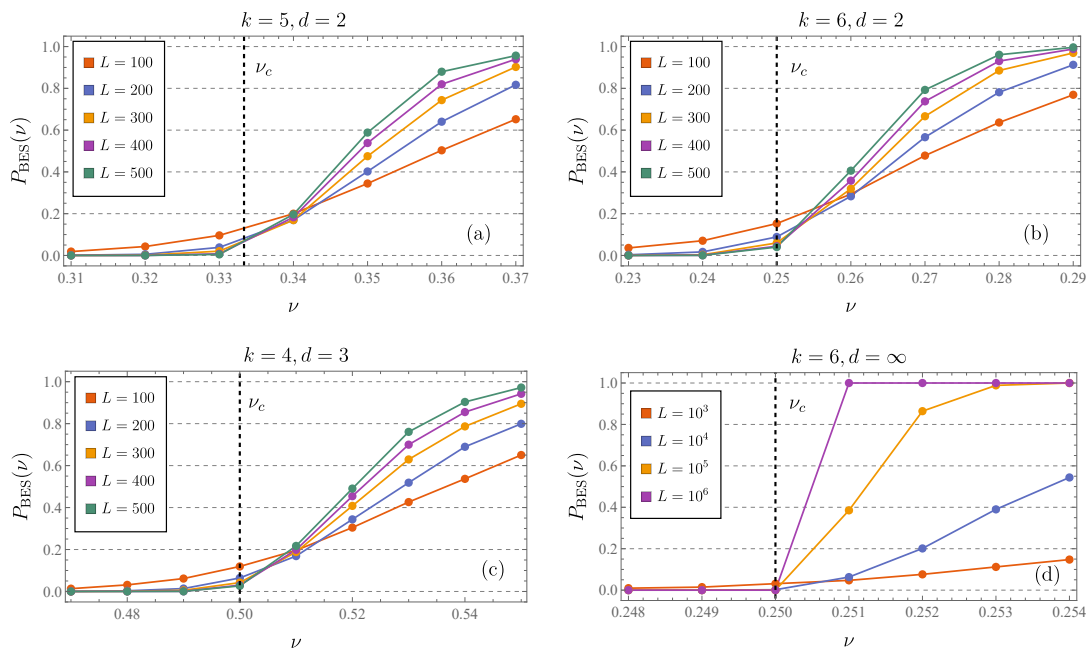


FIG. 7. Success rate $P_{\text{BES}}(\nu)$ of reaching the BES as a function of the filling ν for various choices of d and k . For plots, (a)-(c), the algorithm of Section VIII C was used, and sample sizes were of order $\mathcal{O}(10^5)$ for $L = 100, 200$ and $\mathcal{O}(10^4)$ for $L = 300, 400, 500$. For plot (d), states were mapped to their corresponding FES using the algorithm of Appendix H, from which it was directly determined if the blockage-free FES had been reached. Sample sizes were $\mathcal{O}(10^4)$ for $L = 10^3, 10^4, 10^5$, and $\mathcal{O}(10^3)$ for $L = 10^6$. Error bars for all plots were obtained by dividing the standard deviation associated with each data point by the square root of the sample size, and are mostly too small to see.

“bridge” the holes separating one active region from another.

In Fig. 7(a)-(c), we present the results of applying this algorithm to randomly drawn states with various on-site dimensions d and localities k . We expect these states to be “typical”, and hence to have a vanishingly small intensive center of mass. We note that in each case studied, the success rate of the algorithm tends to 1 with increasing L for $\nu > \nu_c$, indicating the presence of weak fragmentation; whereas it progressively vanishes for $\nu < \nu_c$, which is consistent with the presence of the strongly fragmented phase proved in Section V.

For comparison, we also present numerical results for $d = \infty$ in Fig. 7(d). In this case, we may use the algorithm in Appendix H to map arbitrary initial states to their corresponding FES, as we did in Section VI E; if the FES is blockage-free, then we register a success and if not, then we register a failure. As expected, we see the same overall trend of an increasing success rate for $\nu > \nu_c$ and a decreasing one for $\nu < \nu_c$ as in the finite d case, again highlighting the shared critical density for arbitrary d .

These results suggest that, regardless of the on-site dimension d , the dominant Krylov sectors in the weakly fragmented phase can always be identified as those that contain the BES. This implies that for any d , particles arranged to form a BES can, through k -local dynamics, be mapped to almost all other possible configurations of

particles in a same (N, X) symmetry sector. This explains why the critical density ν_c is independent of d , as for any value of the latter, ν_c is the smallest density at which the BES can span the whole system, and one can hence obtain ergodic behaviour.

VIII. NUMERICAL RESULTS FOR THE RATIO OF DIMENSIONS

In the previous sections we presented strong analytic and numerical evidence of the existence of a universal d -independent transition at the critical filling $\nu_c = (k - 2)^{-1}$. In this section, we numerically determine for $d = 2, 3$ the dimension of the largest Krylov sectors in typical symmetry sectors at different values of the filling ν , so as to characterise the scaling with L of the ratio $r_{d,k}(N, X)$ as a function of ν . In Fig. 8(a)-(b) we report exact numerical results for $r_{2,k}(N, X)$ and $k = 5, 6$ as a function of a few small values of L and a few values of ν . Here (N, X) is always chosen to be the largest symmetry sector for a given N , that is, we always have center of mass located exactly at or just next to the middle of the chain. These values of $r_{2,k}(N, X)$ were obtained by numerically partitioning the chosen (N, X) sector into all its Krylov sectors, identifying the largest one, and dividing the dimension of the latter by the numerically determined $D_{N,X}^{(2)}$. We see how below ν_c the ratio $r_{2,k}(N, X)$

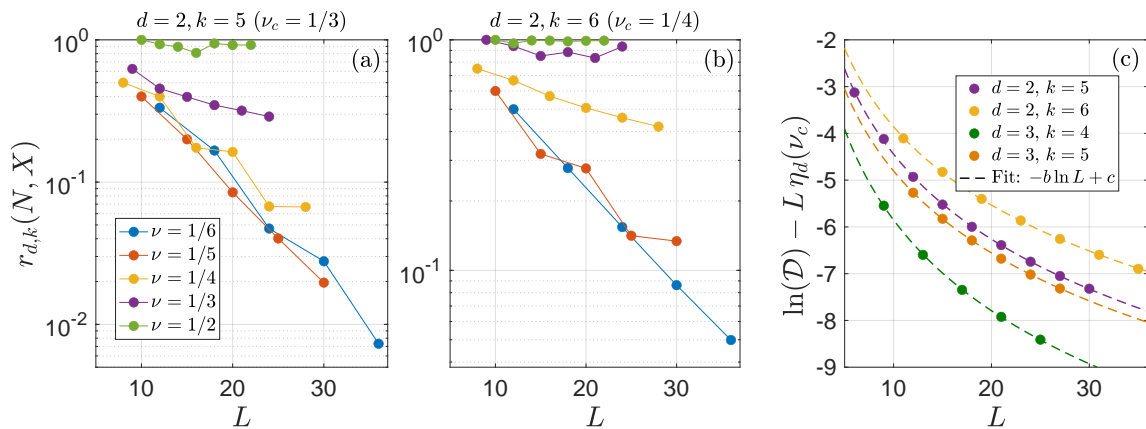


FIG. 8. (a)-(b) Exact values of $r_{2,k}(N, X)$ for the largest symmetry sector (N, X) at each given N and locality $k = 5, 6$. Results are shown for a few sizes L and fillings ν . (c) Values of $\mathcal{D}(L)$ for $d = 2, 3$ and several values of k . The dashed lines are 2-parameter fits to verify that, aside for polynomial corrections in L , $\mathcal{D}(L)$ has dependence on L equal to $\exp(L\eta_d(\nu_c))$.

appears to be decaying exponentially with L , while above ν_c it remains always close to 1, consistently with a phase transition characterised by Eq. (7) happening at ν_c . At the critical filling ν_c we find an intermediate behaviour, with $r_{d,k}(N, X)$ still decaying to zero with L but more slowly than for $\nu < \nu_c$. Following [21] we numerically verify that $r_{d,k}(N, X)$ at $\nu = \nu_c$ decays to zero only polynomially with L , a feature conjectured to hold only at the critical point. Based on the evidence from Section VII we study the dimension of the unique Krylov sector that contains a BES, which is expected to be the largest. In this way we avoid the need to partition the symmetry sector into all of its Krylov subsectors, and thus we manage to reach slightly higher values of L . We always choose $\nu \simeq \nu_c$ and $\nu_x = 1/2$ such that this BES has empty boundary sites and contains no sequence of $k - 2$ holes, as pictured below



We vary L while retaining the general form pictured above, noting that because of the latter one obtains exactly $\nu \rightarrow \nu_c$ for $L \rightarrow \infty$. We call $\mathcal{D}(L)$ the dimension of the Krylov sector that contains such a BES. We numerically compute $\mathcal{D}(L)$ by starting from the BES and applying a very high number of successive random gates to explore the entire Krylov sector. At each discrete time step, a gate is randomly selected from the set of all possible gates compatible with d, k and conservation of N and X . We then count the number of different configurations reached in the stochastic evolution up to a certain time and stop the search when this number remains constant for a long-enough time window. This allows us to reach slightly higher values of L compared to those of Fig. 8(a)-(b) and to study $d = 3$ in addition to $d = 2$. The data in Fig. 8(c) suggest that the ratio of \mathcal{D} over $D_{N,X}^{(d)} = \exp[L\eta_d(\nu) - 2\ln L + \mathcal{O}(L^0)]$ decays to zero

polynomially with L , i.e.

$$\ln \left[\frac{\mathcal{D}(L)}{D_{N,X}^{(d)}(L)} \right] = -\gamma \ln L + \lambda + o(L^0), \quad (60)$$

where γ, λ are L -independent constants and $\gamma > 0$. Indeed, we perform a preliminary 3-parameter fit of the form

$$\ln \mathcal{D}(L) = aL - b \ln L + c. \quad (61)$$

We always find that a coincides with $\eta_d(\nu_c)$ from Section IV up to a 1% error in the worst case. Then we perform the second 2-parameter fit shown in Fig. 8(c)

$$\ln \mathcal{D}(L) - L\eta_d(\nu_c) = -b \ln L + c. \quad (62)$$

We find excellent agreement between the latter and the data, suggesting that the ratio $r_{d,k}$ has critical scaling at ν_c for arbitrary d . This also represents numerical evidence that for $\nu \geq \nu_c$ Krylov sectors that contain BESs have a size whose exponential scaling with L is identical to that of the size of the typical symmetry sector they belong to.

IX. MODELS WITHOUT A PHASE TRANSITION

We now examine special models whose families of typical symmetry sectors are always strongly fragmented, irrespective of the filling ν . This occurs when the lower critical density ν_c and the upper critical density $d - 1 - \nu_c$ coincide, ensuring no phase transition occurs. This overlap implies the relation

$$\nu_c = \frac{1}{k-2} = \frac{d-1}{2} \quad (63)$$

This is satisfied for the values $d = 2, k = 4$ and $d = 3, k = 3$. The models with these parameters are particularly

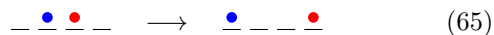
remarkable in that they possess “absolute blockages”, which are particular local configurations of particles or holes that, whenever they occur in a state, necessarily lead to the presence of a sequence of $k - 1$ frozen sites and hence of a blockage. These objects were first studied under the name of “bottlenecks” in Ref. [15], where it was shown that their presence necessarily dynamically disconnects the regions to their right and their left. It is easy to show combinatorially that local configurations of particles that represent absolute blockages appear, for any filling ν , an extensive number of times in each typical state and are evenly-distributed along the chain, and we use this property explicitly for the case of $d = 2, k = 4$ to compute the exact active bubble density function.

A. Absolute blockages

We begin by demonstrating using arguments similar to those in Ref. [15] that for $d = 2, k = 4$, any sequence of 5 holes (or 5 particles by particle-hole symmetry) will necessarily contain at least $k - 1 = 3$ frozen sites, making this an absolute blockage. In this model, only one hopping move is consistent with particle number and dipole moment conservation:



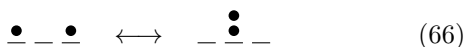
This restricted moveset has important implications for the mobility of particles. Indeed, say we had a particle we wished to move two sites to the right via outward hops. For it to perform its first hop, it would need a particle to its left as in the LHS of Eq. (64). Colouring the right particle in red and the left one in blue, the first hop would look like



Hence, for the red particle to perform a second hop right, the blue particle to its left would have to travel two sites right via outward hops first. However, this requires the presence of a particle to the left of the blue particle, which must also move two sites to the right through outward hops, which in turn necessitates another particle to its left that can perform two outward hops to the right, and so on.

Since this sequence never terminates, no particle can travel two sites in a given direction via outward hops alone. Hence, for any sequence of 5 holes, the middle 3 holes can never be occupied and are thus frozen irrespective of what surrounds them.

For the case of $d = 3, k = 3$, there is again only one hopping move available, this time given by



In this case, any sequence of 4 holes (or 4 sites with 2 particles each) will constitute an absolute blockage, with $k - 1 = 2$ frozen sites in the middle. The derivation can be found in Ref. [15], and follows the logic identical to that of the $d = 2, k = 4$ model.

B. Exact active bubble density for $d = 2, k = 4$

For the special case of $d = 2$ and $k = 4$, the restricted particle mobility discussed in the previous subsection makes it possible to exactly compute $\lim_{L \rightarrow \infty} a_2(x, \ell, k = 4, \nu L, L)$, which is the $k = 4$ density function for individual active bubble configurations as defined in Section VID. We begin by noting a few simple combinatorial results, which are rigorously derived in the Appendix J.

Given m neighbouring sites in an arbitrary state of a $d = 2$ system with size L and N particles, the probability that those sites will contain any particular configuration of x particles is given by

$$\binom{L - m}{N - x} / \binom{L}{N}, \quad (67)$$

where the numerator gives the number of ways to arrange the remaining $N - x$ particles in the system amongst the remaining $L - m$ sites, and the denominator gives the total number of possible states. We note this result is independent of the exact arrangement of the x particles in the configuration. Thus, for example, both particle configurations presented in Eq. (64) could occur on a given sequence of 4 sites with equal probability.

Setting $N = \nu L$ and taking the thermodynamic limit, Eq. (67) simplifies to

$$\nu^x (1 - \nu)^{m-x}, \quad (68)$$

up to $\mathcal{O}(1/L)$ corrections. Hence, a given configuration of x particles over m sites will occur on average $L\nu^x (1 - \nu)^{m-x}$ times in a randomly-chosen state.

In fact, Eq. (68) gives the exact density of occurrences of any given configuration of x particles over m sites in a typical state. This is proven in Appendix J, and has important consequences for the dynamics of the system: in particular, it implies the presence of a finite density of absolute blockages in any typical state, guaranteeing the presence of a finite density of frozen sites, and hence of strong fragmentation at any filling ν by the derivation in Section V.

We shall now use the result in Eq. (68) to compute the active bubble configuration density function $a_2(x, \ell, k = 4, \nu L, L)$ in the thermodynamic limit. It is clear from the above discussion that this function must be of the general form

$$\lim_{L \rightarrow \infty} a_2(x, \ell, k = 4, \nu L, L) = \nu^x (1 - \nu)^{\ell-x} (P_b(\nu))^2,$$

where the function $P_b(\nu)$ is the probability that the particles next to the active bubble configuration, either to the right or the left, will be arranged so as to form a blockage consisting of at least 3 frozen sites. By the restricted mobility derived in Section IX A, the simplest way for this to happen would be if there was a sequence of 4 holes or 4 particles next to the active bubble, resulting in the lower bound

$$P_b(\nu) > \nu^4 + (1 - \nu)^4.$$

In Appendix K, we make use of the restricted mobility to exactly enumerate all possible patterns which result in a blockage of 3 frozen sites, giving the final result

$$P_b(\nu) = (1-\nu)^3 \frac{1-2\nu+2\nu^2-\nu^3+\nu^4}{1-2\nu+3\nu^2-3\nu^3+4\nu^4-3\nu^5+\nu^6} + (\nu \leftrightarrow 1-\nu) \quad (69)$$

Using this result, we may also exactly calculate the bubble density function $\lim_{L \rightarrow \infty} A_2(x, k=4, \nu L, L)$, which gives the exact total density of active bubbles that contain x particles in a thermodynamically-large typical state. For example, for $x=2$, only two active bubble configurations are possible in $k=4$, both of which occupy 4 sites by Eq. (64). Referring to Eq. (50), this immediately gives

$$\lim_{L \rightarrow \infty} A_2(x=2, k=4, \nu L, L) = 2\nu^2(1-\nu)^2(P_b(\nu))^2. \quad (70)$$

The exact active bubble density of bubbles with higher values of x can be computed similarly.

X. ENTANGLEMENT ENTROPY IN THE STRONGLY FRAGMENTED PHASE

A. Type-1 blockages

In generic quantum chaotic systems, eigenstates at finite energy density above the ground state possess volume-law entanglement entropy (EE), with their entropy density for $L \rightarrow \infty$ expected to coincide with the thermodynamic entropy density at the corresponding energy, as computed from e.g. the microcanonical or Gibbs ensembles [2, 31]. In particular, for a Hamiltonian without symmetries defined on the tensor product of local on-site Hilbert spaces, typical eigenstates in the spectrum possess an EE density that coincides with the average EE density of random quantum states, easily computed by the Page formula [32, 33]. Page formula can also be generalised to systems with global symmetries that don't lead to simple tensor product structures [34].

Furthermore, volume law entanglement is also a characteristic feature of typical eigenstates at finite energy densities in integrable models [35]. In this section we argue that in the class of models discussed in this work, the EE of typical eigenstates in N -sectors characterized by $\nu < \nu_c$ follows an *area-law*.

The bipartite EE of each eigenstate within the i -th Krylov sector of an (N, X) sector can be upper bounded by $\ln \mathcal{D}_i^{(d)}(A)$, where $\mathcal{D}_i^{(d)}(A)$ is the dimension of the Krylov sector restricted to the subsystem A of the bipartition [15, 36, 37], where we are assuming $\mathcal{D}_i^{(d)}(A) \leq \mathcal{D}_i^{(d)}(B)$. In particular, this ensures that *all* eigenstates

of strongly fragmented (N, X) families have EE density s upper bounded in the thermodynamic limit by

$$s \leq \lim_{L \rightarrow \infty} \frac{1}{L} \ln \mathcal{D}_{\max}^{(d)} < \lim_{L \rightarrow \infty} \frac{1}{L} \ln D_{N,X}^{(d)}. \quad (71)$$

In quantum chaotic models, the last term in the previous expression would be expected to coincide with the EE density of typical eigenstates in the chosen family of (N, X) sectors, as obtained by generalizations of Page's approach to subsectors of the total Hilbert space [34]. Thus, the inequality in Eq. (71) proves ergodicity breaking at the level of entanglement on the basis of the exponential suppression of the dimension of Krylov sectors compared to the dimension of symmetry sectors. However, given that usually $\mathcal{D}_{\max}^{(d)}$ scales exponentially with L , the inequality in Eq. (71) doesn't prevent eigenstates of strongly fragmented models from possessing volume-law entanglement. It has been first remarked in Ref. [15] that further restrictions on the generation of entanglement can arise from local configurations that completely disconnect the regions of the chain to their left and right. In [15] these disconnections coincided with the "absolute blockages" discussed in Section IX, which exist only in very specific models with $d=2, k=4$ and $d=3, k=3$, which are strongly fragmented irrespective of the filling ν . Given our definition of type-1 blockages from Section III, we now generalise this idea to models with any d and k .

Consider a Krylov sector \mathcal{K} that contains a type-1 block somewhere in the chain. By the definition of Krylov sectors, the Hamiltonian leaves the vector space \mathcal{K} invariant, i.e. $H\mathcal{K} \subseteq \mathcal{K}$. Call $H_{\mathcal{K}}$ the restriction of H to \mathcal{K} . We can always partition the chain by inserting a cut somewhere in the middle of the type-1 blockage, creating in this way two subregions α and β . Then, by definition of type-1 blockages we obtain

$$H_{\mathcal{K}} = H_{\alpha} \otimes \mathbb{I}_{\beta} + \mathbb{I}_{\alpha} \otimes H_{\beta}, \quad (72)$$

where \mathbb{I} represents the identity operator and H_{α}, H_{β} are Hermitian operators. From Eq. (72) it is obvious that the eigenstates of $H_{\mathcal{K}}$, which form a basis of \mathcal{K} , have the form

$$|n, m\rangle = |n\rangle_{\alpha} \otimes |m\rangle_{\beta}, \quad (73)$$

where $|n\rangle_{\alpha}$ and $|m\rangle_{\beta}$ are eigenstates of respectively H_{α} and H_{β} . More in general, if a Krylov sector contains several type-1 blockages which partition the system into G regions α_i [38], then all its eigenstates can be expressed as product states of active regions enclosed by the type-1 blockages

$$|n_1, \dots, n_G\rangle = |n_1\rangle_{\alpha_1} \otimes \dots \otimes |n_G\rangle_{\alpha_G}. \quad (74)$$

From this it is elementary to verify that for any of these eigenstates:

1. The bipartite EE associated with a single entanglement cut located within a type-1 blockage is exactly zero.

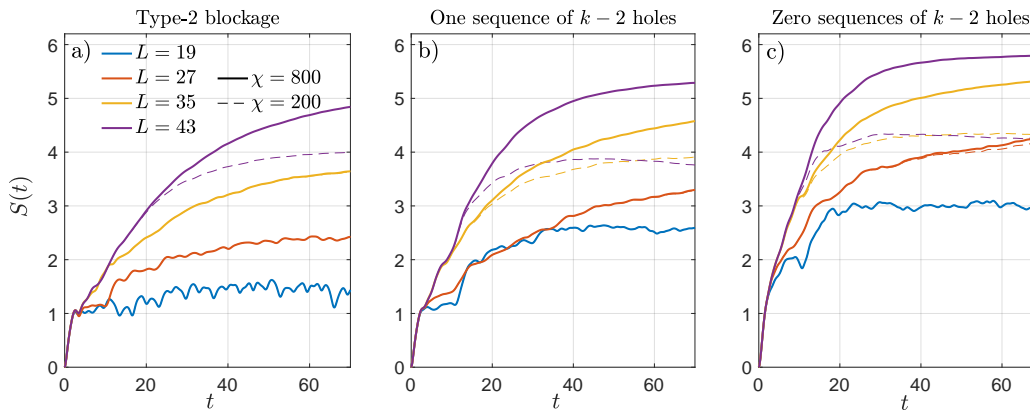


FIG. 9. Time-dependence of the bipartite Von Neumann entropy $S(t)$ under Hamiltonian dynamics computed using tDMRG. The Hamiltonian is characterised by $d = 2$, $k = 6$ and the initial product state is chosen among the set of configurations discussed in Section XB, for various system sizes L . We report tDMRG results for the maximum bond dimension $\chi = 200$ and 800 . (a) Local disturbance coinciding with the simplest kind of type-2 blockage. (b) Local disturbance represented by a single sequence of $k - 2$ holes (no blockage). (c) No disturbance.

2. The bipartite EE associated with a single entanglement cut that has to its left or right a type-1 blockage is upper bounded by $\ln \mathcal{D}^*$, where \mathcal{D}^* is the dimension of the Krylov sector when it is restricted to the “active region” enclosed by the entanglement cut and the type-1 blockage. We notice that for an active region of size ℓ , $\ln \mathcal{D}^* \leq \ell \ln d$.

The previous results trivially generalise to the case in which the entanglement bipartition arises from two entanglement cuts. In Section VI we proved that typical Krylov sectors in any N -family with $\nu < \nu_c$ possess an extensive number of type-1 blockages and that the latter are quite uniformly distributed along the chain. Given the relation between EE and type-1 blockages established above, we conclude that typical eigenstates in these families possess area-law EE, i.e. the bipartite EE (with single entanglement cut) in these eigenstates does not grow with L as the latter is increased to infinity. By similar arguments, the eigenstate expectation values of local observables strongly deviate from the ETH prediction, even beyond what expected on the sole basis of the dimension of Krylov sectors.

The reduction of EE generation due to type-1 blockages also has clear consequences for dynamics. For example, consider the quench dynamics with Hamiltonian H starting from a random product state $|\psi(0)\rangle$ in a fixed N -sector – i.e. a random state belonging to the particle basis – with $\nu < \nu_c$. For large L , this type of state is typically part of a Krylov with an extensive number of type-1 blockages that are uniformly distributed along the chain. Then, as a consequence of Eq. (72), $|\psi(t)\rangle$ at any time t will have the same form of Eq. (74), with typical active regions having L -independent size. This ensures that for typical choices of the entanglement cut(s), its EE saturates to an area-law value at long times. More in general, the decomposition in Eq. (72) proves that the quantum dynamics is decomposed into the independent

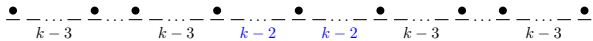
action of extensively many local Hamiltonians on regions of L -independent size, transforming the quantum many-body problem into the sum of extensively many independent few-body problems. This shows that beyond the EE, this strong form of ergodicity breaking also has direct consequences on the quantum dynamics of local operators. We note that these conclusions are not reached if one considers a randomly drawn quantum state in the full Hilbert space. From Eq. (13) we know that typically such quantum states have dominant overlap with (N, X) sectors at half-filling $\nu = (d - 1)/2$ and vanishing intensive center of mass $\nu_{x_0} = 0$, which, aside from the special models discussed in Section IX, are weakly fragmented and thus not dominated by type-1 blockages.

B. Type-2 blockages

We consider the effect of type-2 blockages on the EE, which turns out not to be as drastic as the one of type-1 blockages, leading us to conjecture the presence of an inverse quantum many-body scars phenomenon [24–27] in the family of models discussed in this work.

Given that type-2 blockages prevent transport of particles and dipole moment between the regions to their left and right, their presence along the chain typically reduces the value of $\ln \mathcal{D}_i^{(d)}(A)$ discussed in the previous subsection, thus lowering the maximal eigenstate EE reachable in principle through a bipartition into A and B . This is however only a weak suppression of EE generation, compared to the strong disconnecting effect of type-1 blockages. One might wonder whether a similar kind of strong suppression is produced also by type-2 blockages. However, due to the possibility of the regions to the left and right of a type-2 blockage to interact with the latter, type-2 blockages are not in principle expected to completely block the generation of EE. This is verified

numerically in Fig. 9 using tDMRG [39] for $d = 2$. We consider a chain of length L in a BES which coincides with an FES, in which the boundary sites are occupied and particles are separated by exactly $k - 3$ holes, with the only exception of a local disturbance in the middle of the chain. This is chosen to be a type-2 blockage formed by two sequences of $k - 2$ holes separated by just one particle.



We focus on quantum Hamiltonian dynamics, with H from Eq. (3) characterized by $d = 2$ and $k = 6$, for which we choose the h_j 's to represent a complete set of gates as defined in Section II. We place the entanglement cut somewhere within the type-2 blockage and calculate the Von Neumann entropy $S(t)$ as a function of time. From Fig. 9(a) we see that $S(t)$ is different from zero and becomes larger as L is increased. This must be contrasted with the case in which the local disturbance is a type-1 blockage with entanglement cut within it, for which $S(t) = 0 \forall t, \forall L$. In Fig. 9(b) and 9(c) we produce the same kind of dynamics but replacing the type-2 blockage with, respectively, a single sequence of $k - 2$ holes and no sequence of $k - 2$ holes, as these do not give rise to blockages of any kind. These plots show a very similar evolution for $S(t)$ compared to the type-2 blockage case, confirming that the latter does not lead to any absolute hindrance to the generation of EE. Similar conclusions are reached if one places the entanglement cut just to the left or just to the right of the disturbance. This supports the claim that the bipartite EE with entanglement cut lying in a subregion A that hosts type-2 blockages but not type-1 blockages can have a dependence on the size of A .

To conclude, in the entire region $\nu < \nu_c$ there exist atypical Krylov sectors that contain extensively large “fully-connected” subregions of the chain devoid of type-1 and type-2 blockages. These give rise to eigenstates with volume-law EE, if the entanglement cut lies within one of these fully-connected regions. Even more interesting are the rare Krylov sectors in the interval $(k - 1)^{-1} \leq \nu \leq \nu_c$ which possess an extensive number of type-2 blockages uniformly distributed along the chain, but no type-1 blockages. The numerics above suggests that their eigenstates EE scales beyond any area-law, irrespective of the entanglement cut location. It is an intriguing problem for future work to understand whether the EE of these types of eigenstates follows a volume law or not. Note that this phenomenon of rare eigenstates with volume-law – or beyond area-law – EE, embedded in a sea of area-law eigenstates, could be seen as inverse quantum many-body scars [24–27]. Much remains to be understood about the mechanisms responsible for inverse scars in general, and an analytic understanding of the entanglement structure of states only containing type-2 blockages could reveal a novel scenario in which they can emerge.

XI. CONCLUSION AND OUTLOOK

In this paper, we introduced a number of new approaches for characterising and studying the strongly and weakly fragmented phases of dipole-conserving 1D quantum systems. These allowed us to derive numerous rigorous new results concerning these phases and the transition between them, as well as to develop efficient algorithms for numerically studying these models at large system sizes without relying on approximations. By mapping states in finite d systems to their corresponding fully extended states, we were able to rigorously prove the persistence of blockages for particle filling $\nu < \nu_c = (k - 2)^{-1}$, leading to strong fragmentation in typical symmetry sectors. We were also able to analytically characterise the distribution of blockages and active bubbles in this phase, as well as to prove area-law entanglement scaling in typical states. For the weakly fragmented phase, by developing an efficient algorithm for mapping arbitrary initial states to their corresponding extended blockage-free states at $\nu > \nu_c$ and general d , we provided strong numerical evidence of weak fragmentation in typical symmetry sectors, indicating a universal critical filling of ν_c .

Many of the topics explored in this paper warrant further analysis. It would be useful to better understand the nature and distribution of finite- d blockages in typical states, as well as analytic expressions for the dimensions of the various Krylov sectors at finite d . This could lead to an analytic proof that the critical density equals $\nu_c = (k - 2)^{-1}$ at all d , as well as to exact results concerning the average distribution of blockages and active bubbles. Further analytic understanding of how entanglement entropy scales in the strongly fragmented phase for states with only type-2 blockages would also be valuable, as it may prove the presence of inverse quantum many-body scars in the system.

Several natural generalisations of our work present themselves. It is important to understand whether the methods introduced in this work could be generalised to the case of systems in higher spatial dimensions [15, 40] as well as to systems with more complex symmetries [23, 41, 42] that allow Hilbert space fragmentation. Another interesting direction is to consider the inclusion of ordinary on-site and lattice symmetries, and to study the possible interplay of fragmentation with equilibrium orders mirroring the “localisation protected quantum order” phenomenon of MBL systems [43, 44]. Finally, It would be useful to clarify in what ways our results on the lattice are applicable to ergodicity breaking in continuum dipole-conserving systems [45, 46] where the locality k has a different meaning.

ACKNOWLEDGMENTS

This work was supported by the European Research Council under the Fonds de recherche du Québec via Doctoral Level Grant No. 302311 (J.C.-H.), the Engineer-

ing and Physical Sciences Research Council, Grant No. EP/T517811/1 (R.S.) and the European Union Horizon 2020 Research and Innovation Programme, Grant Agreement No. 804213-TMCS (A.P.).

Appendix A: Uniqueness of fully extended states

In the following appendix, as in most of the paper, we restrict ourselves to systems with open boundary conditions. We define a configuration of N particles in a system of length L with $d = \infty$ to correspond to a “fully extended state” (FES) if no pair of particles within the resulting state can perform an outward hop, that is, there is no point in the state to which an outward hop gate can be applied. It is clear that this implies that in the bulk of the system, all particles must be separated by at least $k - 3$ holes from their neighbours and no particles can be stacked; otherwise, it would still be possible for some particles to perform outward hops. The only exceptions to these rules are at the boundaries: an indefinite number of particles can be stacked on the leftmost and rightmost sites of the system, and there is no lower bound on the number of holes separating each of these stacks from the next closest particle.

An important feature of open boundary systems is that starting from any initial configuration of particles, outward hops cannot be performed indefinitely; a sequence of outward hops must necessarily terminate after a finite number of moves, with the resulting configuration of particles corresponding to an FES. A simple proof of this fact is presented in Ref. [21] and makes use of the quadrupole moment:

$$Q = \sum_{i=0}^{L-1} i^2 n_i, \quad (\text{A1})$$

where as in Eq. (1), n_i counts the number of particles on each site. It is easy to check that any outward hop performed by two particles will necessarily increase the value of Q by 2. However, for finite N and L , there is a clear upper bound on Q , given by the quadrupole moment of the particle configuration in which all particles are stacked on the right boundary site. This proves that, starting from any configuration, an FES must be reached in a finite number of moves.

In this appendix, we prove that in a $d = \infty$ system with open boundary and any locality k , each particle configuration is dynamically connected to *exactly one* FES, i.e. there is one and only one FES to which any given particle configuration can be mapped via a series of k -local hopping moves. This also implies that for $d = \infty$ each Krylov sector contains a single unique FES, by which it can be characterised. This generalises the result of Ref. [21], where uniqueness was proven in the special case of $k = 3$.

We start by proving the following lemma:

Assume that a Krylov sector contains more than one FES. Then it must be possible to map each FES in the sector to at least one other FES in the sector by a sequence of only inward hops followed by a sequence of only outward hops.

In the following, we will generically denote outward hop gates with the letter O and inward hop gates with the letter I , and we will use subscripts to indicate the order in which we apply them. For example, a sequence involving a single inward hop followed by two outward hops and then two further inward hops would be designated by

$$I_5 I_4 O_3 O_2 I_1. \quad (\text{A2})$$

In the reasoning that will follow, the exact nature of each of these hops (i.e. where on the system the hop is performed, and the number of sites separating the hopping particles) will not be important, hence permitting the above simplified notation.

Consider a given initial FES and assume that it is not the unique FES within its Krylov sector. There must therefore exist a sequence of hops that will map it to a different FES. This sequence of moves will necessarily start with some number $n > 0$ of consecutive inward hops I_i , with $i = 1, \dots, n$. Let O_{n+1} denote the first outward hop performed. The sequence of hops up to this point is hence given by

$$\dots O_{n+1} I_n \dots I_1. \quad (\text{A3})$$

Before acting with the next hop in the sequence, we consider “inserting the identity”:

$$(\tilde{I}_m \dots \tilde{I}_1)(\tilde{O}_m \dots \tilde{O}_1) O_{n+1} I_n \dots I_1, \quad (\text{A4})$$

for some set $\{\tilde{O}_i\}_{i=1}^m$ of outward hops with $\tilde{I}_{m-i+1} = \tilde{O}_i^{-1} \forall i$. Given that from any configuration of particles it is always possible to reach an FES by applying a finite number of consecutive outward hops, we may choose the operators $\{\tilde{O}_i\}_{i=1}^m$ such that the state after \tilde{O}_m is applied is an FES. Now, if the FES obtained after the application of \tilde{O}_m is different from the initial one, we have achieved the desired result, since the sequence $(\tilde{O}_m \dots \tilde{O}_1) O_{n+1} I_n \dots I_1$ maps from our initial FES to a different FES. If on the other hand, the resulting FES is identical to the starting one, we have learnt that the subsequence $O_{n+1} I_n \dots I_1$ of inward and outward hops can be replaced by the sequence of only inward hops $\tilde{I}_m \dots \tilde{I}_1$. Iterating this reasoning for every further outward hop O_i appearing in the overall hopping sequence, we see that at some point we will arrive at a sequence of purely inward and purely outward hops connecting our initial FES to a different FES, either by virtue of finding such a sequence of inward and outward hops at some intermediate step, or by virtue of successfully changing the original sequence of mixed inward and outward hops into an equivalent sequence of

purely inward hops followed by purely outward hops.

We now prove the main result of this appendix, i.e. the uniqueness of FESs:

Each Krylov sector of a $d = \infty$ k -local system with open boundaries contains a unique FES.

We proceed inductively. The cases of 1 and 2 particles are easy to verify. Assume that uniqueness holds up to FESs containing $N - 1$ particles and consider an FES composed of N particles. We will prove that there is no sequence of purely inward hops followed by purely outward hops that will map this FES to a different FES. Thus, uniqueness will follow as a direct consequence of our previous lemma. In what follows, we will refer to a sequence of purely inward then purely outward hops as an O/I sequence. We will now explore different structures of FESs on a case-by-case basis.

Case 1. Assume that in the FES there is at least one pair of particles separated by a sequence of $k - 1$ or more empty sites. We apply an O/I sequence with the aim of obtaining a different FES. During the application of the inward hops, the particles to the right and left of the separation of $k - 1$ holes cannot interact with each other by k -locality. Hence, the particles on each side of the $k - 1$ empty sites form in their own right independent FESs, and so by our inductive hypothesis, the sequence of outward hops can only map them back to their initial positions. Hence, the original FES is re-obtained.

Case 2. Assume that in the FES there is no pair of particles separated by $k - 1$ or more holes, but there are two pairs or more separated by $k - 2$ holes. Assume that two of these pairs are next to each other.

$$\cdots \frac{\bullet}{k-2} \cdots \frac{\bullet}{k-2} \cdots \quad (\text{A5})$$

If the particle in the middle doesn't move during the inward dynamics of the O/I sequence, then the particles to its left cannot interact with particles to its right, and by induction the only FES that can be reached is the original one via the same logic as in case 1. If the particle in the middle moves during the inward dynamics, then in performing an inward hop with one of its neighbouring particles, it will necessarily create a spacing of at least $k - 1$ holes between itself and its other neighbouring particle. This will again split the state into disconnected left and right regions during the O/I sequence, and we may again use our inductive hypothesis to see that the same FES will be retrieved at the end of the sequence.

We next assume that there are no two sequences of $k - 2$ holes next to each other in the FES, i.e. there is at least one sequence of $k - 3$ holes separating each pair of sequences of $k - 2$ holes. Consider the two sequences of

$k - 2$ holes that are closest to each other:

$$\cdots \frac{\bullet}{k-2} \cdots \frac{\bullet}{k-3} \cdots \frac{\bullet}{k-3} \cdots \frac{\bullet}{k-2} \cdots \quad (\text{A6})$$

If, during the inward hops of the O/I sequence, any of the particles between the two sets of $k - 2$ holes remains immobile, then we again have by our induction hypothesis that the original FES is retrieved after the outward hops. Assume that this is not the case, i.e. all particles between the two sets of $k - 2$ holes perform an inward hop at some point. Consider the leftmost of these particles, which is on the right side of the left sequence of $k - 2$ holes. If this particle performs an inward hop with the particle to its right, this will necessarily separate it by at least $k - 1$ holes from the particle on its left, and the inductive hypothesis can be applied again. If this particle performs a hop instead with the particle to its left, this will create a spacing of at least $k - 2$ holes between it and the particle to its right. If the resulting spacing is of more than $k - 2$ holes due to other inward hops in the sequence, then the inductive hypothesis can be applied. If it equals $k - 2$ holes, then once more, unless the two particles on either side of these $k - 2$ holes perform an inward hop, the regions on either side of them will be dynamically disconnected and the inductive hypothesis can be applied. A hop between the two particles, however, will again necessarily create a new spacing of at least $k - 2$ holes to its right.

By iterating the above analysis, we see that at each step we reduce the distance between the sequence of $k - 2$ holes on the right of the configuration in Eq. (A6) and the next nearest sequence of $k - 2$ holes on its left. Eventually, we must again arrive at a scenario with two neighbouring sequences of $k - 2$ holes separated by a single particle, and we may use the same reasoning as in the scenario presented in Eq. (A5).

Case 3. Assume that in the FES there is at most one pair of particles separated by $k - 2$ holes, with all the other pairs being separated by $k - 3$ holes (or less if there is overlap with the boundary). We will now prove that two different FESs of this type must have different dipole moments X . Given that the dynamics considered in this work conserve X and that the FESs from cases 1 and 2 have already been shown to be unique, this proves uniqueness of the case 3 FESs as well.

We first consider the case of FESs that don't overlap with the boundary sites. We denote by i_0 the site of the leftmost particle and assume that the m -th particle from the left is separated from the previous one by $k - 2$ holes, with all other pairs of particles being separated by $k - 3$ holes.

$$\cdots \frac{1}{k-3} \cdots \frac{m-1}{k-3} \frac{m}{k-2} \cdots \frac{N}{k-3} \cdots \quad (\text{A7})$$

If there is no pair of particles separated by $k - 2$ holes, we choose by convention to set $m = N + 1$, hence $2 \leq m \leq N + 1$. The dipole moment of the configuration in Eq. (A7) is then

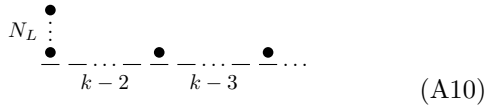
$$X = N i_0 - m + h(k, N), \quad (\text{A8})$$

where $h(k, N) = (k - 2)N(N - 1)/2 + N + 1$ doesn't depend on m or i_0 . We now imagine a different FES of the same type, which must possess different values of i_0 , m or both. Its dipole moment would thus read

$$X' = N i'_0 - m' + h(k, N). \quad (\text{A9})$$

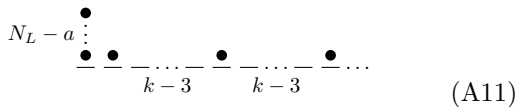
It is elementary to see that the equation $X = X'$ has no solution because $|i_0 - i'_0|$ is an integer and $2 \leq m' \leq N + 1$. Hence when there is no overlap with the boundary, we have shown that FESs of the type of Eq. (A7) are uniquely determined.

We next allow for the possibility of overlap with the boundary. Hence we are considering FESs in which at most one pair of particles is separated by $k - 2$ sites, and all other pairs are separated by $k - 3$ sites, up to the possible exception of particle stacking on the boundary and a separation of fewer than $k - 3$ sites between particles on the boundary and the next nearest particles. We will show that the dipole moment X of such an FES uniquely determines the number of particles stacked on the right and left boundary sites. To begin with, we consider the case of the left boundary site. Say there are $N_L > 0$ particles stacked on top of it. The highest dipole moment X_{\max} achievable in this case is associated with the configuration



$$\begin{array}{c} \bullet \\ \vdots \\ N_L \\ \bullet \\ \dots \\ k-2 \\ \bullet \\ \dots \\ k-3 \\ \bullet \\ \dots \end{array} \quad (\text{A10})$$

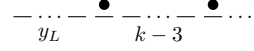
Here, after the sequence of $k - 2$ holes, we repeat only sequences of $k - 3$ holes until either all N particles are positioned or, if the right boundary is reached first, all remaining particles are stacked on the right boundary. Next, consider an integer $a > 0$ and say we construct our FES with $N_L - a > 0$ particles on the left boundary. In this case the lowest dipole moment X_{\min} is achieved with the configuration



$$\begin{array}{c} \bullet \\ \vdots \\ N_L - a \\ \bullet \\ \bullet \\ \dots \\ k-3 \\ \bullet \\ \dots \\ k-3 \\ \bullet \\ \dots \end{array} \quad (\text{A11})$$

Here again, we only repeat sequences of $k - 3$ holes between particles until all N particles are placed or we reach the right boundary and the remaining particles are stacked. By comparing Eq. (A10) and Eq. (A11), it is clear that $X_{\min} > X_{\max}$. Thus an FES of the type considered here with $N_L > 0$ particles on the left boundary cannot be dynamically connected to an FES with $N_L - a > 0$ particles on it and vice versa.

We next consider an FES with $N_L = 0$ and $y_L \geq 0$ empty sites between the left boundary and the first particle. The lowest dipole moment X_{\min}^* compatible with the FES structure we are considering is achieved in the configuration



$$\begin{array}{c} \bullet \\ \dots \\ y_L \\ \bullet \\ \dots \\ k-3 \\ \bullet \\ \dots \end{array}$$

Once again sequences of $k - 3$ holes are repeated until the N particles or positioned or the right boundary is reached. Similarly to before it is elementary to check that $X_{\min}^* > X_{\max}$.

We have thus shown that, for an FES of the type studied in case 3, the dipole moment X uniquely determines the number of particles N_L on the left boundary, including the possibility of $N_L = 0$. Likewise, an identical demonstration shows that X also determines the number N_R of particles on the right boundary site. What remains to be determined are the positions of the particles in the bulk of the system; but with N_L and N_R already known, the positions of the remaining particles are also uniquely determined by the dipole moment using the same logic as for the configuration in Eq. (A7). This completes the proof.

A notable property of the FESs discussed in case 3 is that, unlike the FESs discussed in cases 1 and 2, they do not have any regions that are disconnected under dynamical evolution. For the case of fillings $N/L \geq \nu_c = (k - 2)^{-1}$, we refer to case 3 FESs as “blockage-free FESs”, and we discuss them in more detail in Section III C. Their particular structure will be of import to our discussion of the weakly Hilbert space fragmented phase in Section VII, where we shall identify dominant Krylov sectors in typical symmetry sectors of $d = \infty$ systems as those sectors that contain blockage-free FESs.

Appendix B: Proof of 2-colour connectivity

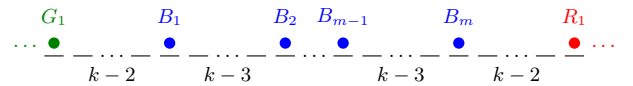


FIG. 10. Configuration of particles in an FES from Fig. 3(b)-(c), which leads to the formation of a type-2 blockage. Regions separated by a type-2 edge (i.e. a sequences of $k - 2$ holes in an FES) host particles of different colour. We name the m particles in the blue region B_1, \dots, B_m , while the right-most green particle and left-most red particle are respectively $G1$ and $R1$.

The proof of the 2-colour connectivity introduced in Section III A is identical in spirit to the proof discussed in case 2 of Appendix A. However, for completeness and in order to make explicit use of the colour scheme used in defining the 2-colour connectivity, we present a separate proof in this appendix.

It is enough to prove the statement for a subregion of the chain containing 3 colours, as the result trivially generalises to the whole system. We can thus refer to the particle configurations, colours, and labels from Fig. 10. We start by noticing that because of uniqueness of the FES, from any configuration in the Krylov, we can reach the FES by performing only outward hops. This automatically implies that any given configuration can be reached starting from the FES and performing only inward hops. Call “central” the region consisting of the two type-2 edges (i.e. sequences of $k - 2$ holes) and all the sites between them. Assume that there is a configuration of particles \mathcal{C} in the Krylov sector that violates the 2-colour connectivity. This means that wherever in the central region we place a cut between two sites, during the series of inward hops from the FES to \mathcal{C} there must be at least one inward hop that involves a particle on the left and one on the right of the cut. This implies that at least one inward hop involving G_1 and B_1 from Fig. 10 must occur before these interact with any other particle, otherwise a sequence of $k - 1$ holes is created between them, preventing any future inward hop between the two. Thus at some point during the series of inward hops B_1 is moved for the first time and goes at least one site to its left. This necessarily creates a separation of $k - 2$ or more holes between B_1 and B_2 . Given the assumption on \mathcal{C} , this separation must necessarily be of $k - 2$ holes, otherwise inward hops between B_1 and B_2 would be prevented and the 2-colour connectivity would be respected. We can now repeat the same reasoning used for G_1 and B_1 , which were separated by $k - 2$ holes, for B_1 and B_2 . In this way we keep propagating to the right a sequence of $k - 2$ holes. Clearly, by analogous reasoning the sequence of $k - 2$ holes that originally separate B_m from R_1 must propagate to the left. Thus, at some point two sequences of $k - 2$ holes must be next to each other, with a single particle in the middle that has not been part of any inward hop yet. By the assumption on \mathcal{C} , the particle in the middle must perform an inward hop, and this necessarily creates a sequence of $k - 1$ holes. By placing a cut anywhere between two sites that are part of this sequence of $k - 1$ holes, we manage to partition the system into two independent subregions that never interact and that contain at most 2 different colours. This contradicts the assumption on \mathcal{C} and proves that any configuration of particles in the Krylov sector respects the 2-colour connectivity.

Appendix C: Existence of blockage-free FESs and BESs for any N and X

We have shown in Appendix A that fixed L and N with $N/L \geq \nu_c$, two different blockage-free FESs necessarily have different dipole moments X . In this appendix, we address the *existence* of a blockage-free FES (or of a FES consisting of a local BES surrounded by empty sites up to the boundaries, if $N/L < \nu_c$) for any value of X com-

patible with a fixed pair of N and L . In this appendix we refer generically both to a blockage-free FES and for $\nu < \nu_c$ to an FES composed of a local BES plus the empty sites as a “BFES”.

The configuration with N particles with minimal dipole moment is the one in which all particles are stacked on the left boundary. We call its dipole moment X_L^* . Similarly, the configuration with maximal dipole moment has all particles stacked on the right boundary, with dipole moment X_R^* . We now present a simple algorithm to construct BFESs that have any dipole moment X between X_L^* and X_R^* . Importantly, every move we perform in the following brings us from a BFES to another BFES, i.e., we never leave this class of BFESs.

We fix N and L and imagine starting from the configuration in which all the particles are stacked on the left boundary. Thus, we have $N_L = N$, where N_L is the number of particles on the left boundary. The first move takes one particle from the left stack and puts it on top of the site next to it, leading to $N_L = N - 1$ and $X = X_L^* + 1$. We can continue increasing the value of X in steps of 1 by moving the same particle to the right until there are $k - 2$ holes between this and the left boundary. The next move is to take another particle from the left stack, that is, $N_L - 1 \rightarrow N_L - 2$, and place it over the site next to it. Then we alternate in moving the rightmost particle and the intermediate particle of one site to the right, so to have at most one sequence of $k - 2$ holes after each of these steps. This lasts until there are $k - 2$ holes between the intermediate particle and the left stack, at which point we again take a particle from the left stack and place it over the site next to it. We then repeat the process of iteratively moving of one site to the right the particles that are not on the left stack, starting from the rightmost one, arriving to the one closest to the left boundary, and then restarting from the rightmost one unless between the left boundary and the first particle to its right there are $k - 2$ holes. In the latter case we remove an additional particle from the left stack. In this way, we can continue to generate BFESs that differ in dipole moment of exactly 1 unit at each step.

At some point, the left boundary will necessarily remain without particles. The algorithm in this case runs identically to before, without the step in which we remove a particle from the left stack. The final scenario to take into consideration is when we reach the right boundary with the rightmost particle, irrespective of whether this happens before or after the left boundary has been emptied. Also in this case the algorithm remains the same, with the only modification that when between the right boundary and the first particle to its left there are no holes, the next right hop of this particle brings it onto the right boundary. This increases over time the number of particles on the right stack, until we place all the N particles on it, reaching X_R^* .

This, together with the results from Appendix A, proves that for any values of N and L , exists *one and*

only one BFES for each value of X compatible with N and L .

It is apparent that a same derivation can be used to show the existence of a blockage-free extended state (BES) (see Section VII) at finite d for any N and X symmetry sector as well. In this case, we begin with the particle configuration for a given N and L in which all particles are involved in a pile-up on the left of the system, i.e. the leftmost $\lfloor N/(d-1) \rfloor$ sites have occupancy $d-1$, with the next site over having $N - \lfloor N/(d-1) \rfloor$ particles. The steps followed are almost identical to the BFES case, with the main difference being that instead of new particles being taken from the leftmost site of the system, they are taken from the rightmost site of the pile-up, which is still non-empty. Likewise, as the particles are moved to the right of the system, instead of all stacking on the rightmost site, they will fill up the sites one by one to their maximal $d-1$ occupancy, starting from the rightmost site and progressing left. Otherwise, the algorithm used is the same, and the proof also holds at finite d .

Appendix D: Scaling of the size of symmetry sectors

We start by analysing the symmetry sectors where only N is fixed. For any finite d we clearly have the following.

$$(1 + z + \dots + z^{d-1})^L = \sum_{N=0}^{(d-1)L} D_N^{(d)} z^N, \quad (\text{D1})$$

where $D_N^{(d)}$ is the dimension of the symmetry sector with N particles in the case of maximal occupation per site equal to $d-1$. Eq. (D1) can be re-written as

$$(1 + z + \dots + z^{d-1})^L = \sum_{\substack{e_0, e_1, \dots, e_{d-1}=0 \\ e_0 + e_1 + \dots + e_{d-1} = L}}^L \frac{L!}{e_0! e_1! \dots e_{d-1}!} \prod_{n=1}^{d-1} z^{n e_n}. \quad (\text{D2})$$

Thus, finding $D_N^{(d)}$ amounts to summing all the multinomial coefficients in the previous expression associated with sets of multiplicities $\{e_i\}$ such that

$$\sum_{n=0}^{d-1} e_n = L \quad \sum_{n=0}^{d-1} n e_n = N. \quad (\text{D3})$$

For any fixed N and d , the number of different sets $\{e_i\}$ satisfying Eq. (D3) scales at most polynomially with L . This implies that if one of these sets $\{e_i\}$ has a multinomial coefficient that exponentially dominates in L over the others, its exponential scaling determines the function $\eta_d(\nu)$ introduced in Section IV. By particle-hole symmetry we can restrict our attention to fillings $\nu \leq (d-1)/2$ without loss of generality. Using Stirling's

asymptotic formula we easily get

$$\ln \left[\frac{L!}{e_0! e_1! \dots e_{d-1}!} \right] = -L \sum_{n=0}^{d-1} \varepsilon_n \ln \varepsilon_n + \mathcal{O}(\ln L), \quad (\text{D4})$$

where we have defined $\varepsilon_n = e_n/L$. We can maximize by the method of Lagrange multipliers the leading term in the previous expression subject to the constraints in Eq. (D3), which we rewrite as

$$\begin{aligned} h_1(\varepsilon_1, \dots, \varepsilon_{d-1}) &= \sum_{n=0}^{d-1} \varepsilon_n - 1 = 0 \\ h_2(\varepsilon_1, \dots, \varepsilon_{d-1}) &= \sum_{n=0}^{d-1} n \varepsilon_n - \nu = 0. \end{aligned} \quad (\text{D5})$$

We thus look for the stationary points of the function

$$- \sum_{n=0}^{d-1} \varepsilon_n \ln \varepsilon_n - q h_1 - \tilde{q} h_2. \quad (\text{D6})$$

These are given by

$$\varepsilon_n^* = e^{-1-q} t^n \quad \forall n \quad t \equiv e^{-\tilde{q}}. \quad (\text{D7})$$

Assume that $0 \leq t < 1$. By imposing the constraints in Eq. (D5) on the set $\{\varepsilon_n^*\}$ we obtain

$$e^{1+q} = \frac{1-t^d}{1-t}, \quad (\text{D8})$$

$$\nu = d + \frac{t}{1-t} - \frac{d}{1-t^d}. \quad (\text{D9})$$

Note that in Eq. (D9) we obtain $\nu = 0$ by setting $t = 0$ and $\nu \rightarrow (d-1)/2$ in the limit $t \rightarrow 1^-$. By continuity, there always exists a solution $0 \leq t < 1$ to the equation Eq. (D9) in the domain of interest $0 \leq \nu < (d-1)/2$, and thus our previous assumption on the domain of t is justified. We also notice that the right-hand side of Eq. (D9) is a strictly increasing function in the interval $0 \leq t < 1$ and thus the solution $t = t(\nu, d)$ of Eq. (D9) is unique. We can now use the functional form of the maxima Eq. (D7) together with Eq. (D8) and Eq. (D9) to obtain

$$\eta_d(\nu) = - \sum_{n=0}^{d-1} \varepsilon_n^* \ln \varepsilon_n^* = \ln \left[\frac{1-t^d}{1-t} \right] - \nu \ln t. \quad (\text{D10})$$

This is an implicit expression for $\eta_d(\nu)$ as a function of $t(\nu, d)$, valid for any d . The solution $t(\nu, d)$ can be easily determined analytically in the case of $d = 2$ yielding $\eta_2(\nu)$ from Eq. (12), while allowing $d \rightarrow \infty$ one recovers $\eta_\infty(\nu)$ again from Eq. (12). For $d = 3$ the solution t is given by

$$t(\nu, 3) = \frac{1 - \nu - \sqrt{1 + 6\nu - 3\nu^2}}{2(\nu - 2)}, \quad (\text{D11})$$

from which $\eta_3(\nu)$ is readily obtained using Eq. (D10). The strict concavity of $\eta_d(\nu)$ for $d = 2, 3$ and ∞ follows

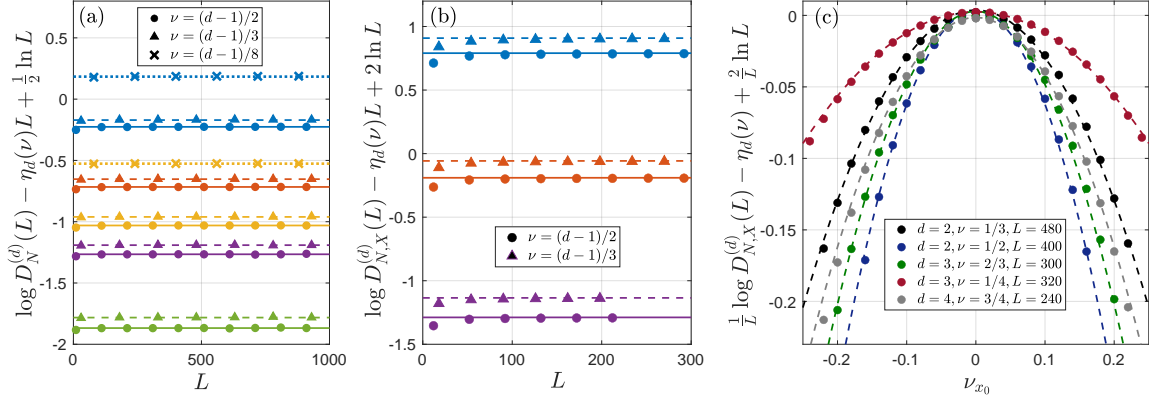


FIG. 11. (a) Scaling of $D_N^{(d)}(L)$ for d equal to 2, 3, 4, 5 and 9, respectively in blue, red, yellow, purple and green. For $\nu = (d-1)/2$, $\eta_d(\nu) = \ln d$, while for the others fillings $\eta_d(\nu)$ is computed analytically for $d = 2, 3$ and by numerically solving Eq. (D9) for $d = 4, 5, 9$. The horizontal lines coincide with the L independent constants appearing in Eq. (11). (b) Scaling of $D_{N,X}^{(d)}(L)$, where $x = X/N$ coincides with the center of the chain. Colour scheme and values of $\eta_d(\nu)$ as in Figure (a). The horizontal lines are the estimated values for the L -independent constants appearing in Eq. (13) and obtained as the parameter a in a two-parameter fit $a - b/x$. (c) Scaling of $D_{N,X}^{(d)}(L)$ as a function of the intensive center of mass ν_{x_0} with origin in the center of the chain, for fixed values of d, ν and L . The dashed lines are 2-parameter quadratic fits $a - bx^2$, $b > 0$. These have been performed excluding a few points at the boundaries of the ν_{x_0} -range displayed in the figure, so to focus on the small- ν_{x_0} regime at the basis of the quadratic expansion in Eq. (14).

easily from the fact that $\eta_d''(\nu) < 0$ for any ν in the domain $0 \leq \nu \leq (d-1)/2$. In the general d case, the value of $\eta_d(\nu)$ at a fixed ν can be found by numerically solving Eq. (D9) and inserting the solution t in Eq. (D10). Furthermore, by differentiating Eq. (D9) with respect to ν , we can express both $\partial_\nu t$ and $\partial_\nu^2 t$ as functions of d, ν and $t(\nu, d)$ itself. This allows us to analytically express $\eta_d''(\nu)$ as a function of the latter variables by using Eq. (D10)

$$\eta_d''(\nu) = Z(\nu, d, t(\nu, d)). \quad (\text{D12})$$

We don't report explicitly the function Z , as the latter involves sums of many terms and its determination requires only simple algebraic manipulations. Then, the value of $\eta_d''(\nu)$ for any fixed ν and any generic d can be obtained by numerically solving Eq. (D9) to obtain $t(\nu, d)$, and using the latter in the third argument of the function Z . We have applied this procedure to a large number of different d values and always found that the function $\eta_d''(\nu)$ is strictly negative in the entire interval $0 \leq \nu \leq (d-1)/2$. By particle-hole symmetry the same is true for $(d-1)/2 \leq \nu \leq d-1$.

In Fig. 11(a) we verify numerically that the asymptotic functional form of $D_N^{(d)}(L)$ coincides with Eq. (11) for

generic d values other than $d = 2$ and ∞ . Here the value of $D_N^{(d)}$ is computed numerically using Eq. (D1) for several choices of d and ν .

Similarly to Eq. (D1), we can obtain the values of $D_{N,X}^{(d)}$ as

$$\prod_{n=0}^{L-1} (1 + zy^n + z^2y^{2n} + \dots + z^{d-1}y^{(d-1)n}) = \sum_{N,X} D_{N,X}^{(d)} z^N y^X. \quad (\text{D13})$$

In Ref. [28] a sharp asymptotic formula for $D_{N,X}^{(\infty)}(L)$ has been derived. In our formalism this is given by

$$\ln D_{N,X}^{(\infty)}(L) = L [r + 2s\nu_x - \nu \ln(1 - e^{-r-s})] - 2 \ln L + \mathcal{O}(L^0). \quad (\text{D14})$$

Here $r = r(\nu, \nu_x)$ and $s = s(\nu, \nu_x)$ are L -independent functions of the filling and the intensive center of mass implicitly defined as the unique positive real solutions of the following set of coupled equations [28]

$$\frac{1}{\nu} = \frac{1}{s} \ln \left(\frac{e^{r+s} - 1}{e^r - 1} \right) - 1, \quad (\text{D15})$$

$$\frac{\nu_x}{\nu} = \frac{s \ln(1 - e^{-r-s}) + \text{dilog}(1 - e^{-r}) - \text{dilog}(1 - e^{-r-s})}{s^2},$$

where

$$\text{dilog}(x) \equiv \int_1^x dt \frac{\ln t}{1-t} \quad |1-x| < 1. \quad (\text{D16})$$

Note that we are restricting ν_x to $\nu_x \leq 1/2$ without loss of generality. For $\nu_x = 1/2$ the solutions to the set Eq. (D15) is

$$r = \ln(1+\nu) \quad s = 0, \quad (\text{D17})$$

from which we obtain Eq. (13) with $d = \infty$ and $\Lambda_\infty(\nu, 1/2) = 0$. For small negative values of $\nu_{x_0} = \nu_x - 1/2$ we can study the set Eq. (D15) perturbatively in ν_{x_0} and obtain the following expansion for r and s

$$\begin{aligned} r &= \ln(1+\nu) + \frac{6\nu\nu_{x_0}}{1+\nu} + \mathcal{O}(\nu_{x_0}^2), \\ s &= -\frac{12\nu\nu_{x_0}}{1+\nu} + \mathcal{O}(\nu_{x_0}^2). \end{aligned} \quad (\text{D18})$$

Substituting this into Eq. (D14) yields Eq. (13) for $d = \infty$ with $\Lambda_\infty(\nu, \nu_x)$ expanded as in Eq. (14). Note that the analytic determination of $\lambda_\infty(\nu)$ that appears in Eq. (14) requires knowledge of higher-order terms in the expansion Eq. (D18).

We finally show that it is possible to derive an exact asymptotic formula for $D_{N,X}^{(2)}$ based on the knowledge of $D_{N,X}^{(\infty)}$. A known generalization of the binomial theorem, see e.g. [47], gives

$$\begin{aligned} \prod_{n=0}^{L-1} (1+zy^n) &= \\ &= \sum_{N=0}^L \sum_{j=0}^{N(L-N)} D_{N,j}^{(\infty)}(L-N) z^N y^{j+N(N+1)/2}. \end{aligned} \quad (\text{D19})$$

Comparing Eq. (D19) with Eq. (D13) we realize that

$$D_{N,X}^{(2)}(L) = D_{N,\tilde{X}}^{(\infty)}(\tilde{L}), \quad (\text{D20})$$

where $\tilde{L} = L - N$, $\tilde{X} = X - N(N+1)/2$ and N, X belong to the domain allowed by $d = 2$. Similarly to the definitions of ν and ν_{x_0} we can define $\tilde{\nu} = N/\tilde{L}$ and $\tilde{\nu}_{x_0} = \tilde{X}/(N\tilde{L}) - 1/2$. In the range $0 < \nu < 1$ of interest we have

$$\tilde{\nu} = \frac{\nu}{1-\nu} \quad \tilde{\nu}_{x_0} = \frac{\nu_{x_0}}{1-\nu} + \mathcal{O}(L^{-1}). \quad (\text{D21})$$

Using the previous two equations together with Eq. (D20) we arrive at the asymptotic expression Eq. (13) for $d = 2$. In particular, for small ν_{x_0} values we obtain

$$\begin{aligned} \ln D_{N,X}^{(2)}(L) &= \ln D_{N,\tilde{X}}^{(\infty)}(\tilde{L}) \\ &= L \left[(1-\nu) \eta_\infty(\tilde{\nu}) - \frac{\lambda_\infty(\tilde{\nu})}{1-\nu} \nu_{x_0}^2 + o(\nu_{x_0}^2) \right] \\ &\quad - 2 \ln L + \mathcal{O}(L^0). \end{aligned} \quad (\text{D22})$$

From this we see that

$$\lambda_2(\nu) = \frac{\lambda_\infty(\tilde{\nu})}{1-\nu}. \quad (\text{D23})$$

It is elementary to verify using Eq. (12) that

$$(1-\nu) \eta_\infty(\tilde{\nu}) = \eta_2(\nu), \quad (\text{D24})$$

as required by Eq. (13).

The asymptotic value of $D_{N,X}^{(d)}(L)$ for a dipole moment with center of mass $x(L)$ coinciding with the centre of the chain is numerically studied in Fig. 11(b) for a few finite d values, and coincides with the one reported in Eq. (13). Fig. 11(c) studies the dependence of $D_{N,X}^{(d)}$ on ν_{x_0} , for small values of the latter, at fixed L and for different finite d values. The 2-parameter quadratic fits match the data very well, confirming that $\ln D_{N,X}^{(d)}/L - \eta_d(\nu)$ is at leading order in ν_{x_0} a quadratic function of the latter for generic d , as expressed by Eq. (14). The coefficient in front of the quadratic term of the fit is an estimate for the value of $\lambda_d(\nu)$ from Eq. (14).

Appendix E: Strong fragmentation in atypical (N, X) families

In this appendix we briefly discuss atypical families of (N, X) sectors, which even together contain only an exponentially vanishing fraction of all configurations associated with a given $N = \nu L$ sector. As clear from the analysis of Sections V A and V B, the presence of a non-zero density of type-1 or type-2 blockages for $\nu < (k-2)^{-1}$ holds regardless of the value of ν_{x_0} . Thus, the physics of atypical families of (N, X) sectors characterised in the thermodynamic limit by $\nu_{x_0} \neq 0$ and $\nu < (k-2)^{-1}$ is still dominated by an extensive number of sites involved in blockages.

Proving strong fragmentation in atypical families following simple arguments similar to the ones employed for typical families requires the determination of the function $\Lambda_d(\nu, \nu_x)$ appearing in Eq. (13), a task that goes beyond the numerical results discussed in Appendix D. However, consider the domain $\nu < (k-1)^{-1}$, where necessarily a fraction $f > 0$ of all sites is involved in a type-1 blockage. Call $\Delta_d(\nu, f)$ the difference

$$\Delta_d(\nu, f) = g_d(0|\nu, f) - \eta_d(\nu) < 0. \quad (\text{E1})$$

If ν_{x_0} is different from zero in the thermodynamic limit, Eq. (21) can be replaced by

$$\lim_{L \rightarrow \infty} \frac{1}{L} \ln r_{d,k}(N, X) \leq \Delta_d(\nu, f) + \Lambda_d(\nu, \nu_x). \quad (\text{E2})$$

This trivially proves that all the atypical families with $|\nu_{x_0}|$ different from zero but sufficiently small and $\nu < (k-1)^{-1}$ are strongly fragmented, with ratio $r_{d,k}$ decaying to zero exponentially with L . This is because, due

to Eq. (14), there always exists a non-zero value of $|\nu_{x_0}|$ below which the left-hand side of Eq. (E2) is negative.

More in general, for $\nu < (k-2)^{-1}$ and without requiring explicit knowledge of $\Lambda_d(\nu, \nu_x)$, if one can prove that in the largest Krylov subsectors of an atypical family, one of the extensively many blockages partitions the system into two extensive subregions that both contain an exponentially large number of configurations according to the scaling in Eq. (13), then application of Eq. (18) would ensure that the ratio $r_{d,k}$ decays to zero at least as L^{-2} , as seen from Eq. (30) when one sets $G = 2$. Similar reasoning can also be applied to cases with $G > 2$ by making use of the disconnecting property of multiple blockages.

We notice that it is possible that in addition to weak-to-strong fragmentation transitions induced by tuning ν , similar transitions might be induced by varying ν_{x_0} . In particular, in families with ν_{x_0} significantly different from 0 and $\nu < \nu_c$, it might be possible that the dipole polarisation constrains the majority of particles into a subregion of the chain with a local density of particles larger than ν_c , thus locally suppressing the presence of blockages. This mechanism might be at the basis of a transition from weak to strong fragmentation within N -families characterised by $\nu < \nu_c$. We leave the study of this interesting problem for future work.

Appendix F: Calculation of densities of various particle configurations

In this appendix, we compute several functions of use for Section VI.

1. Calculation of $b_1(k, n, \ell)$ and $b_1^\infty(k, n, \ell)$

Here we compute an exact expression for the functions $b_1(k, N, L)$ and $b_1^\infty(k, N, L)$, which for $d = 2$ and $d = \infty$ respectively give the total number of ways to arrange n particles over ℓ sites such that they satisfy the no-propagation constraints

$$i_n^0 \geq (n-1)(k-2) \quad (\text{F1})$$

For $d = 2$, we have

$$b_1(k, N, L) = \sum_{i_N=(N-1)(k-2)}^{L-1} \cdots \sum_{i_2=(k-2)}^{i_3-1} \sum_{i_1=0}^{i_2-1} 1 \quad (\text{F2})$$

This sum is identical to

$$b_1(k, N, L) = b'_1(k, N, L) = \sum_{i_N=N(k-2)}^y \cdots \sum_{i_2=2(k-2)}^{i_3-1} \sum_{i_1=k-2}^{i_2-1} 1 \quad (\text{F3})$$

when $y = \ell + k - 3$. We will now prove that

$$b'_1(k, N, L) = \frac{y - N(k-2) + 1}{y - N + 1} \binom{y}{N} \quad (\text{F4})$$

inductively in N . The case $N = 1$ is trivial. Assume that the formula holds up to $N - 1$, and consider it for N . We then find

$$\begin{aligned} b'_1(k, N, L) &= \sum_{i_N=N(k-2)}^y D'_k(N-1, i_N-1) = \sum_{i_N=N(k-2)}^y \frac{i_N - (N-1)(k-2)}{i_N - N} \binom{i_N-1}{N-1} \\ &= \sum_{i_N=N(k-2)}^y \left[\binom{i_N}{N-1} - (k-2) \binom{i_N-1}{N-2} \right] = \left(\sum_{i_N=N-1}^y - \sum_{i_N=N-1}^{N(k-2)-1} \right) \left[\binom{i_N}{N-1} - (k-2) \binom{i_N-1}{N-2} \right] \\ &= \binom{y+1}{N} - (k-2) \binom{y}{N-1} = \frac{y - N(k-2) + 1}{y - N + 1} \binom{y}{N}, \end{aligned} \quad (\text{F5})$$

where in the before-last step we made use of the hockey stick identity. Setting $y = L + k - 3$ we obtain the desired result:

$$b_1(k, N, L) = \binom{L + (k-2)}{N} \frac{L - (N-1)(k-2)}{L + (k-2)} \quad (\text{F6})$$

As concerns the $d = \infty$ case, due to stacking we have

$$b_1^\infty(k, n, \ell) = \sum_{i_N=(N-1)(k-2)}^{L-1} \cdots \sum_{i_2=(k-2)}^{i_3} \sum_{i_1=0}^{i_2} 1. \quad (\text{F7})$$

Following identical logic to the previous derivation, one

can then show

$$\beta_1^\infty(k, N, L) = \frac{L - (N - 1)(k - 2)}{L + k - 2} \binom{L + k + N - 3}{N} \quad (\text{F8})$$

For a particular local configuration of x particles over m sites in a $d = 2$ system, this sum equals the average density of occurrences of that configuration amongst states with N particles and L sites such that the particles to the right and left of the configuration satisfy the no-propagation condition of Eq. 31. The average is carried out over an entire N sector. The bounds on the sum over N_R are given by

$$N_{\min} = \max \left(0, N - \left\lfloor \frac{L - L_R - m + k - 3}{k - 2} \right\rfloor \right), \quad (\text{F10})$$

$$N_{\max} = \min \left(N, \left\lfloor \frac{L_R + k - 3}{k - 2} \right\rfloor \right), \quad (\text{F11})$$

The sum on the right-hand side of Eq. (F9) involves polynomially many in L terms. We will show that a subset of the summands exponentially dominates in L over the others, and thus the leading order of the total sum coincides with the sum of this subset. Using Eq. (F6) we re-write the product of b_1 's in Eq. (F9) as

$$\begin{aligned} b_1(N_R, L_R) b_1(N - N_R - x, L - L_R - m) \\ = \binom{L_R}{N_R} \binom{L - L_R}{N - N_R} \alpha(k, x, m, N, L, N_R, L_R). \end{aligned} \quad (\text{F12})$$

It is easy to check that $\alpha(k, x, m, N, L, N_R, L_R)$ is $\mathcal{O}(L^0)$ and thus the only exponential dependence on L comes from the product of the two binomials. We introduce the intensive quantities

$$\ell_R = \frac{L_R}{L} \quad \nu_R = \frac{N_R}{L}, \quad (\text{F13})$$

and define

$$\begin{aligned} M_{\nu, \ell_R}(\nu_R) &= \binom{L_R}{N_R} \binom{L - L_R}{N - N_R} / \binom{L}{N} \\ &= \binom{\ell_R L}{\nu_R L} \binom{(1 - \ell_R)L}{(\nu - \nu_R)L} / \binom{L}{\nu L}. \end{aligned} \quad (\text{F14})$$

Using Stirling's formula for the asymptotic value of the binomials, we find that $M_{\nu, \ell_R}(\nu_R)$ is given by a product

$$M_{\nu, \ell_R}(\nu_R) = \left[M_{\nu, \ell_R}^{(1)}(\nu_R) \right]^L M_{\nu, \ell_R}^{(2)}(\nu_R) L^{-1/2}, \quad (\text{F15})$$

2. Lower bound on the density of particular particle configurations

We will next compute a function which has several applications in the main text. In particular, we compute the thermodynamic limit of the function

$$P(x, m, k, N, L) = \frac{\sum_{L_R=0}^{L-m} \sum_{N_R=N_{\min}}^{N_{\max}} b_1(k, N_R, L_R) b_1(k, N - N_R - x, L - L_R - m)}{L \binom{L}{N}}. \quad (\text{F9})$$

where both $M_{\nu, \ell_R}^{(1)}$ and $M_{\nu, \ell_R}^{(2)}$ are $\mathcal{O}(L^0)$. It is easy to show that $M_{\nu, \ell_R}^{(1)}$ has only one global maximum for $\nu_R^* = \nu \ell_R$, where it takes the value

$$M_{\nu, \ell_R}^{(1)}(\nu_R^*) = 1. \quad (\text{F16})$$

Taylor expanding $M_{\nu, \ell_R}^{(1)}$ in a small neighborhood around ν_R^* we get

$$\begin{aligned} \left[M_{\nu, \ell_R}^{(1)}(\nu_R) \right]^L &= \\ \exp \left\{ -L \left[\frac{(\nu_R - \nu_R^*)^2}{2\sigma^2} + \mathcal{O}((\nu_R - \nu_R^*)^3) \right] \right\}, \end{aligned} \quad (\text{F17})$$

with

$$\sigma^2 = \ell_R(1 - \ell_R)\nu(1 - \nu). \quad (\text{F18})$$

In the thermodynamic limit we can transform the sum over N_R into an integral

$$L^{-1/2} \sum_{N_R} = L^{1/2} \frac{1}{L} \sum_{N_R=N_{\min}}^{N_{\max}} \rightarrow L^{1/2} \int_{\nu_R^{\min}}^{\nu_R^{\max}} d\nu_R, \quad (\text{F19})$$

where the factor $L^{-1/2}$ comes from Eq. (F15). From Eq. (F17) it is clear that, aside from corrections that go to zero faster than any power law in L , only a small neighborhood around ν_R^* of width of the order of $1/\sqrt{L}$ contributes to the integral. In this neighborhood we can neglect the $\mathcal{O}((\nu_R - \nu_R^*)^3)$ term from Eq. (F17). Thus, by defining

$$\tilde{\alpha}_{k, x, m, \nu, \ell_R}(\nu_R) = \alpha(k, x, m, \nu L, L, \nu_R L, \ell_R L), \quad (\text{F20})$$

we can rewrite Eq. (F9) as

$$\begin{aligned} P(x, m, k, \nu L, L) &= \\ \int_0^1 d\ell_R \int_{-\infty}^{\infty} d\nu_R \tilde{\alpha}_{k, x, m, \nu, \ell_R}(\nu_R) M_{\nu, \ell_R}^{(2)}(\nu_R) \frac{e^{-\frac{(\nu_R - \nu_R^*)^2}{2\sigma^2/L}}}{1/\sqrt{L}} \\ &\quad + \varepsilon(L), \end{aligned} \quad (\text{F21})$$

where $\varepsilon(L)$ goes to zero faster than any power law in L . Notice that in the previous expression we have extended the integral boundaries to $\pm\infty$ and absorbed the

associated error inside $\varepsilon(L)$. Given that only a $\mathcal{O}(1/\sqrt{L})$ region around ν_R^* contributes to the integral in Eq. (F21), we can expand $\tilde{A}_{k,x,m,\nu,\ell_R} M_{\nu,\ell_R}^{(2)}$ in powers of $(\nu_R - \nu_R^*)$, obtaining

$$\begin{aligned} \tilde{\alpha}_{k,x,m,\nu,\ell_R}(\nu_R) M_{\nu,\ell_R}^{(2)}(\nu_R) = \\ \frac{1}{\sqrt{2\pi\sigma^2}} \nu^x (1-\nu)^{m+2-2(k-1)} (1-\nu/\nu_c)^2 + \mathcal{O}(\nu_R - \nu_R^*) . \end{aligned} \quad (\text{F22})$$

The odd powers in this expansion don't contribute to the final result as they vanish within the remaining Gaussian integral, while each $(\nu_R - \nu_R^*)^{2n}$ with $n \geq 1$ contributes an order $\mathcal{O}(L^{-n})$. Thus we only need to worry about the leading order in Eq. (F22), which brings us to

$$\begin{aligned} P(x, m, k, \nu L, L) = \\ \int_0^1 d\ell_R \nu^x (1-\nu)^{m+2-2(k-1)} (1-\nu/\nu_c)^2 \int_{-\infty}^{\infty} d\nu_R \frac{e^{-\frac{(\nu_R - \nu_R^*)^2}{2\sigma^2/L}}}{\sqrt{2\pi\sigma^2/L}} \\ + \mathcal{O}(1/L) . \end{aligned} \quad (\text{F23})$$

Given that the Gaussian integral in the previous equation is properly normalized, carrying the integral through we obtain

$$\lim_{L \rightarrow \infty} P(x, m, k, \nu L, L) = \nu^x (1-\nu)^{m+2-2(k-1)} (1-\nu/\nu_c)^2 \quad (\text{F24})$$

This can be used to obtain the type-1 blockage density of Eq. (41) by setting $m = 2k - 4$ and $x = 1$, as well as the active bubble configuration density of Eq. (53) by setting $m = \ell + 2(k - 1)$.

The corresponding function for $d = \infty$ is given by

$$P^\infty(x, m, k, N, L) = \frac{\sum_{L_R=0}^{L-m} \sum_{N_R=N_{\min}}^{N_{\max}} b_1^\infty(k, N_R, L_R) b_1^\infty(k, N - N_R - x, L - L_R - m)}{L \binom{L+N-1}{N}} . \quad (\text{F25})$$

The thermodynamic limit expression derived using an identical approach, and found to be

$$\begin{aligned} \lim_{L \rightarrow \infty} P^\infty(x, m, k, \nu L, L) = \\ \nu^x (1+\nu)^{-(x+m+2-2(k-1))} (1-\nu/\nu_c)^2 \end{aligned} \quad (\text{F26})$$

From this we obtain the type-1 blockage density of Eq. (45) by setting $x = 1$ and $m = 2k - 4$, and the active bubble configuration density of Eq. (57) by setting $m = \ell + 2(k - 1)$.

Appendix G: Lower bounds on $A_2(x, k, N, L)$ and $A_\infty(x, k, N, L)$

In this section, we proceed to explicitly compute some lower bounds on the $d = 2$ and $d = \infty$ active bubble density functions, $A_2(x, k, \nu L, L)$ and $A_\infty(x, k, \nu L, L)$, as defined in Section VID, for various values of k and x . We begin with the simplest case of $A_\infty(x, k, \nu L, L)$, which we will lower bound for $k = 7$ and from $x = 2$ to $x = 6$. We have that

$$\begin{aligned} A_\infty(x, k = 7, \nu L, L) = \\ \sum_{\ell=1+5(x-1)}^{1+6(x-1)} m_\infty(x, \ell, k = 7) a_\infty(x, \ell, k = 7, N, L), \end{aligned} \quad (\text{G1})$$

The summation bounds are derived from Eqs. (52) (which also holds for $d = \infty$) and (56) in the main text, where a lower bound on $a_\infty(x, \ell, k = 7, N, L)$ in the thermodynamic limit is also provided. Hence all that remains to be calculated are the multiplicities $m_\infty(x, \ell, k = 7)$. This can be done methodically with the aid of a computer as follows. For each value of ℓ in the summation, $m_\infty(x, \ell, k = 7)$ will equal the sum of the dimensions of all local Krylov sectors with a corresponding local FES consisting of $\ell - (1 + 5(x - 1))$ pairs of particles separated by $k - 2$ holes and $1 + 6(x - 1) - \ell$ pairs of particles separated by $k - 3$ holes. For example, $m_\infty(x, \ell = 1 + 5(x - 1), k = 7)$ will equal the dimension of the local Krylov sector that contains the local FES in which all pairs of particles are separated by $k - 3$ holes. On the other hand, $m_\infty(x, \ell = 2 + 5(x - 1), k = 7)$ will equal the sum of the dimensions of the $x - 1$ local Krylov sectors defined by the local FESs with exactly one pair of particles separated by $k - 2$ holes; and so on. The dimensions of the local Krylov sector associated with a given local FES can be determined by starting from that FES, then computing all possible states that can be reached from the FES via a series of inward hop operators. This necessarily maps out the whole of the FES, as by the result in Appendix A, any state in a Krylov sector of a $d = \infty$ system can be reached by starting from the FES and applying inward hops. We present all the multiplicity values derived in this fashion in the table below,

where the boxes filled are those between the bounds of ℓ_{\min} and ℓ_{\max} :

$m_{\infty}(x, \ell, k = 7)$						
	$\ell = 1 + 5(x - 1)$	$\ell = 2 + 5(x - 1)$	$\ell = 3 + 5(x - 1)$	$\ell = 4 + 5(x - 1)$	$\ell = 5 + 5(x - 1)$	$\ell = 6 + 5(x - 1)$
x=2	3	4				
x=3	18	42	7			
x=4	131	462	108	19		
x=5	1111	5268	1446	408	40	
x=6	10462	62185	18688	6723	1077	97

We next consider, for $k = 5$, the $d = 2$ multiplicity function $m_2(x, \ell, k = 5)$. Although a given active bubble configuration cannot necessarily attain its corresponding local FES for d finite, one can show via brute force enumeration that for the values $x = 2$ to $x = 5$ that we

consider, this will always be the case. Hence the local Krylov sectors for these values of x can be determined by starting from the corresponding local FES and mapping out all states attainable via a combination of inward and outward hops. This then yields the results

$m_2(x, \ell, k = 5)$					
	$\ell = 1 + 5(x - 1)$	$\ell = 2 + 5(x - 1)$	$\ell = 3 + 5(x - 1)$	$\ell = 4 + 5(x - 1)$	$\ell = 5 + 5(x - 1)$
x=2	2	2			
x=3	5	12	3		
x=4	15	62	27	5	
x=5	56	318	180	62	8

Appendix H: Algorithm for efficiently mapping to the FES

In this appendix, we present an algorithm for efficiently mapping from an initial state at any d to its corresponding FES in the FES picture. This algorithm makes use of the following property: if we have either a single site with one or more particles, or else (for $k \geq 4$) a collection of sites all of which contain at least one particle and which are separated by at most $k - 4$ holes from each other, then if the particles on those sites are expanded to their corresponding local FES, that local FES will be a local blockage-free FES uniquely determined by the number and dipole moment of the particles. This result follows immediately from the 2-colour dynamics discussed in Section III A and the uniqueness result of Appendix A. The algorithm for expanding to an FES is then as follows.

- Divide the state into “blockage-free groups” of occupied sites separated by $k - 4$ holes or fewer from each other (or in the case of $k = 3$, simply individual occupied sites).
- For each blockage-free group, use the number of particles it contains as well as its local dipole moment to compute the leftmost and rightmost site it will occupy when expanded into a local FES.
- Merge any pair of blockage-free groups for which the corresponding local FESs are separated by $k - 4$

sites or less (or for which the local FESs overlap, in the case of $k = 3$), and compute the bounds of the new resulting local FES. Repeat this merging procedure until no further merging can occur.

- Use the particle number and dipole moment of each blockage-free group to determine the location of each of the particles in the corresponding local FES, and use these results to construct the FES of the entire system.

We next present how to calculate the leftmost and rightmost sites of the local FES corresponding to a blockage-free group, as well as the positions of the particles in the local FES. Since the local FES is ergodic, it will have at most one pair of particles separated by $k - 2$ holes and all others separated by $k - 3$ holes up to a possible pile-up at the boundary. We begin by considering the case where there is no overlap in the local FES with the boundary. Say that the blockage-free group has n particles and a dipole moment p . Let i_l denote the leftmost site of the local FES and i_f denote the rightmost. Furthermore, let $j \in \{1, \dots, n\}$ denote the index of the particle to the left of which there is a spacing of $k - 2$ holes (so if there are $k - 2$ holes between the first and second particles, $j = 1$). If there are no spacings of $k - 2$ holes, then $j = n$. In this case, the local dipole moment

equals

$$\begin{aligned} p &= n i_1 + \sum_{m=1}^{n-1} m(k-2) + (n-j) \\ &= n i_1 + n(n-1)(k-2)/2 + (n-j). \end{aligned} \quad (\text{H1})$$

From this equation one easily finds that

$$\begin{aligned} i_1 &= \lfloor (p - n(n-1)(k-2)/2)/n \rfloor \\ j &= n(i_1 + 1) + n(n-1)(k-2)/2 - p \\ i_f &= i_1 + (n-1)(k-2) + (1 - \delta_{j,n}) \end{aligned} \quad (\text{H2})$$

We next consider the case where the local FES overlaps with exactly one boundary. We assume it to be the left boundary (with the derivation for the right boundary following identical logic). Let m_l denote the number of particles piled up on the left boundary, i_1 the site of the leftmost particle *not on the boundary* of the local FES, $j \in \{1, \dots, n - m_l\}$ the index amongst those particles textitnot on the boundary of the particle to the right of which there are $k - 2$ holes (with $j = n - m_l$ if there is none) and i_f the site of the rightmost particle. In this case, the dipole moment equals

$$p = m_l + (n - m_l) i_1 + (n - m_l)(n - m_l - 1)(k - 2)/2 + (n - m_l - j). \quad (\text{H3})$$

We know that in the above equation, $2 \leq i_1 \leq k$. We proceed as follows: we know that of the possible configurations of the remaining $n - m_l$ particles, the one with the smallest dipole moment is given by $i_1 = 2$ and $j = n - m_l$. Hence, if we set $i_1 = 1$ and j to these values in the above equation and solve for m_l , then that solution rounded up to the next integer (if the solution isn't already an integer) will give m_l . Indeed, by the proof of uniqueness of the FES in Appendix A, if m_L were lower or higher than this value, then it would be impossible to arrange the particles not on the boundary to obtain the dipole moment p . With m_L determined, the remaining variables can be solved, as before, by determining the positions of the particles in the local FES.

We finally consider the case where the local FES in fact spans the whole system, with particles on both boundaries. In this case, let m_l be the numbers of particles on the left boundary, m_c the number of particles on neither boundary, i_1 the site of the leftmost particle not on a boundary, i_f the site of the rightmost particle not on a boundary, and $j \in \{1, \dots, n - m_l - m_c\}$ the index of the particle to the right of which a sequence of $k - 2$ holes are situated. Noting this implies there are $n - m_l - m_c$ particles on the right boundary, we then have that

$$p = m_l + m_c i_1 + m_c(m_c - 1)(k - 2)/2 + (m_c - j) + (n - m_l - m_c)L. \quad (\text{H4})$$

We know that $m_c \leq \lceil (L - 2)/(k - 2) \rceil$, and that the smallest dipole moment for a given m_l is achieved when m_c saturates this bound and $i_1 = 2$, $j = m_c$. Plugging these values into the above equation, solving for m_l , and rounding up to the nearest integer gives the value of m_l .

The value of m_r , the number of particles on the right boundary, can be determined using an identical method, following which m_c , i_1 , j , and i_f can be determined.

Appendix I: Proof of the CS-to-BES algorithm

In this appendix, we prove the algorithm described in Section VIII B for mapping a contracted state to a blockage-free extended state. We will focus on the case of $d = 2$ for simplicity, from which it is clear how to generalise to higher d . We recall that the algorithm in question is given by

- For site $i \in \{0, \dots, L - 1\}$ in increasing order, if the sites i and $i + k - 1$ are within the bounds of the system and have occupancy 1 and all sites in-between them are empty, apply the gate $U_{i, i+k-1}^+$. Repeat the loop over sites until it is no longer possible to apply this gate.
- For $\ell = k - 4$ to $\ell = 1$ in decreasing order, for site $i \in \{0, \dots, L - 1\}$ in increasing order, if the sites i and $i + \ell + 2$ are within the system and have occupancy 1 and all sites in-between are empty, apply the gate $U_{i, i+\ell+2}^+$; otherwise, if the sites i and $i + \ell + 3$ are within the system and have occupancy 1 and all sites in-between are empty, apply $U_{i, i+\ell+3}^+$.
- For $\ell = 1$ to $\ell = k - 4$ in increasing order, for site $i \in \{0, \dots, L - 1\}$ in increasing order, apply the gate $U_{i, i+\ell+2}^+$ if possible, and if not then apply the gate $U_{i, i+\ell+3}^+$ if possible.

To prove that this algorithm works, we recall that the CS for $d = 2$ consists of a series of clusters of particles, each separated by one hole from its neighbours. By a cluster, we mean a group of occupied neighbouring sites. We also recall that at most one of these clusters will contain $k - 2$ particles; the rest will all contain $k - 3$ particles, up to the possible exception of the leftmost and rightmost clusters, which may contain fewer particles.

Let us label the clusters in a given CS by an index $j = 1, \dots, N_C$, where N_C is the initial total number of particle clusters. As the algorithm is carried out, new clusters may form to the left and right of the existing ones. When a new cluster is formed to the left, we take the range of j to extend downward, so a first new leftward cluster will have $j = 0$, a second new one will have $j = -1$, and so on. Likewise, when new clusters are formed to the right, the upper range of the index i extends beyond N_C . We will denote the number of particles in each cluster by c_j . When, after a series of hops, $c_j = 0$ this will indicate there are no particles left in the cluster (hence the holes that were originally on either side of the cluster become adjacent); we will continue to label the ‘‘empty cluster’’ however to preserve notational consistency.

Let us consider the first step in the algorithm. If there is no cluster of size $k - 2$, this step does not have an

impact. If there is such a cluster, then say it is at index j , such that $c_j = k - 2$, and that the leftmost particle in it is at site i . After the outward hop gate $U_{i-1, i+k-2}^+$ is applied to it, the following changes in cluster size will occur:

$$\begin{aligned} c_j &= k - 4, \\ c_{j+1} &= c_{j+1} + 1, \\ c_{j-1} &= c_{j-1} + 1. \end{aligned}$$

If the new value of c_{j+1} satisfies $c_{j+1} < k - 2$, then no further hops are applied until the algorithm loops back round to the first site. If $c_{j+1} = k - 2$ on the other hand, then the outward hop operator is applied again, resulting in

$$\begin{aligned} c_{j+1} &= k - 4, \\ c_j &= k - 3, \\ c_{j+2} &= c_{j+2} + 1. \end{aligned}$$

Again, a further hop operator will only be applied if $c_{j+2} = k - 2$; these outward hops will continue until an outward hop occurs in which no cluster of size $k - 2$ is formed, or else a cluster of size $k - 2$ is formed which overlaps with the boundary (in which the particles just contribute to the pile-up at the boundary) at which point the algorithm loops back to the first site.

When the algorithm loops back to the first site and runs through again, then $c_{j-1} \leq k - 2$, and all other clusters (up to the possible exception of the boundary) have size less than $k - 2$. If $c_{j-1} < k - 2$, then the first step of the algorithm terminates. If $c_{j-1} = k - 2$, then the same series of hops is performed again, with the end result that either $c_{j-2} = k - 2$ or else no cluster away from the boundaries has size $k - 2$. This continues until there are no clusters of size $k - 2$ not on the boundary left, which must eventually occur due to the finite size of the system.

We then consider the second step of the algorithm. For each value of ℓ , at the beginning of the loop, $\ell + 1$ is the size of the largest clusters present, and at the end of the loop, ℓ is the size of the largest clusters present (disregarding boundaries). To demonstrate this, we note that it is easy to show following identical logic to the last step that by the end of each loop over all sites, the number of clusters of size $\ell + 1$ is lesser or equal to what it was before the loop over all sites; and furthermore that if it is equal, then the index of the leftmost cluster of size $\ell + 1$ has decreased by 1. Hence, repeated application of the loop over all sites eventually results in the absence of any clusters of size ℓ away from the boundaries. The loop over the values of ℓ itself eventually results in all clusters away from the boundaries having a size of at most 1, and hence in all particles not in boundary pile-ups being separated by at least one (and at most 2) holes from their neighbours.

The third step of the algorithm follows identical logic in reverse. For each value of ℓ , at the start all particles

are separated by at least ℓ and at most $\ell + 1$ holes from their neighbours, and by the end they are all separated by at least $\ell + 1$ and at most $\ell + 2$ holes. By the end of the algorithm, all particles are separated by at least $k - 3$ and at most $k - 2$ holes. However, it is easy to check that there can only be one instance of $k - 2$ holes, since if there were two or more, then following logic identical to that in step 2 of the uniqueness proof in Appendix A, it would be impossible via a series of solely inward hops to arrive at a type-1 CS, but this must be possible since the sequence of outward hops we applied in our algorithm can be reversed.

In the case of general finite d , the ‘‘clusters’’ become groups of neighbouring sites with occupancies $d - 1$. The first step of the algorithm removes any cluster of $k - 2$ sites, and the second step removes any clusters of even one site, as it results in a state where no sites aside from boundary pile-ups have occupancy $d - 1$. The third step then completes the expansion to the BES. The proof of the general d algorithm is almost identical to that presented above for $d = 2$.

Appendix J: Characterizing typical states for $d = 2$

As seen in Eq. (11), the logarithm of the total number of particle configurations in a family of $N = \nu L$ sectors for $d = 2$ is given by

$$\ln D_N^{(2)}(L) = \ln \binom{L}{N} = L \eta_2(\nu) + \mathcal{O}(\ln L), \quad (\text{J1})$$

with $\eta_2(\nu)$ defined in Eq. (12). In each of these configurations, call N_n the number of particles that are separated by exactly $n \geq 0$ holes from the first particle to their right (for the right-most particle in the system n is the number of holes to its right up to the right-boundary), and call $f_n = N_n/N$ their fractions over the total number of particles. In this Appendix we characterise the fractions f_n in typical states of $d = 2$ systems at fixed fillings $0 < \nu < 1 = d - 1$.

We start by noticing that counting all the configurations in an N sector is equivalent to counting all the possible ways, compatible with the size L , of assigning right-sequences of n holes to each of the N particles in the system, i.e.

$$\sum_{\{N_n\}} \frac{N!}{N_0! N_1! \dots N_{\Gamma-1}!} = D_N^{(2)}(L), \quad (\text{J2})$$

where $\Gamma - 1 = L - N$ and the sum is over all sets $\{N_n \mid n = 0, \dots, \Gamma - 1\}$ that satisfy the constraints

$$\sum_{n=0}^{\Gamma-1} N_n = N \quad \sum_{n=0}^{\Gamma-1} n N_n = L - N. \quad (\text{J3})$$

The value of $\Gamma = L - N$ has been derived from the previous constraints by setting $N_0 = N - 1$ and $N_{\Gamma-1} = 1$.

A first question is: how many different sets $\{N_n\}$ satisfy Eq. (J3)? We notice that the equations in Eq. (J3) are identical to the ones in Eq. (1) for $d = \infty$, via the identifications

$$L \rightarrow \Gamma \equiv L', \quad N \rightarrow N \equiv N', \quad X \rightarrow L - N \equiv X'. \quad (\text{J4})$$

This means that the number of distinct sets $\{N_n\}$ satisfying Eq. (J3) coincides with $D_{N',X'}^{(\infty)}(L')$. Given that

$$\nu'_x = \frac{X'}{N'L'} = \frac{1}{\nu L} = \mathcal{O}(L^{-1}), \quad (\text{J5})$$

$D_{N',X'}^{(\infty)}(L')$ must scale with L much more slowly than $D_{N,X}^{(\infty)}(L)$ for typical (N, X) sectors with $\nu_x = 1/2$. However, we cannot calculate $D_{N',X'}^{(\infty)}$ by direct application of the formulas for $D_{N,X}^{(\infty)}$ discussed in Section IV and Appendix D, as those were derived under the assumption of $0 < \nu_x < 1$, which guarantees that $\ln D_{N,X}^{(\infty)} = \mathcal{O}(L)$. This suggests that the leading order of $\ln D_{N',X'}^{(\infty)}(L')$ should be $\mathcal{O}(L^\gamma)$ with $0 < \gamma < 1$. Calculating numerically $D_{N',X'}^{(\infty)}(L')$ as a function of a few values of L we obtain $\gamma = 1/2$.

Given that only $\mathcal{O}(\exp c\sqrt{L})$ sets $\{N_n\}$ appear in the sum Eq. (J2), with c an L -independent constant, if a restricted class of these sets is associated with multinomials that exponentially dominate in L over all the others, this class alone determines the fraction f_n in typical states. The asymptotic scaling of

$$\ln \left[\frac{N!}{N_0!N_1! \dots N_{\Gamma-1}!} \right] = L M_{\{N_n\}} + \mathcal{O}(\ln L) \quad (\text{J6})$$

can be studied exactly with the same method based on Stirling's asymptotic formula and employed in Appendix D for the multinomials

$$\frac{L!}{e_0!e_1! \dots e_{d-1}!}, \quad (\text{J7})$$

which were subject to the constraints in Eq. (D3), which are functionally identical to Eq. (J3). In particular, we can directly use here the results from Appendix D via the identifications

$$\begin{aligned} \frac{L!}{(\varepsilon_0 L)! \dots (\varepsilon_{d-1} L)!} &\rightarrow \frac{N!}{(f_0 N)! \dots (f_{\tilde{\Gamma}-1} N)!}, \\ \sum_{n=0}^{d-1} \varepsilon_n = 1 &\rightarrow \sum_{n=0}^{\tilde{\Gamma}-1} f_n = 1, \\ \sum_{n=0}^{d-1} n \varepsilon_n = \nu &\rightarrow \sum_{n=0}^{\tilde{\Gamma}-1} n f_n = \frac{1}{\nu} - 1, \end{aligned} \quad (\text{J8})$$

where $\tilde{\Gamma} < \Gamma$ is a new cutoff to be determined a posteriori by requiring that $N_n \geq 1 \forall n = 0, \dots, \tilde{\Gamma}$. The previous inequality is necessary to justify the application

of Stirling's formula, which is quite accurate even for N_n as small as 1, but certainly not for $N_n = 0$. From the results of Appendix D we automatically deduce that the maximum of $M_{\{N_n\}}$ from Eq. (J6) is given by

$$M_{\{f_n^* N\}} = \nu \ln \left(\frac{1 - t^{\tilde{\Gamma}}}{1 - t} \right) - (1 - \nu) \ln t, \quad (\text{J9})$$

$$f_n^* = \frac{N_n^*}{N} = \frac{1 - t}{1 - t^{\tilde{\Gamma}}} t^n, \quad (\text{J10})$$

where $0 < t < 1$ is the unique solution of

$$\frac{1}{\nu} - 1 = \tilde{\Gamma} + \frac{t}{1 - t} - \frac{\tilde{\Gamma}}{1 - t^{\tilde{\Gamma}}}. \quad (\text{J11})$$

We now assume that $\tilde{\Gamma}$ is an increasing function of L which diverges in the thermodynamic limit and we will check this at the end. This allows to determine the solution t of Eq. (J11) in terms of the expansion

$$t = 1 - \nu + \mathcal{O} \left[(1 - \nu)^{\tilde{\Gamma}} \right], \quad (\text{J12})$$

which is consistent with $0 < t < 1$. From this we obtain

$$M_{\{f_n^* N\}} = \eta_2(\nu) + \mathcal{O} \left[(1 - \nu)^{\tilde{\Gamma}} \right], \quad (\text{J13})$$

$$f_n^* = \nu(1 - \nu)^n + \mathcal{O} \left[(1 - \nu)^{\tilde{\Gamma}} \right]. \quad (\text{J14})$$

The fact that the leading order of the maximum $L M_{\{f_n^* N\}}$ coincides with the leading order of $\ln D_N^{(2)}(L)$, see Eq. (J1), was expected from Eq. (J2). To determine $\tilde{\Gamma}$ we now impose that $N_{\tilde{\Gamma}-1}^* = 1$, so to ensure $N_n^* \geq 1 \forall n = 0, \dots, \tilde{\Gamma} - 1$. This implies

$$\frac{1}{N} = f_{\tilde{\Gamma}-1}^* = \mathcal{O} \left[(1 - \nu)^{\tilde{\Gamma}} \right] \rightarrow \tilde{\Gamma} = \mathcal{O}(\ln N). \quad (\text{J15})$$

This proves that $\tilde{\Gamma}$ is an increasing function of L which diverges in the thermodynamic limit, consistent with our previous assumption. Note that the typicality class which includes an infinitesimal neighborhood around the maxima f_n^* contains a fraction of all configurations that tends to 1 exponentially fast with L .

The previous results can be interpreted in a simple way through the lens of the central limit theorem. Imagine generating a random configuration of particles and holes in the chain of size L by drawing a particle on each site with probability ν and a hole with probability $1 - \nu$. For large L the central limit theorem guarantees that, in any state generated in this way, the global filling is very close to ν , with fluctuations around this value of order $\mathcal{O}(1/\sqrt{L})$. This means that for asymptotically large L this class of randomly generated states reflects the average properties over the set of $D_{\nu L}^{(2)}(L)$ states with filling

ν on a chain of size L . We can then ask what the expectation value is of N_n in the randomly generated set of states. This is given by the probability of having (after any particle) n consecutive holes followed by another particle, times the total number of particles in the system

$$\langle N_n \rangle = \langle N \rangle (1 - \nu)^n \nu = L \nu^2 (1 - \nu)^n. \quad (\text{J16})$$

The previous result coincides with Eq. (J14), as expected from the fact that our typicality class dominates in the determination of any average over the entire set of states. Exploiting this equivalence between average properties over sets of randomly drawn states and properties of single states in a typicality class, we can generalise our previous results to the following statement:

In typical states of $d = 2$ systems with global filling ν there are

$$L \nu^p (1 - \nu)^h + o(L) \quad (\text{J17})$$

occurrences of $p + h$ consecutive sites hosting p particles and h holes arranged in a fixed chosen configuration.

Appendix K: Deriving $P_b(\nu)$ for $d = 2, k = 4$

We aim to derive an exact expression for the function $P_b(\nu)$, which for $k = 4$ and $d = 2$ gives the probability that, starting from a given site (and assuming the preceding 2 sites are part of an active bubble), a pattern of particles and holes will arise such that the first three sites in the pattern are frozen sites.

We begin by noting that the first three sites in the pattern must either all be holes or particles. This is because the preceding 2 sites are part of an active bubble, and so they must consist of one particle and one hole, with the respective positions of the particle and hole swapping as the system evolves with time. Hence, if the first three sites of the pattern contained both particles and holes, it is easy to see this would allow a hopping move to occur via interaction with a particle in the active bubble, and so the 3 sites would not all be frozen.

In view of this result, we proceed to decompose our function as

$$P_b(\nu) = (1 - \nu)^3 p_b(\nu) + \nu^3 p_b(1 - \nu),$$

where $p_b(\nu)$ is the probability that starting from a given site, a pattern will arise such that the first site in the pattern is either empty or, if it contains a particle, the particle will be unable to perform an outward hop. Hence, if the three sites next to the active bubble are holes, $p_b(\nu)$ is the probability that the following sites will be configured such that those 3 holes are frozen; and likewise, if the three sites are particles, then $p_b(1 - \nu)$ gives the probability that those three particles will be frozen.

To make the computation of $p_b(\nu)$ more intuitive to follow, instead of expressing it as a sum over powers of ν and $(1 - \nu)$, we will express it as a sum over sequences of “0” (indicating a hole) and “1” (indicating a particle),

with the rule $0 \rightarrow (1 - \nu)$ and $1 \rightarrow \nu$. By definition, we immediately have that

$$p_b(\nu) = 0 + 1 \dots, \quad (\text{K1})$$

where by \dots we mean that further terms need to be specified in the sequence to ensure that the starting particle in it cannot hop outward. If the first 1 is followed by a 0 then another 1, we find ourselves in the same situation: the first particle in the sequence cannot hop outward only if the newly added particle cannot hop outward. This pattern repeats itself if we add on indefinitely many further terms of the form 01, and so

$$p_b(\nu) = 0 + 1 \left(\sum_{i=0}^{\infty} (01)^i \right) \dots \quad (\text{K2})$$

The next term we could add to the sequence is either a 00 or a 11 (since a 10 would allow the first particle in the sequence to perform an outward hop). A 00 already achieves the goal of preventing an outward hop. A 11 on the other hand requires that more of the sequence be specified to ensure an outward hop cannot happen. Hence we have

$$p_b(\nu) = 0 + 1 \left(\sum_{i=0}^{\infty} (01)^i \right) (00 + 11 \dots) \quad (\text{K3})$$

If we have a 11 term, we must ensure that the second of these two particles cannot perform an inward hop with the remaining particles in the sequence. If we add a 01 to the sequence, then we have the same situation: we must ensure that the latest particle added to the sequence cannot perform an inward hop. Thus we have

$$p_b(\nu) = 0 + 1 \left(\sum_{i=0}^{\infty} (01)^i \right) (00 + 11 \left(\sum_{i=0}^{\infty} (01)^i \right) \dots) \quad (\text{K4})$$

If we add on a further 1 after this, then the inward hop cannot occur and we are done. If we add on a 00, then we must add on a third 0, as a 001 would allow an inward hop with the before-last particle. Thus

$$p_b(\nu) = 0 + 1 \left(\sum_{i=0}^{\infty} (01)^i \right) (00 + 11 \left(\sum_{i=0}^{\infty} (01)^i \right) (1 + 000 \dots)) \quad (\text{K5})$$

For the final term, we note that our aim is achieved only if the last sequence 000 is followed by a fourth hole 0, or else by a particle 1 that cannot perform an outward hop. We therefore have

$$p_b(\nu) = 0 + 1 \left(\sum_{i=0}^{\infty} (01)^i \right) (00 + 11 \left(\sum_{i=0}^{\infty} (01)^i \right) (1 + 000 p_{nh}(\nu))) \quad (\text{K6})$$

Substituting $(1 - \nu)$ for 0 and ν for 1 in the above equation and solving it, we obtain our desired result:

$$p_b(\nu) = \frac{1 - 2\nu + 2\nu^2 - \nu^3 + \nu^4}{1 - 2\nu + 3\nu^2 - 3\nu^3 + 4\nu^4 - 3\nu^5 + \nu^6} \quad (\text{K7})$$

- [1] J. M. Deutsch, Eigenstate thermalization hypothesis, *Reports on Progress in Physics* **81**, 082001 (2018).
- [2] A. P. Luca D’Alessio, Yariv Kafri and M. Rigol, From quantum chaos and eigenstate thermalization to statistical mechanics and thermodynamics, *Advances in Physics* **65**, 239 (2016).
- [3] R. Nandkishore and D. A. Huse, Many-body localization and thermalization in quantum statistical mechanics, *Annual Review of Condensed Matter Physics* **6**, 15 (2015).
- [4] P. W. Anderson, Absence of diffusion in certain random lattices, *Phys. Rev.* **109**, 1492 (1958).
- [5] D. Basko, I. Aleiner, and B. Altshuler, Metal–insulator transition in a weakly interacting many-electron system with localized single-particle states, *Annals of Physics* **321**, 1126 (2006).
- [6] D. A. Abanin, E. Altman, I. Bloch, and M. Serbyn, Colloquium: Many-body localization, thermalization, and entanglement, *Rev. Mod. Phys.* **91**, 021001 (2019).
- [7] C. Chamon, Quantum glassiness in strongly correlated clean systems: An example of topological overprotection, *Phys. Rev. Lett.* **94**, 040402 (2005).
- [8] J. Haah, Local stabilizer codes in three dimensions without string logical operators, *Phys. Rev. A* **83**, 042330 (2011).
- [9] S. Vijay, J. Haah, and L. Fu, A new kind of topological quantum order: A dimensional hierarchy of quasiparticles built from stationary excitations, *Phys. Rev. B* **92**, 235136 (2015).
- [10] R. M. Nandkishore and M. Hermele, Fractons, *Annual Review of Condensed Matter Physics* **10**, 295 (2019).
- [11] M. Pretko, X. Chen, and Y. You, Fracton phases of matter, *International Journal of Modern Physics A* **35**, 2030003 (2020).
- [12] A. Gromov and L. Radzihovsky, Colloquium: Fracton matter, *Rev. Mod. Phys.* **96**, 011001 (2024).
- [13] S. Pai, M. Pretko, and R. M. Nandkishore, Localization in fractonic random circuits, *Phys. Rev. X* **9**, 021003 (2019).
- [14] P. Sala, T. Rakovszky, R. Verresen, M. Knap, and F. Pollmann, Ergodicity breaking arising from hilbert space fragmentation in dipole-conserving hamiltonians, *Phys. Rev. X* **10**, 011047 (2020).
- [15] V. Khemani, M. Hermele, and R. Nandkishore, Localization from hilbert space shattering: From theory to physical realizations, *Phys. Rev. B* **101**, 174204 (2020).
- [16] Z.-Y. Wang, S. Takayoshi, and M. Nakamura, Spin-chain description of fractional quantum hall states in the jain series, *Phys. Rev. B* **86**, 155104 (2012).
- [17] E. J. Bergholtz, M. Nakamura, and J. Suorsa, Effective spin chains for fractional quantum hall states, *Physica E: Low-dimensional Systems and Nanostructures* **43**, 755 (2011), nanoPHYS 09.
- [18] W. Morong, F. Liu, P. Becker, K. S. Collins, L. Feng, A. Kyprianidis, G. Pagano, T. You, A. V. Gorshkov, and C. Monroe, Observation of stark many-body localization without disorder, *Nature* **599**, 393 (2021).
- [19] E. van Nieuwenburg, Y. Baum, and G. Refael, From bloch oscillations to many-body localization in clean interacting systems, *Proceedings of the National Academy of Sciences* **116**, 9269 (2019).
- [20] A. Morningstar, V. Khemani, and D. A. Huse, Kinetically constrained freezing transition in a dipole-conserving system, *Phys. Rev. B* **101**, 214205 (2020).
- [21] C. Pozderac, S. Speck, X. Feng, D. A. Huse, and B. Skinner, Exact solution for the filling-induced thermalization transition in a one-dimensional fracton system, *Phys. Rev. B* **107**, 045137 (2023).
- [22] C. Wang and Z.-C. Yang, Freezing transition in the particle-conserving east model, *Phys. Rev. B* **108**, 144308 (2023).
- [23] S. Moudgalya and O. I. Motrunich, Hilbert space fragmentation and commutant algebras, *Phys. Rev. X* **12**, 011050 (2022).
- [24] N. S. Srivatsa, H. Yarloo, R. Moessner, and A. E. B. Nielsen, Mobility edges through inverted quantum many-body scarring, *Phys. Rev. B* **108**, L100202 (2023).
- [25] Q. Chen and Z. Zhu, Inverting multiple quantum many-body scars via disorder, *Phys. Rev. B* **109**, 014212 (2024).
- [26] N. S. Srivatsa, R. Moessner, and A. E. B. Nielsen, Many-body delocalization via emergent symmetry, *Phys. Rev. Lett.* **125**, 240401 (2020).
- [27] M. Iversen, N. S. Srivatsa, and A. E. B. Nielsen, Escaping many-body localization in an exact eigenstate, *Phys. Rev. B* **106**, 214201 (2022).
- [28] S. Melczer, G. Panova, and R. Pemantle, Counting partitions inside a rectangle, *SIAM Journal on Discrete Mathematics* **34**, 2388 (2020).
- [29] This homogeneity over extensive subregions is expected from simple arguments. Indeed, for asymptotically large values of L we can imagine generating a random state by randomly associating a site $i = 0, \dots, L - 1$ with each particle, avoiding occupations beyond $d - 1$. In the vast majority of states generated in this way, any extensive subregion is expected to have a filling identical to the global filling ν .
- [30] S. Wiseman and E. Domany, Lack of self-averaging in critical disordered systems, *Phys. Rev. E* **52**, 3469 (1995).
- [31] J. R. Garrison and T. Grover, Does a single eigenstate encode the full hamiltonian?, *Phys. Rev. X* **8**, 021026 (2018).
- [32] D. N. Page, Average entropy of a subsystem, *Phys. Rev. Lett.* **71**, 1291 (1993).
- [33] S. Sen, Average entropy of a quantum subsystem, *Phys. Rev. Lett.* **77**, 1 (1996).
- [34] E. Bianchi, L. Hackl, M. Kieburg, M. Rigol, and L. Vidmar, Volume-law entanglement entropy of typical pure quantum states, *PRX Quantum* **3**, 030201 (2022).
- [35] T. LeBlond, K. Mallayya, L. Vidmar, and M. Rigol, Entanglement and matrix elements of observables in interacting integrable systems, *Phys. Rev. E* **100**, 062134 (2019).
- [36] S. Moudgalya, B. A. Bernevig, and N. Regnault, Quantum many-body scars and hilbert space fragmentation: a review of exact results, *Reports on Progress in Physics* **85**, 086501 (2022).
- [37] Z.-C. Yang, F. Liu, A. V. Gorshkov, and T. Iadecola, Hilbert-space fragmentation from strict confinement, *Phys. Rev. Lett.* **124**, 207602 (2020).
- [38] Remember that there always is the additional freedom in partitioning the chain into α_i subregions due to the possible different choices for the location of the cut within each type-1 blockage.

- [39] M. Fishman, S. R. White, and E. M. Stoudenmire, The ITensor Software Library for Tensor Network Calculations, [SciPost Phys. Codebases](#), **4** (2022).
- [40] J. Lehmann, P. S. de Torres-Solanot, F. Pollmann, and T. Rakovszky, Fragmentation-induced localization and boundary charges in dimensions two and above, [SciPost Phys.](#) **14**, 140 (2023).
- [41] P. Sala, J. Lehmann, T. Rakovszky, and F. Pollmann, Dynamics in systems with modulated symmetries, [Phys. Rev. Lett.](#) **129**, 170601 (2022).
- [42] J. Iaconis, A. Lucas, and R. Nandkishore, Multipole conservation laws and subdiffusion in any dimension, [Phys. Rev. E](#) **103**, 022142 (2021).
- [43] D. A. Huse, R. Nandkishore, V. Oganesyan, A. Pal, and S. L. Sondhi, Localization-protected quantum order, [Phys. Rev. B](#) **88**, 014206 (2013).
- [44] S. A. Parameswaran and R. Vasseur, Many-body localization, symmetry and topology, [Reports on Progress in Physics](#) **81**, 082501 (2018).
- [45] A. Prakash, A. Goriely, and S. L. Sondhi, Classical non-relativistic fractons, [Phys. Rev. B](#) **109**, 054313 (2024).
- [46] A. Prakash, Y. Sadki, and S. L. Sondhi, Machian fractons, hamiltonian attractors, and nonequilibrium steady states, [Phys. Rev. B](#) **110**, 024305 (2024).
- [47] L. Takács, Some asymptotic formulas for lattice paths, [Journal of Statistical Planning and Inference](#) **14**, 123 (1986).